A Class of Simple Biomolecular Antithetic Proportional-Integral-Derivative Controllers

Maurice Filo[1] and Mustafa Khammash[1,*]

[1]ETH Zürich Department of Biosystems Science and Engineering
[*]Correspondence: mustafa.khammash@bsse.ethz.ch

Abstract

Proportional-Integral-Derivative (PID) feedback controllers have been the most widely used controllers in the industry for almost a century. This is mainly due to their simplicity and intuitive operation. Recently, motivated by their success in various engineering disciplines, PID controllers found their way into molecular biology. In this paper, we consider the mathematical realization of (nonlinear) PID controllers via biomolecular interactions in both the deterministic and stochastic settings. We propose several simple biomolecular PID control architectures that take into consideration the biological implementation aspect. We verify the underlying PID control structures by performing a linear perturbation analysis and examine their effects on the (deterministic and stochastic) performance and stability. In fact, we demonstrate that different proportional controllers exhibit different capabilities of enhancing the dynamics and reducing variance (cell-to-cell variability). Furthermore, we propose a simple derivative controller that is mathematically realized by cascading the antithetic integral controller with an incoherent feedforward loop without adding any additional species. We demonstrate that the derivative component is capable of enhancing the transient dynamics at the cost of boosting the variance, which agrees with the well known vulnerability of the derivative controller to noise. We also show that this can be mitigated by carefully designing the inhibition pathway of the incoherent feedforward loop. Throughout the paper, the stochastic analysis is carried out based on a tailored moment-closure technique and is also backed up by simulations.

1 Introduction

One of the most salient features of biological systems is their ability to adapt to their noisy environments. For example, cells often regulate gene expression to counteract all sorts of intrinsic and extrinsic noise in order to maintain a desirable behavior in a precise and timely fashion. This resilience toward undesired disturbances is often achieved via feedback control that has proved to be ubiquitous in both natural (e.g. [1–3]) and engineered systems (e.g. [4,5]). In fact, synthetically engineering biomolecular controllers is gaining a wide attention from biologists and engineers (e.g. [6–14]).

A standard general setup for feedback controllers is depicted as a block diagram (refer to Box 1: A Primer on Block Diagrams) in Panel A of Figure 1. The "Plant" block represents the process to be controlled. It can be actuated through its input, denoted here by u, to dynamically manipulate its output of interest, denoted here by y. The objective of such control systems is to design a feedback controller that *automatically* actuates the plant in a smart autonomous fashion and guarantees that the output y meets certain performance goals despite the presence of disturbances in the plant. These performance goals include (but are not limited to)

- **Robust Perfect Adaptation (RPA)**: This property is the biological analogue of the notion of *Robust Steady-State Tracking* (RSST) that is well known in control theory [15]. A controller achieves RPA (or equivalently RSST) if it drives the steady state of the plant output y to a constant value – prescribed by the user as a set point or reference (denoted by r in Figure 1)– which does not depend on the initial conditions and/or plant uncertainties. Furthermore, the steady state of the output has to be immune to constant disturbances in the plant. If the controller does not possess the RPA feature, a steady-state error emerges when exogenous disturbances strike the plant (refer to Panel B of Figure 1).

- **Stability Enhancement**: The plant might be unstable when operating in a certain regime, that is the output y does not converge to a fixed steady-state value. An example of such instabilities is a divergent response where y grows unboundedly. Another example is when the output y exhibits a sustained oscillation and never converges to the desired set point r (refer to Panel B of Figure 1). A typical

performance objective of the controller is to enhance the stability of the system, that is, shrink the operating regimes where the dynamics are unstable.

Box 1. A Primer on Block Diagrams

In classical control theory, block diagrams are used to visually represent (deterministic) dynamical systems with inputs and outputs. In a fairly general setting, a dynamical system $\mathcal{M}$ can be written as a set of differential equations coupled with another set of algebraic equations given by

$$\mathcal{M} : \begin{cases} \dot{x} = f(x, u); & x(0) = x_0 \\ y = g(x, u), \end{cases}$$

where x is called the state variable with initial condition x_0, u is the input, and y is the output. Note that, for simplicity, x, u and y are all considered to be scalar functions of time (scalar signals); however, the extension to vector-valued signals is straightforward. One can think of $\mathcal{M}$ as a dynamical mapping that maps the input signal u to the output signal y. In the rest of this box, we set the initial condition to zero for simplicity (and without loss of generality). This dynamical system $\mathcal{M}$ can be represented as a block diagram depicted in Panel A. This block takes u as an input indicated by the inward arrow, and yields y as the output indicated by the outward arrow. Note that inputs to a block are not affected by the block itself, only outputs are affected. Outputs can serve as inputs to other blocks, and inputs can be incoming as feedback from the output of other blocks (see Panel A of Figure 1 for example). As a result, one of the nice features of a block diagram is to decompose the overall dynamics into multiple modularized sub-dynamical systems, each having a specialized operation.

Block diagrams are especially useful for linear dynamical systems such as the system to the left in Panel B. In this system, the input-output relationship, in the time domain, is given by a linear differential (and algebraic) equation, where ω_c is a constant. This relationship can be equivalently expressed in the Laplace domain, by taking the Laplace transforms. With slight abuse of notation, let $x(s), u(s)$ and $y(s)$ denote the Laplace transforms of $x(t), u(t)$ and $y(t)$, respectively, with s being the Laplace variable. Note that we drop t and s when the considered domain (time/Laplace) is clear. Then it is straightforward to show that the input-output relationship in the Laplace domain reduces to a multiplication operation $y(s) = M(s)u(s)$, where $M(s) := \frac{\omega_c}{s+\omega_c}$ is called the transfer function of the block. Hence, for linear dynamical systems, the output of a block in the Laplace domain is simply the product between the block's transfer function and its input. This example block operates as a low pass filter that filters out high frequencies, particularly those higher than the cutoff frequency ω_c [16, Figure 8.15]. Note that in the limit, as $\omega_c \to \infty$, this block becomes the identity operator: $y = u$.

Panel C shows other commonly used blocks representing four linear dynamical systems: (1) a summation junction that sums (and/or subtracts) its inputs, (2) an integral block which integrates the input in time and is equivalent to dividing by s in the Laplace domain, (3) a proportional block which multiplies its input by a constant, and (4) a derivative block which differentiates its input in time and is equivalent to multiplying by s in the Laplace domain. The transfer functions of the integral, proportional and derivative blocks are thus $K_I/s, K_P$ and $K_D s$, respectively, as depicted in Panel C.

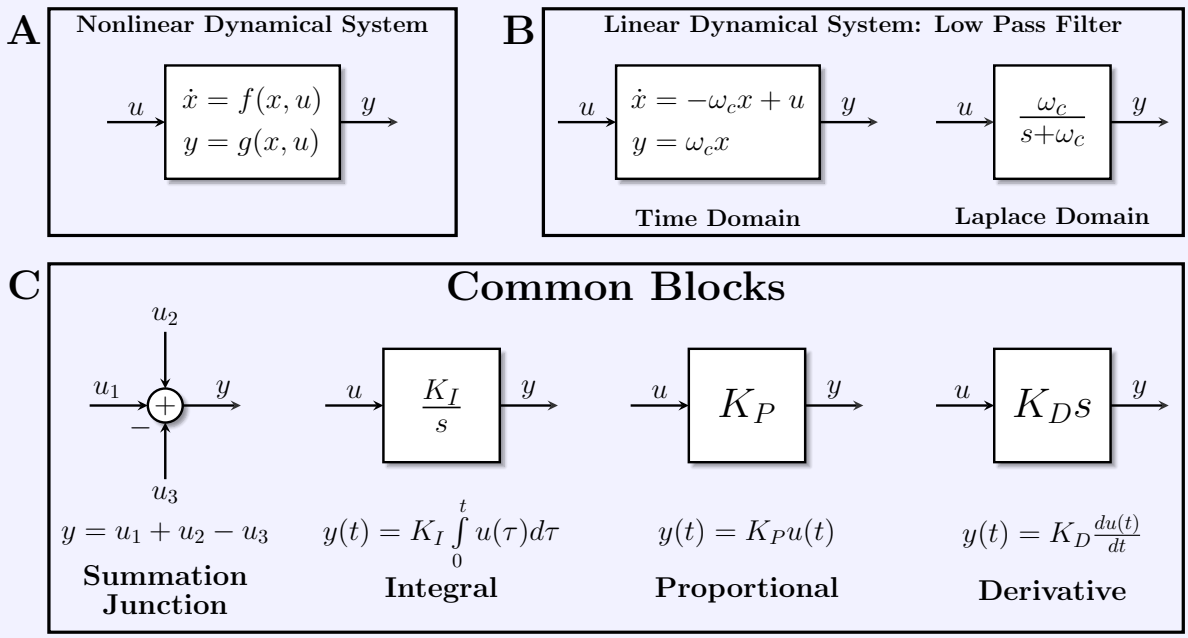

- **Desirable Transient Response**: Building a controller that achieves RPA is perhaps the most basic and essential requirement; however, a high performance controller has to fulfill additional requirements that are equally as important. For example, even though a controller is designed to ensure RPA (and stability), the transient dynamics might still be very slow to reach the desired (robust) steady state. This undesirable sluggish response, in some situations, can practically destroy the theoretically guaranteed RPA. Other examples of undesirable transient dynamical responses include overshoots and damped oscillations (refer to Panel B of Figure 1). A typical performance objective is to design a controller that yields a smooth transient response which is fast enough but doesn't overshoot or oscillate too much.

- **Variance Reduction**: This is a performance objective that is less common in classical control theory. When the dynamics are stochastic, it is common to study the time evolution of the output probability distribution and its moments such as the mean and variance. A natural performance objective is to design a controller that tightens the probability distribution around the mean, e.g. reduce the variance. This could be particularly useful in biology for reducing cell-to-cell variability.

Control theory developed a wide set of tools to design feedback controllers that meet certain performance objectives. For instance, it is well known in control theory (internal model principle [17]) that a controller should involve an Integral (I) action to be able to achieve RSST (or equivalently RPA). Furthermore, Proportional-Integral-Derivative (PID) feedback controllers – first rigorously introduced by Nicolas Minorsky [18] around a hundred years ago – adds a Proportional (P) and Derivative (D) action to the Integrator (I) to be able to tune the transient dynamics and enhance stability while preserving RPA. Interestingly, after almost a century, PID controllers are still the most widely used controllers in industrial applications spanning a broad range of engineering disciplines such as mechanical and electrical engineering ([19–21]).

Originally, PID feedback controllers were designed to control mechanical (later, electrical) systems such as automatic ship steering (later, telephone engineering systems) [22]. Such control systems involve controlling quantities that can take both negative and positive values such as angles, velocities, electric currents, voltages, etc... Furthermore, traditional PID controllers possess linear dynamics since all three operations of a PID are linear. Two classes of linear PID controllers, adopted from [16, Chapter 10], are shown in Panels C and D of Figure 1. In the first architecture shown in Panel C, the error signal $e(t) := r - y(t)$ is fed into the three (P, I, and D) components. The outputs of the three components are summed up to yield the control action u which serves as the actuation input to the plant as demonstrated in Panel A. In the second architecture shown in Panel D, the controller has two degrees of freedom since both the error e and the output y are used separately and simultaneously. Particularly, the error is fed into the integrator, while the output is fed into the proportional and derivative components. Observe that both architectures require that the integrator operates on the error (and not the output). This is necessary to achieve RSST and can be easily seen using a very simple argument explained next. Let $u_I(t)$ denote the output of the integrator, that is

$$u_I(t) := K_I \int_0^t e(\tau)d\tau \qquad \Longrightarrow \qquad \dot{u}_I(t) = K_I e(t). \tag{1}$$

Assuming that the dynamics are stable (that is, converge to a fixed point), then at steady state we have $\lim_{t\to\infty} \dot{u}_I(t) = 0$. This implies that, at steady state (assuming stability), the error $e := r - y$ has to be zero, and thus $\lim_{t\to\infty} y(t) = r$, hence achieving the steady-state tracking property. Observe that this argument does not depend on the plant, hence achieving the robustness property.

For mechanical and electrical systems, the linearity of the PID controllers is convenient because of the availability of basic physical parts (e.g. dampers, springs, RLC circuits, op-amps, etc...) that are capable of realizing these linear dynamics. However, this realization quickly becomes challenging when designing biomolecular controllers. This difficulty arises because (a) biomolecular controllers have to respect the structure of BioChemical Reaction Networks (BCRN), and (b) the quantities to be controlled (protein copy numbers or concentrations) cannot be negative (see [23] for positive integral control). Furthermore, the dynamics of biochemical reactions are inherently nonlinear. To achieve RPA, BCRN realizations of standalone Integral (I) controllers initially received the widest attention [24–29]. In previous work [26], the Antithetic Integral Feedback (AIF) controller was introduced to realize integral action that ensures RPA. In fact, more recently, it was shown in [9] that the antithetic motif is necessary to achieve RPA in arbitrary intracellular networks with noisy dynamics. A detailed mathematical analysis of the performance tradeoffs that may arise in the AIF controller is presented in [30,31], and optimal tuning is treated in [32]. Furthermore, practical design aspects, particularly the dilution effect of controller species, are addressed in [28,29]. Biological implementations of various biomolecular integral controllers appeared in bacteria *in vivo* [6,8,9] and *in vitro* [13], and more recently in mammalian cells [14].

In the pursue of designing high performance controllers while maintaining the RPA property, BCRN realizations of PI and PID controllers started receiving more focused attention [33–38]. Particularly in [33], a

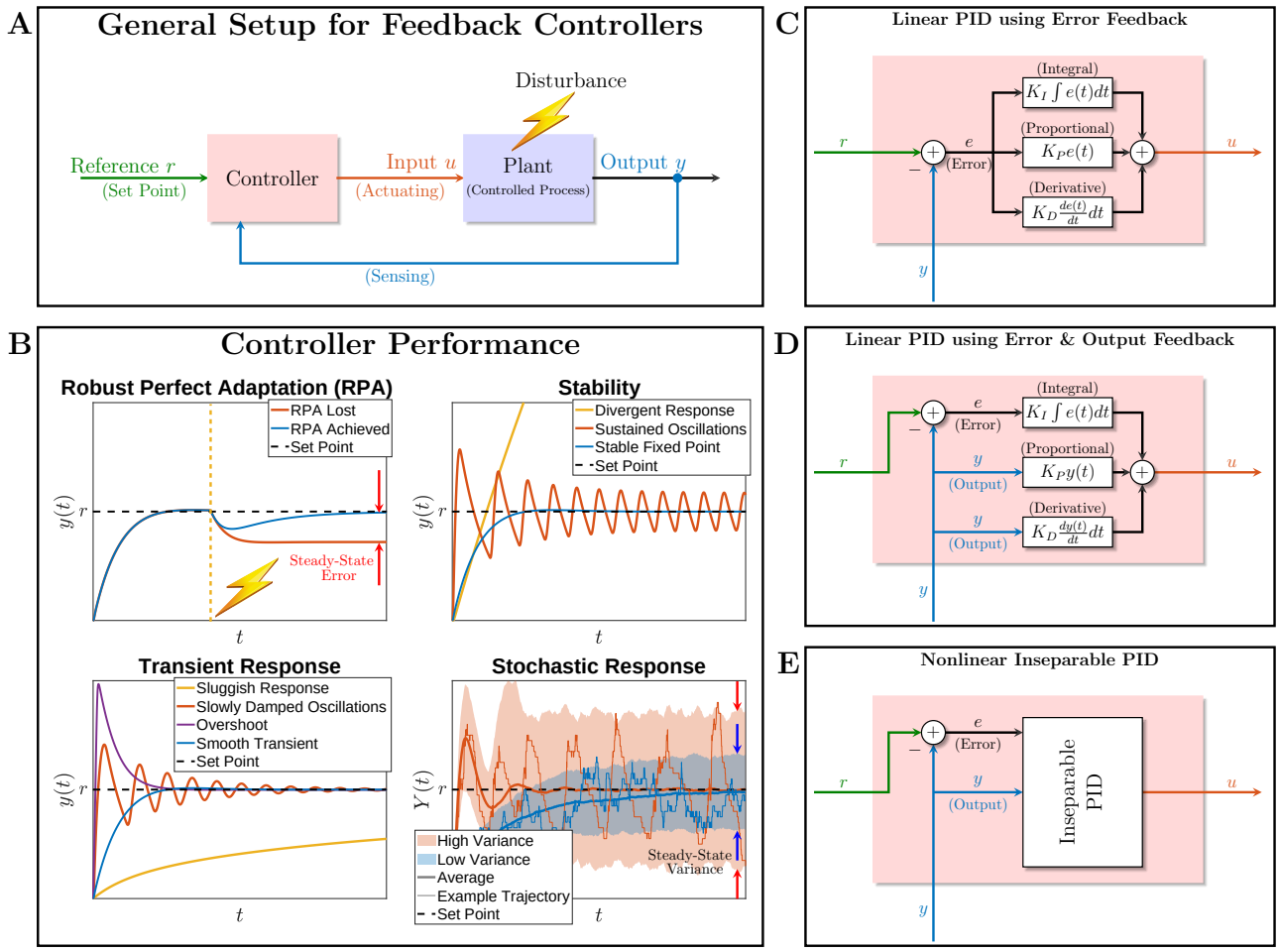

Figure 1: **Feedback Controller Design and Performance. (A)** The output to be controlled is fed back into the controller via some sensing mechanism. The controller exploits the set point, that is typically "dialed in" by the user and computes the suitable control action to be applied to the plant (or process) via some actuation mechanism. The goal of the control action is to steer the output to the desired set point despite external (or even internal) disturbances. **(B)** A demonstration of various performance goals that are typically targeted when designing the controller. **(C), (D), and (E)** Various PID control architectures. The classical designs in (C) and (D) involve separate linear P, I and D operations that are added together to yield the control action u. The difference between (C) and (D) is in the controller input: in (C) the error signal is the only input, while in (D) the error signal is fed into the I component whereas the output signal is fed into the P and D components . In this paper, we propose PID control architectures that fit in the more general class depicted in (E) where the PID components are nonlinear and inseparable. This gives more design flexibility for biomolecular controllers.

proportional component is separately appended to the antithetic integral motif via a repressing hill-type function to tune the transient dynamics and reduce the variance. The resulting PI controller follows the concept of Panel D where error and output feedback are used to build separate (but nonlinear) P and I components. Several successful attempts were carried out to realize a BCRN capable of approximating derivatives [39–42]. However, the first focused work on BCRN realizations of a full PID controller was done in [35], where the authors introduce more controller species for the derivative component to follow the concept of Panel C in Figure 1. The resulting PID controller uses error feedback to build separate nonlinear P, I, and D components and successfully improves the dynamic performance in the deterministic setting. Using a different approach, [37] and [38] exploit the dual-rail representation from [24], where additional species are introduced to overcome the non-negativity challenge of the realized PID controller. The authors demonstrate the resulting improvement of the performance in the deterministic setting. On a different note, [36] analyzed the effects of separate proportional and derivative controllers on (bursty) gene expression models in the stochastic setting.

Interestingly, all previous research in this direction have two intimately related aspects in common. Firstly, the P, I, and D components are realized separately such that they enter the dynamics additively. This aspect is motivated by traditional PID controllers where the controller dynamics are constrained to be linear, and thus the three components has to be added up (rather than multiplied for example). However, since feedback mechanisms in BCRNs are inherently nonlinear, there is no reason to restrict the controller to have linear dynamics and/or additive components. Secondly, the proposed derivative control designs introduce additional species to realize the controller, and thus making the biological implementation more difficult. To this end, we consider in this paper (more general) nonlinear PID controllers that do not have to be explicitly separable

into their three (P, I and D) components. This allows controllers to involve P, I , and D architectures in one (inseparable) block as depicted in Panel E of Figure 1 where both, error and output, feedbacks are allowed. The nonlinearity and inseparability features of the proposed PI and PID controllers provide more flexibility in the BCRN design and allows simpler architectures that do not require introducing additional species to the standalone integral controller. Note that, one can convert such inseparable PIDs with output and error feedbacks to only error feedback by introducing a single additional controller species (similar to [35]). However, in this paper, we use both error and output feedback to keep the controller designs as simple as possible and to maintain the two degrees of freedom in the actuation.

The paper is organized as follows. A general framework for biomolecular feedback controllers is introduced in the subsequent section. Then, in Section 3, several Proportional-Integral (PI) Feedback controllers are proposed and analyzed in both the deterministic and stochastic settings. Next, a simple Derivative (D) component is appended to the PI controller in Section 4. Simulations are carried out to assess the performance and is also validated by a theoretical analysis. Finally, we conclude in Section 5.

2 General Framework for Biomolecular Feedback Controllers

The framework for feedback control systems is traditionally described through block diagrams (e.g. Panel A of Figure 1). In this section, we lay down a general framework for feedback control systems where both the plant and the controller are represented by Biochemical Reaction Networks (BCRN). With this framework, the controller can either represent an actual biomolecular circuit or it can be implemented as a mathematical algorithm *in silico* [43–45] to regulate a biological circuit (through light for example [46]).

2.1 Open Loop Description: an Arbitrary Plant

Consider a general plant, depicted in Figure 2, comprised of L species $\mathbf{X} := \{\mathbf{X_1}, \mathbf{X_2}, \cdots, \mathbf{X_L}\}$ that react with each other through K reaction channels labeled as $\mathcal{R} := \{\mathcal{R}^1, \mathcal{R}^2, \cdots, \mathcal{R}^K\}$. Each reaction $\mathcal{R}^k$ ($k = 1, 2, \cdots, K$) has a stoichiometry vector denoted by $\zeta_k \in \mathbb{Z}^L$ and a propensity function $\lambda_k : \mathbb{N}_0^L \to \mathbb{R}_*^+$. Let $S := \begin{bmatrix}\zeta_1 & \zeta_2 & \cdots & \zeta_K\end{bmatrix} \in \mathbb{Z}^{L\times K}$ denote the stoichiometry matrix and let $\lambda := \begin{bmatrix}\lambda_1 & \lambda_2 & \cdots & \lambda_K\end{bmatrix}^T$ denote the (vector-valued) propensity function. Then, the plant constitutes a BCRN that is fully characterized by the triplet $\mathcal{N}_{ol} := (\mathbf{X}, S, \lambda)$ which we shall call the "open-loop" system.

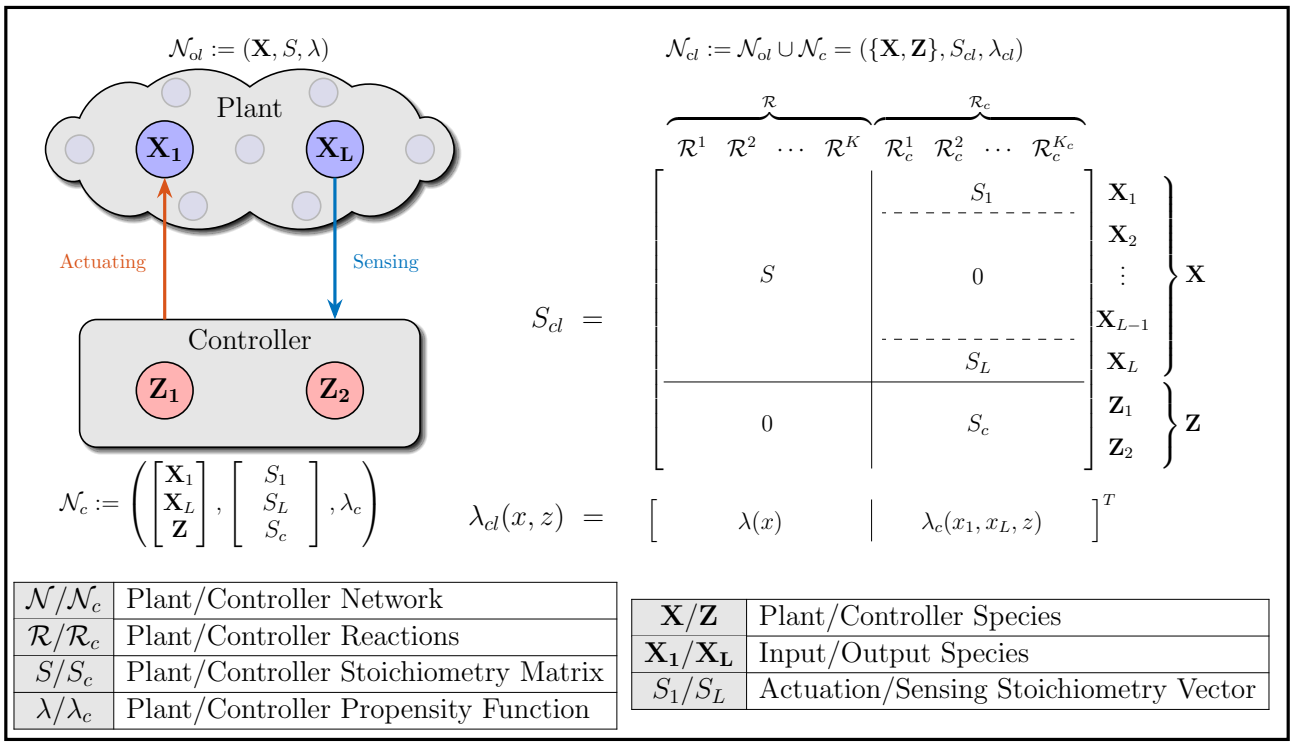

$\mathcal{N}/\mathcal{N}_c$	Plant/Controller Network
$\mathcal{R}/\mathcal{R}_c$	Plant/Controller Reactions
S/S_c	Plant/Controller Stoichiometry Matrix
λ/λ_c	Plant/Controller Propensity Function

$\mathbf{X}/\mathbf{Z}$	Plant/Controller Species
$\mathbf{X_1}/\mathbf{X_L}$	Input/Output Species
S_1/S_L	Actuation/Sensing Stoichiometry Vector

Figure 2: **A Framework for Feedback Control of (Bio)chemical Reaction Networks.** An arbitrary plant is comprised of L species $\{\mathbf{X_1}, \mathbf{X_2}, ..., \mathbf{X_L}\}$ reacting with each other. Species $\mathbf{X_L}$, by definition, is the output of interest to be controller, while $\mathbf{X_1}$ is assumed to be the only accessible input species that can be "actuated" by the controller network. The closed-loop system, with stiochiometry matrix S_{cl} and propensity function λ_{cl}, denotes the overall feedback interconnection between the plant and controller networks.

2.2 Feedback Controller & Closed Loop Description

The goal of this work is to design a controller network, denoted by $\mathcal{N}_c$, that is connected in feedback with the plant network $\mathcal{N}_{ol}$, as illustrated in Figure 2, to meet certain performance objectives such as those mentioned in the Section 1. To keep the controller simple, the number of controller species is restricted to only two, that is $\mathbf{Z} := \{\mathbf{Z_1}, \mathbf{Z_2}\}$. We assume that all the plant species are inaccessible by the controller except for species $\mathbf{X_1}$ and $\mathbf{X_L}$. Particularly, the controller "senses" the plant output species $\mathbf{X_L}$, then "processes" the sensed signal via the controller species $\mathbf{Z_1}$ and $\mathbf{Z_2}$, and finally "actuates" the plant input species $\mathbf{X_1}$. The controller species are allowed to react with each other and with the plant input/output species through K_c reaction channels labeled as $\mathcal{R}_c := \{\mathcal{R}_c^1, \mathcal{R}_c^2, \cdots, \mathcal{R}_c^{K_c}\}$. Let $\bar{S}_c \in \mathbb{Z}^{4\times K_c}$ and $\lambda_c : \mathbb{N}_0^4 \to (\mathbb{R}_*^+)^{K_c}$ denote the stoichiometry matrix and propensity function of the controller, respectively.

Since the controller reactions $\mathcal{R}_c$ involve the controller species $\mathbf{Z}$ and the plant input/output species $\mathbf{X_1}/\mathbf{X_L}$, the stoichiometry matrix $\bar{S}_c$ can be partitioned as

$$\bar{S}_c := \begin{bmatrix} S_1 \\ S_L \\ S_c \end{bmatrix},$$

where S_1 and $S_L \in \mathbb{Z}^{1\times K_c}$ encrypt the stoichiometry coefficients of the plant input and output species $\mathbf{X_1}$ and $\mathbf{X_L}$, respectively, among the controller reaction channels $\mathcal{R}_c$. Furthermore, $S_c \in \mathbb{Z}^{2\times K_c}$ encrypts the stoichiometry coefficients of the controller species $\mathbf{Z_1}$ and $\mathbf{Z_2}$. Hence, to design a controller network $\mathcal{N}_c$ for a particular plant, it is sufficient to specify S_1, S_L, S_c and λ_c.

Finally, the closed-loop system constitutes the open-loop network appended by the controller network so that it includes all the plant and controller species $\mathbf{X_{cl}} := \{\mathbf{X}, \mathbf{Z}\}$ and reactions $\mathcal{R}_{cl} := \{\mathcal{R}, \mathcal{R}_c\}$. Thus, the closed loop network, $\mathcal{N}_{cl} := \mathcal{N}_{ol} \cup \mathcal{N}_c$, can be fully represented by the closed-loop stoichiometry matrix S_{cl} and propensity function λ_{cl} shown in Figure 2. We close this section, by noting that although we restrict the controller to involve only two species communicating with two other species in the plant, this framework can be easily generalized to more species. The major flavor of this paper is to maintain the simplicity of the biomolecular controller design which motivates our restriction to only two controller species $\mathbf{Z_1}$ and $\mathbf{Z_2}$.

3 Antithetic Proportional-Integral Feedback (APIF) Controllers

Equipped with the BCRN framework for feedback control systems, we are now ready to propose several PI feedback controllers that are capable of achieving various performance objectives. All of the proposed controllers involve the antithetic integral motif introduced in [26] to ensure RPA. However, other additional motifs are appended to the antithetic motif to realize a proportional (P) control action.

3.1 Network Description

Consider the closed-loop network, depicted in Figure 3, where an arbitrary plant is connected in feedback with a class of controllers that we shall call APIF controllers. Observe that there are three different inhibition actions color coded as orange, purple and green. Each inhibition action gives rise to a single class of the proposed APIF controllers. Particularly, when no inhibition is present, we obtain the standalone AIF controller of [26] whose reactions are summarized in the first table of Figure 3. Whereas, APIF of Class 1 (resp. Class 2) involves the inhibition of $\mathbf{X_1}$ by $\mathbf{X_L}$ (resp. $\mathbf{Z_2}$), and APIF of Class 3 involves the inhibition of $\mathbf{Z_1}$ by $\mathbf{X_L}$. Furthermore, each APIF class encompasses various types of controllers depending on the inhibition mechanisms that enter the controller network as actuation reactions. We consider three types of biologically-relevant inhibition mechanisms.

- **Additive Inhibition**: In this mechanism, the inhibitor species produces the inhibited species separately at a decreasing hill-type rate. For instance, in the case of APIF Class 1 with additive inhibition (second row of the orange table in Figure 3), both $\mathbf{Z_1}$ and $\mathbf{X_L}$ produce $\mathbf{X_1}$ separately, but $\mathbf{Z_1}$ acts as an activator while $\mathbf{X_L}$ acts as a repressor. This separate inhibition can be captured by modeling the production of $\mathbf{X_1}$ (that is the positive actuation reaction $\mathcal{R}_a^+$) with an *additive* hill-type propensity given by $h^+(z_1, x_L) = kz_1 + \frac{\alpha}{1+(x_L/\kappa)^n}$, where n, α and κ denote the hill coefficient, maximal production rate and repression coefficient, respectively. The first term gives the integral (I) action, and the second term gives the proportional (P) action. In fact, this APIF is the closest control architecture to [33] and [35], since the P and I components are additive and separable (see Figure 1, Panels (C) and (D)).

- **Multiplicative Inhibition**: In this mechanism, the inhibitor *competes* with an activator over a production reaction. For instance, in the case of APIF Class 1 with multiplicative inhibition (third row of the orange table in Figure 3), $\mathbf{X_L}$ inhibits the production of $\mathbf{X_1}$ by $\mathbf{Z_1}$. This can be captured by modeling the production of $\mathbf{X_1}$ with a *multiplicative* hill-type propensity given by $h^+(z_1, x_L) = kz_1 \times \frac{1}{1+(x_L/\kappa)^n}$.

Observe that in this scenario, the proportional (P) and integral (I) control actions cannot be separated; instead, this actuation reaction $\mathcal{R}_a^+$ encodes both PI actions in one shot.

- **Degradation Inhibition**: In this mechanism, the inhibitor invokes a negative actuation reaction that degrades the inhibited species. For instance, in the case of APIF Class 1 with degradation inhibition (fourth row of the orange table in Figure 3), $\mathbf{Z_1}$ produces $\mathbf{X_1}$ (positive actuation reaction $\mathcal{R}_a^+$) and $\mathbf{X_L}$ degrades $\mathbf{X_1}$ (negative actuation reaction $\mathcal{R}_a^-$). For generality, if the degradation is assumed to be n-cooperative, the dynamics can be captured by using a positive actuation with propensity $h^+(z_1) = kz_1$ and a negative actuation with propensity $h^-(x_1, x_L) = \delta x_1 x_L^n$. Hence the overall actuation propensity is defined as $h(z_1, x_1, x_L) := h^+(z_1) - h^-(x_1, x_L)$.

Considering all three APIF classes with the various inhibition mechanisms, Figure 3 proposes eight different APIF control architectures. Note that, it can be shown that a degradation inhibition in the case of APIF Class 3 would destroy the RPA property and is thus omitted. All of these controllers are compactly represented by one general closed loop stoichiometry matrix S_{cl} and propensity function λ_{cl} shown in Figure 3. The various architectures can be easily obtained by properly selecting the functions $h := h^+ - h^-$ and g from the tables of Figure 3. We shall call the function h (resp. g) as the actuation (resp. reference) propensity for reasons that will be apparent in the subsequent section. In fact, the theoretical analysis that is carried out in the rest of the section applies for any function h that is smooth and monotonically increasing (resp. decreasing) in z_1 (resp. z_2, x_1 and x_L), and any function g that is smooth and monotonically increasing (resp. decreasing) in μ (resp. x_L).

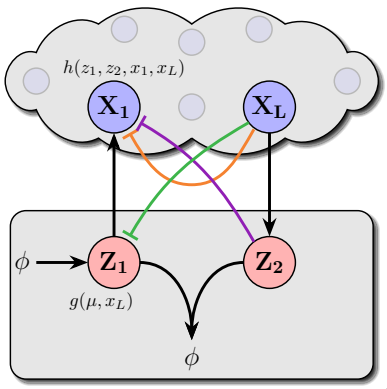

$$S_{cl} = \begin{array}{c} \begin{array}{cccccccc} \mathcal{R}^1 & \mathcal{R}^2 & \cdots & \mathcal{R}^K & \mathcal{R}_s & \mathcal{R}_q & \mathcal{R}_r & \mathcal{R}_a^+ & \mathcal{R}_a^- \end{array} \\ \left[\begin{array}{cccc|ccccc} & & & & 0 & 0 & 0 & 1 & -1 \\ & & & & & & & & \\ & S & & & & 0 & & & \\ & & & & & & & & \\ & & & & 0 & 0 & 0 & 0 & 0 \\ \hline & & & & 0 & -1 & 1 & 0 & 0 \\ & 0 & & & 1 & -1 & 0 & 0 & 0 \end{array}\right] \end{array} \begin{array}{l} \mathbf{X}_1 \\ \mathbf{X}_2 \\ \vdots \\ \mathbf{X}_{L-1} \\ \mathbf{X}_L \\ \mathbf{Z}_1 \\ \mathbf{Z}_2 \end{array} \begin{array}{l} \left.\begin{array}{l} \\ \\ \\ \\ \\ \end{array}\right\} \mathbf{X} \\ \left.\begin{array}{l} \\ \end{array}\right\} \mathbf{Z} \end{array}$$

$$\lambda_{cl}(x, z) = \left[\begin{array}{cccc|ccccc} \mathcal{R}^1 & \mathcal{R}^2 & \cdots & \mathcal{R}^K & \mathcal{R}_s & \mathcal{R}_q & \mathcal{R}_r & \mathcal{R}_a^+ & \mathcal{R}_a^- \\ & \lambda(x) & & & \theta x_L & \eta z_1 z_2 & g(\mu, x_L) & h^+(z_1, z_2, x_L) & h^-(z_2, x_1, x_L) \end{array}\right]^T$$

Actuation Propensity: $h(z_1, z_2, x_1, x_L) := h^+(z_1, z_2, x_L) - h^-(z_2, x_1, x_L)$

AIF	Reference Rxn: $\mathcal{R}_r$	Actuation Rxn: $\mathcal{R}_a$	Sensing Rxn: $\mathcal{R}_s$	Sequestration Rxn: $\mathcal{R}_q$	$h(z_1, z_2, x_1, x_L)$	$g(\mu, x_L)$
	$\phi \xrightarrow{\mu} \mathbf{Z_1}$	$\mathbf{Z_1} \xrightarrow{k} \mathbf{Z_1} + \mathbf{X_1}$	$\mathbf{X_L} \xrightarrow{\theta} \mathbf{X_L} + \mathbf{Z_2}$	$\mathbf{Z_1} + \mathbf{Z_2} \xrightarrow{\eta} \phi$	kz_1	μ

APIF Class 1	Inhibition Type	Actuation Rxns	Actuation Propensity h
	Additive	$\mathcal{R}_a^+ : \ \phi \longrightarrow \mathbf{X_1}$	$kz_1 + \frac{\alpha}{1+(x_L/\kappa)^n}$
	Multiplicative	$\mathcal{R}_a^+ : \ \phi \longrightarrow \mathbf{X_1}$	$\frac{kz_1}{1+(x_L/\kappa)^n}$
	Degradation	$\mathcal{R}_a^+ : \ \mathbf{Z_1} \longrightarrow \mathbf{Z_1} + \mathbf{X_1}$ $\mathcal{R}_a^- : \ \mathbf{X_1} + \mathbf{X_L} \longrightarrow \mathbf{X_L}$	$kz_1 - \delta x_1 x_L^n$

APIF Class 2	Inhibition Type	Actuation Rxns	Actuation Propensity h
	Additive	$\mathcal{R}_a^+ : \ \phi \longrightarrow \mathbf{X_1}$	$kz_1 + \frac{\alpha}{1+(z_2/\kappa)^n}$
	Multiplicative	$\mathcal{R}_a^+ : \ \phi \longrightarrow \mathbf{X_1}$	$\frac{kz_1}{1+(z_2/\kappa)^n}$
	Degradation	$\mathcal{R}_a^+ : \ \mathbf{Z_1} \longrightarrow \mathbf{Z_1} + \mathbf{X_1}$ $\mathcal{R}_a^- : \ \mathbf{X_1} + \mathbf{Z_2} \longrightarrow \mathbf{Z_2}$	$kz_1 - \delta x_1 z_2^n$

APIF Class 3	Inhibition Type	Reference Rxn	Reference Propensity g
	Additive	$\phi \xrightarrow{g(\mu, x_L)} \mathbf{Z_1}$	$\mu + \frac{\alpha}{1+(x_L/\kappa)^n}$
	Multiplicative	$\phi \xrightarrow{g(\mu, x_L)} \mathbf{Z_1}$	$\frac{\mu}{1+(x_L/\kappa)^n}$

Figure 3: **Antithetic Proportional-Integral Feedback (APIF) Controllers.** Three different classes of Proportional-Integral controllers are proposed by appending the standalone antithetic integral feedback (AIF) controller with three (color-coded) inhibitions. Different biologically-relevant inhibition mechanisms are described in the tables for each class. The inhibition mechanisms include additive repression, competitive inhibition (multiplicative) and degradation. All eight controllers are compactly represented by the closed-loop stoichiometry matrix S_{cl} and propensity function λ_{cl} by choosing the suitable actuation propensity function h from the tables.

3.2 Deterministic Steady-State Analysis: Robust Perfect Adaptation

The deterministic dynamics of the closed loop systems, for all the APIF controllers given in Figure 3 can be compactly written as a set of *Ordinary Differential Equations* (ODEs) given by

$$\begin{cases} \dot{x} = f(x) + h(z_1, z_2, x_1, x_L)e_1 \\ \dot{z}_1 = g(\mu, x_L) - \eta z_1 z_2 \\ \dot{z}_2 = \theta x_L - \eta z_1 z_2, \end{cases} \tag{2}$$

where $f(x) := S\lambda(x)$ and $e_1 := \begin{bmatrix} 1 & 0 & \cdots & 0 \end{bmatrix}^T \in \mathbb{R}^L$. Note that the actuation and reference propensities h and g take different forms for different APIF control architectures as depicted in Figure 3. The fixed point of the closed loop dynamics cannot be calculated explicitly for a general plant; however, the output component (x_L) of the fixed point solves the following algebraic equation

$$g(\mu, \bar{x}_L) = \theta \bar{x}_L, \tag{3}$$

where over-bars denote steady-state values, that is $\bar{x}_L := \lim_{t\to\infty} x_L(t)$. Two observations can be made based on (3). The first observation is that (3) has a unique nonnegative solution since g is a monotonically non-increasing function in x_L. The second observation is that (3) does not depend on the plant. As a result, if the closed loop system is stable (i.e. the dynamics converge to a fixed point), then the output concentration converges to a unique set-point that is independent of the plant. This property is valid for any initial condition, and is referred to as *Robust Perfect Adaptation* (RPA). Particularly, for the AIF and APIF of Class 1 and 2, the reference propensity is $g(\mu, x_L) = \mu$, and thus $\bar{x}_L = \frac{\mu}{\theta}$. Furthermore, for the APIF of Class 3, $\bar{x}_L$ solves a polynomial equation of degree $n+1$ given by

$$\begin{aligned} &\text{Additive Inhibition:} && \bar{x}_L^{n+1} - \frac{\mu}{\theta}\bar{x}_L^n + \kappa^n \bar{x}_L - \kappa^n \frac{\mu+\alpha}{\theta} = 0 \\ &\text{Multiplicative Inhibition:} && \bar{x}_L^{n+1} + \kappa^n \bar{x}_L - \kappa^n \frac{\mu}{\theta} = 0. \end{aligned} \tag{4}$$

For example, for a hill coefficient $n = 1$, the unique non-negative steady state (assuming closed-loop stability) of the output concentration is given by

$$\begin{aligned} &\text{Additive Inhibition:} && \bar{x}_L = \frac{\frac{\mu}{\theta} - \kappa + \sqrt{\left(\kappa + \frac{\mu}{\theta}\right)^2 + 4\kappa\frac{\mu}{\theta}}}{2} \\ &\text{Multiplicative Inhibition:} && \bar{x}_L = \frac{\kappa}{2}\left(\sqrt{1 + \frac{4}{\kappa}\frac{\mu}{\theta}} - 1\right). \end{aligned} \tag{5}$$

Clearly, $\bar{x}_L$ depends only on controller parameters μ, θ, and κ, and is thus robust to constant disturbances in plant parameters. In conclusion, all the proposed APIF controllers maintain the RPA property that is obtained by the antithetic integral motif (assuming closed-loop stability), while additional control knobs are introduces to enhance other performance objectives.

3.3 Verification of the Control Structure via Linear Perturbation Analysis

In this section, we verify analytically that all the proposed APIF controllers indeed involve Proportional (P) and Integral (I) control actions. To do that, a linear perturbation analysis is carried out where we examine the linearized dynamics around the fixed point. Let $\begin{bmatrix} \tilde{x}^T & \tilde{z}_1 & \tilde{z}_2 \end{bmatrix}^T$ denote the perturbation from the fixed point $\begin{bmatrix} \bar{x}^T & \bar{z}_1 & \bar{z}_2 \end{bmatrix}^T$ of (2). To carry out a linear perturbation analysis we assume that the reference signal μ is allowed to slightly vary in time around a nominal constant reference $\bar{\mu}$. That is, we have

$$\tilde{x}(t) = x(t) - \bar{x}; \quad \tilde{z}_1(t) = z_1(t) - \bar{z}_1; \quad \tilde{z}_2(t) = z_2(t) - \bar{z}_2; \quad \tilde{\mu}(t) = \mu(t) - \bar{\mu}.$$

The linearized dynamics can thus be written as

$$\begin{aligned} \dot{\tilde{x}} &= A\tilde{x} + (\sigma_1 \tilde{z}_1 - \sigma_2 \tilde{z}_2 - \sigma_3 \tilde{x}_1 - \sigma_4 \tilde{x}_L)\, e_1 \\ \dot{\tilde{z}}_1 &= \sigma_5 \tilde{\mu} - \sigma_6 \tilde{x}_L - \eta \bar{z}_2 \tilde{z}_1 - \eta \bar{z}_1 \tilde{z}_2 \\ \dot{\tilde{z}}_2 &= \theta \tilde{x}_L - \eta \bar{z}_2 \tilde{z}_1 - \eta \bar{z}_1 \tilde{z}_2, \end{aligned}$$

where $A := \partial f(\bar{x})$, $\partial h(\bar{z}_1, \bar{z}_2, \bar{x}_1, \bar{x}_L) =: \begin{bmatrix} \sigma_1 & -\sigma_2 & -\sigma_3 & -\sigma_4 \end{bmatrix}$, and $\partial g(\bar{\mu}, \bar{x}_L) =: \begin{bmatrix} \sigma_5 & -\sigma_6 \end{bmatrix}$, such that $\sigma_1, \sigma_5 > 0$ and $\sigma_2, \sigma_3, \sigma_4, \sigma_6 \geq 0$.

The underlying control structure is most easily uncovered and visualized by drawing the block diagram of the linearized dynamics (refer to Box 1: A Primer on Block Diagrams). Taking the Laplace transforms yields

$$\begin{aligned}
\tilde{x}_L(s) &= e_L^T \left(sI - \bar{A}\right)^{-1} e_1 \tilde{u}(s); \qquad \text{where} \quad \bar{A} := A - \sigma_3 e_1 e_1^T \\
\tilde{u}(s) &= \sigma_1 \tilde{z}_1(s) - \sigma_2 \tilde{z}_2(s) - \sigma_4 \tilde{x}_L(s) \\
\tilde{z}_1(s) &= \frac{\sigma_5 \tilde{\mu}(s) - \sigma_6 \tilde{x}_L(s) - \eta \bar{z}_1 \tilde{z}_2(s)}{s + \eta \bar{z}_2} \\
\tilde{z}_2(s) &= \frac{\theta \tilde{x}_L(s) - \eta \bar{z}_2 \tilde{z}_1(s)}{s + \eta \bar{z}_1}.
\end{aligned}$$

Next, we express $\tilde{z}_1(s)$ and $\tilde{z}_2(s)$ in terms of $\tilde{\mu}(s), \tilde{x}_L(s)$ and the error defined as $\tilde{e}(s) := \tilde{\mu}(s) - \left(\frac{\theta+\sigma_6}{\sigma_5}\right) \tilde{x}_L(s)$. We have

$$\begin{aligned}
\tilde{z}_1(s) &= \left[\sigma_5 \tilde{\mu}(s) - \sigma_6 \tilde{x}_L(s) + \frac{\eta \bar{z}_1 \sigma_5}{s} \tilde{e}(s)\right] \frac{1}{s + \eta\left(\bar{z}_1 + \bar{z}_2\right)} \\
\tilde{z}_2(s) &= \left[\theta \tilde{x}_L(s) - \frac{\eta \bar{z}_2 \sigma_5}{s} \tilde{e}(s)\right] \frac{1}{s + \eta\left(\bar{z}_1 + \bar{z}_2\right)}.
\end{aligned}$$

Substituting for $\tilde{z}_1(s)$ and $\tilde{z}_2(s)$ in $\tilde{u}(s)$ and collecting similar terms yield

$$\tilde{u}(s) = \left[\sigma_1 \tilde{\mu}(s) + \frac{\eta\left(\sigma_1 \bar{z}_1 + \sigma_2 \bar{z}_2\right)}{s} \tilde{e}(s) - \frac{\sigma_2 \theta + \sigma_1 \sigma_6}{\sigma_5} \tilde{x}_L(s)\right] \frac{\sigma_5}{s + \eta\left(\bar{z}_1 + \bar{z}_2\right)} - \sigma_4 \tilde{x}_L(s).$$

This is the controller transfer function that relates the control action $\tilde{u}$ to the reference signal $\tilde{\mu}$, the error signal $\tilde{e}$ and the plant output $\tilde{x}_L$ in the Laplace domain. Therefore, equipped with the controller and plant transfer functions given by

$$\begin{aligned}
&\textbf{Controller:} \quad \tilde{u}(s) = \left[K_F \tilde{\mu}(s) + \frac{K_I}{s} \tilde{e}(s) - K_{P_2} \tilde{x}_L(s)\right] \frac{\omega_c}{s + \omega_c} - K_{P_1} \tilde{x}_L(s) \\
&\textbf{Plant:} \quad \tilde{x}_L(s) = P(s) \tilde{u}(s); \\
&\text{where:} \quad \begin{cases} K_F = \dfrac{\sigma_1 \sigma_5}{\eta(\bar{z}_1 + \bar{z}_2)}, \quad K_I = \sigma_5 \dfrac{\sigma_1 \bar{z}_1 + \sigma_2 \bar{z}_2}{\bar{z}_1 + \bar{z}_2}, \quad K_S = \dfrac{\theta + \sigma_6}{\sigma_5}, \qquad K_{P_1} = \sigma_4, \\ K_{P_2} = \dfrac{\sigma_2 \theta + \sigma_1 \sigma_6}{\eta(\bar{z}_1 + \bar{z}_2)}, \quad \omega_c = \eta(\bar{z}_1 + \bar{z}_2), \qquad P(s) = e_L^T \left(sI - \bar{A}\right)^{-1} e_1, \end{cases}
\end{aligned} \tag{6}$$

we can now draw the block diagram shown in Figure 4 which compactly encompasses all of the proposed APIF architectures. In particular, for the standalone AIF controller, both proportional gains K_{P_1} and K_{P_2} are set to zero. For the APIF controller of Class 1 (resp. Class 2 & 3), the proportional gain K_{P_2} (resp. K_{P_1}) is set to zero. The remaining gains K_I, K_F, and K_S are obtained by calculating the $\sigma_i s$ for the various APIF controllers (Appendix A), and the results are shown the table of Figure 4. Observe that, for all the proposed architectures, there is an Integral (I) and a Proportional (P) control action. In fact, since the controller acts on both the error signal $\tilde{e}$ and the output signal $\tilde{x}_L$, then the PI architecture (of the linearized dynamics) resembles the setting given in Panel D of Figure 1. The main differences are two additional blocks:

- **Feedforward Block:** This block is a consequence of the positivity of the nonlinear dynamics. The reference signal $\tilde{\mu}$ "lifts" the dynamics towards the positive orthant, by adding the feedforward term to the integrated error.
- **Low Pass Filter:** This block is a dynamical system that filters fast signals with frequencies higher than the cutoff frequency $\omega_c = \eta(\bar{z}_1 + \bar{z}_2)$. This block is a consequence of the time dynamics of the nonlinear sequestration reaction.

As demonstrated in Figure 4, for the APIF controllers of Class 1 ($K_{P_1} > 0, K_{P_2} = 0$), the Proportional control action $K_{P_1} \tilde{x}_L$ is instantaneous since it is fed back to the plant as is and without any filtering (that involves time dynamics). In contrast, for the APIF controllers of Class 2 and 3 ($K_{P_1} = 0, K_{P_2} > 0$), the Proportional control action $K_{P_2} \tilde{x}_L$ is not instantaneous since it is passed through a low pass filter before it is fed back to the plant. This low pass filtering step arises because the output species does not actuate the input species immediately like the APIF controllers of Class 1; instead, the output actuates the input via an intermediate controller species: $\mathbf{Z_2}$ (for Class 2) and $\mathbf{Z_1}$ (for Class 3). This low pass filter typically delays the Proportional control action, and as a result – depending on the performance objective and particular plant at hand – it can have a negative or positive effect on the closed loop dynamics.

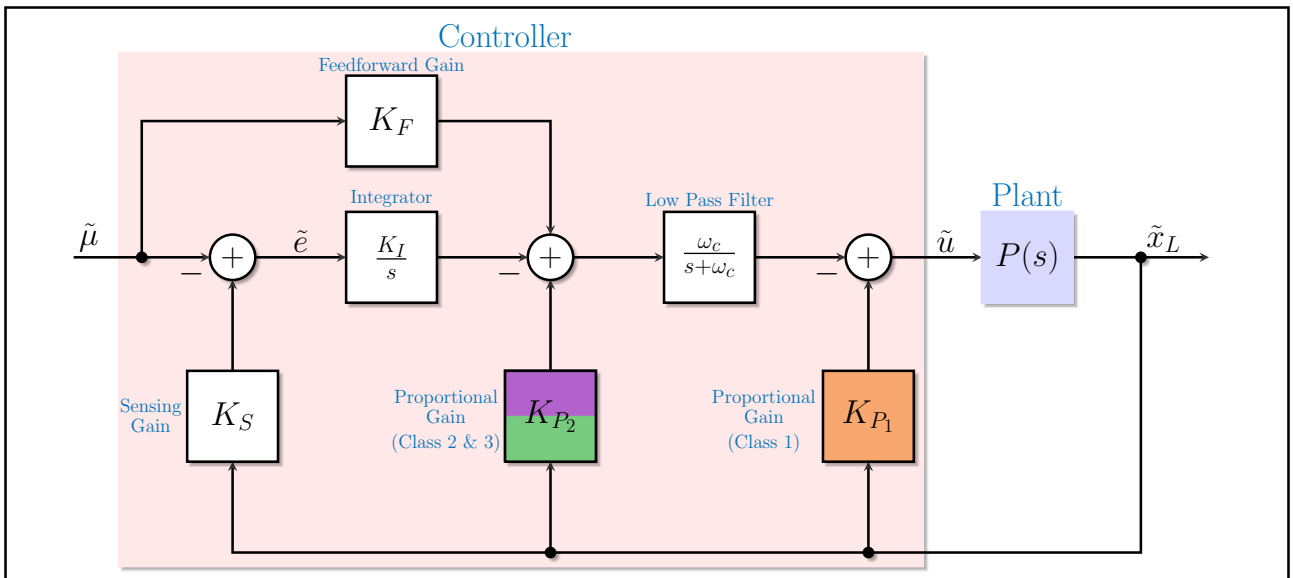

Class	Inhibition	K_I	K_S	K_{P_1}	K_{P_2}	K_F
AIF	None	$k\frac{\bar{z}_1}{\bar{z}_1+\bar{z}_2}$	θ	0	0	$\frac{k}{\eta(\bar{z}_1+\bar{z}_2)}$
APIF Class 1	Additive	$k\frac{\bar{z}_1}{\bar{z}_1+\bar{z}_2}$	θ	$\frac{\alpha}{\kappa}\frac{n(\bar{x}_L/\kappa)^{n-1}}{[1+(\bar{x}_L/\kappa)^n]^2}$	0	$\frac{k}{\eta(\bar{z}_1+\bar{z}_2)}$
	Multiplicative	$\frac{k}{1+(\bar{x}_L/\kappa)^n}\frac{\bar{z}_1}{\bar{z}_1+\bar{z}_2}$	θ	$\frac{k\bar{z}_1}{\kappa}\frac{n(\bar{x}_L/\kappa)^{n-1}}{[1+(\bar{x}_L/\kappa)^n]^2}$	0	$\frac{1}{1+(\bar{x}_L/\kappa)^n}\frac{k}{\eta(\bar{z}_1+\bar{z}_2)}$
	Degradation	$k\frac{\bar{z}_1}{\bar{z}_1+\bar{z}_2}$	θ	$n\delta\bar{x}_1\bar{x}_L^{n-1}$	0	$\frac{k}{\eta(\bar{z}_1+\bar{z}_2)}$
APIF Class 2	Additive	$\left(k\bar{z}_1+\alpha\frac{(\bar{z}_2/\kappa)^n}{(1+(\bar{z}_2/\kappa)^n)^2}\right)\frac{1}{\bar{z}_1+\bar{z}_2}$	θ	0	$\frac{\alpha\theta}{\kappa\eta(\bar{z}_1+\bar{z}_2)}\frac{n(\bar{z}_2/\kappa)^{n-1}}{[1+(\bar{z}_2/\kappa)^n]^2}$	$\frac{k}{\eta(\bar{z}_1+\bar{z}_2)}$
	Multiplicative	$k\frac{\bar{z}_1}{\bar{z}_1+\bar{z}_2}\frac{1+(n+1)(\bar{z}_2/\kappa)^n}{[1+(\bar{z}_2/\kappa)^n]^2}$	θ	0	$k\frac{\bar{z}_1}{\bar{z}_1+\bar{z}_2}\frac{\theta}{\kappa\eta}\frac{n(\bar{z}_2/\kappa)^{n-1}}{[1+(\bar{z}_2/\kappa)^n]^2}$	$\frac{1}{1+(\bar{z}_2/\kappa)^n}\frac{k}{\eta(\bar{z}_1+\bar{z}_2)}$
	Degradation	$\frac{k\bar{z}_1+n\delta\bar{x}_1\bar{z}_2^n}{\bar{z}_1+\bar{z}_2}$	θ	0	$\frac{n\delta\theta\bar{x}_1\bar{z}_2^{n-1}}{\eta(\bar{z}_1+\bar{z}_2)}$	$\frac{k}{\eta(\bar{z}_1+\bar{z}_2)}$
APIF Class 3	Additive	$k\frac{\bar{z}_1}{\bar{z}_1+\bar{z}_2}$	$\theta+\frac{\alpha}{\kappa}\frac{n(\bar{x}_L/\kappa)^{n-1}}{[1+(\bar{x}_L/\kappa)^n]^2}$	0	$\frac{k\alpha}{\kappa\eta(\bar{z}_1+\bar{z}_2)}\frac{n(\bar{x}_L/\kappa)^{n-1}}{[1+(\bar{x}_L/\kappa)^n]^2}$	$\frac{k}{\eta(\bar{z}_1+\bar{z}_2)}$
	Multiplicative	$\frac{k}{1+(\bar{x}_L/\kappa)^n}\frac{\bar{z}_1}{\bar{z}_1+\bar{z}_2}$	$\theta\left[1+(\bar{x}_L/\kappa)^n\right]+\bar{\mu}/\kappa\frac{n(\bar{x}_L/\kappa)^{n-1}}{[1+(\bar{x}_L/\kappa)^n]^2}$	0	$\frac{k\bar{\mu}}{\kappa\eta(\bar{z}_1+\bar{z}_2)}\frac{n(\bar{x}_L/\kappa)^{n-1}}{[1+(\bar{x}_L/\kappa)^n]^2}$	$\frac{1}{1+(\bar{x}_L/\kappa)^n}\frac{k}{\eta(\bar{z}_1+\bar{z}_2)}$

Figure 4: **Block Diagram of the APIF controllers.** This block diagram compactly represents the dynamics (in the Laplace domain) of the linearized closed-loop systems obtained by all the APIF controllers proposed in Figure 3 . Particularly, APIF controllers of Class 1 (resp. 2 and 3) give rise to the proportional gain K_{P_1} (resp. K_{P_2}). The low pass filter in between demonstrates the instantaneous (resp. filtered) proportional control action of the APIF controllers of Class 1 (resp. 2 and 3). The table shows the PI gains as a function of the various biological parameters.

Note that, if the sequestration reaction is fast enough (η is large), the effects of the feedforward block and low pass filter become negligible. This can be observed by examining the asymptotic limit, as $\eta \to \infty$, that yields

$$\lim_{\eta\to\infty} K_F = 0 \qquad \text{and} \qquad \lim_{\eta\to\infty}\left|\frac{\omega_c}{s+\omega_c}\right| = 1.$$

Consequently, as $\eta \to \infty$, the PI architecture of the linearized dynamics becomes exactly the same as that given in Panel D of Figure 1.

Lastly, observe in the table of Figure 4 that the various PID gains may depend mutually on the same controller parameters. As an example, for Class 1 with multiplicative inhibition, the controller parameter κ can tune both the proportional gain K_{P_1} and the integral gain K_I simultaneously. This is a consequence of the inseparability of the original nonlinear PID architecture. In contrast, for Class 1 with additive inhibition, the controller parameter α can tune the proportional gain K_{P_1} only. We will show next, that this simultaneous tuning of the PID gains, with a single controller parameter, may yield better stability properties and performance.

3.4 Deterministic Stability Analysis & Performance Assessment

To compare the stability properties of the various proposed APIF controllers, we consider a particular plant, depicted in Panel A of Figure 5, that is comprised of two species $\mathbf{X_1}$ and $\mathbf{X_2}$ (that is, $L = 2$). This plant may represent a gene expression network where $\mathbf{X_1}$ is the mRNA that is translated to a protein $\mathbf{X_2}$ at a rate k_1. The degradation rates of $\mathbf{X_1}$ and $\mathbf{X_2}$ are denoted by γ_1 and γ_2, respectively. The closed-loop stoichiometry

matrix and propensity function are also shown in Panel A. Using the Routh-Hurwitz stability criterion, one can establish the exact conditions of (linear) stability of the fixed point (Equation (13) in Appendix A) for the various proposed APIF controllers. These conditions, once satisfied, guarantee that the dynamics converge to the fixed point when the trajectory is in the basin of attraction.

For the remainder of this section, we consider fast sequestration reactions, that is η is large. Under this assumption, one can obtain simpler stability conditions that are calculated in Appendix A, and tabulated in Panel B of Figure 5. The stability conditions are given as inequalities that has to be satisfied by the various parameters of the closed-loop systems. A particularly significant lumped parameter is $\rho := \frac{kk_1\theta}{\gamma_1\gamma_2(\gamma_1+\gamma_2)}$ that depends only on the plant and standalone AIF controller parameters.

To study the stabilizing effect of the appended proportional (P) component, we fix all the parameters related to the plant and standalone AIF controller (hence ρ is fixed), and investigate the effect of the other controller parameters related to the appended proportional component. By examining the table in Panel B, one can see that, compared to the standalone AIF, the APIF controller of Class 1 with multiplicative (resp. degradation) inhibition enhances stability regardless of the exact values of κ (resp. δ) and n. This gives rise to a structural stability property: adding these types of proportional components guarantees better stability without having to fine-tune parameters.

In contrast, although the APIF controller of Class 1 with additive inhibition may enhance stability, special care has to be taken when tuning α. In fact, if α is tuned to be larger than a threshold given by $\frac{\gamma_1\gamma_2}{k_1}r\left[1+(r/\kappa)^n\right]$, then stability is lost. Panel C of Figure 5 elaborates more on this type of APIF controller. Three cases arise here. Firstly, if $\rho < 1$, that is the standalone AIF already stabilizes the closed-loop dynamics, then the (α, κ)-parameter space is split into a stable and unstable region. In the latter (α is larger than the threshold), z_2 grows to infinity, and the output x_2 never reaches the desired set point $r = \mu/\theta$. Secondly, if $1 < \rho < 2$, that is the standalone AIF is unstable, then the (α, κ)-parameter space is split into three regions: (1) a stable region, (2) an unstable region with divergent response similar to the previous scenario where $\rho < 1$, and (3) another unstable region where persistent oscillations emerge as depicted in the bottom plot of Panel C. Note that the closer ρ is to 2, the narrower the stability region is. Thirdly, for $\rho > 2$, the stable region disappears and thus this APIF controller has no hope of stabilizing the dynamics without re-tuning the parameters related to the standalone AIF controller (e.g. k and/or θ). Clearly, multiplicative and degradation inhibitions outperform additive inhibition if stability is a critical objective. To this end, Panel D of Figure 5 shows how the settling time and overshoot can be tuned by the controller parameters α, κ, and δ for additive, multiplicative, and degradation inhibitions, respectively. It is shown that with multiplicative and degradation inhibition, one can simultaneously suppress oscillations (settling time) and remove overshoots. In contrast, a proportional component with additive inhibition can suppress oscillations but is not capable of removing overshoots as illustrated in the simulations of Panel D to the right. Furthermore, one can lose stability if α is increased above a threshold as mentioned earlier. Nevertheless, for multiplicative and degradation inhibitions, increasing the controller parameters (κ^{-1}, δ) too much can make the response slower but can never destroy stability.

The other two classes (2 and 3) are shown to be undesirable in enhancing stability. Observe that for Class 2, the stability conditions are the same as the standalone AIF controller (in the limit as $\eta \to \infty$) with an exception in the case of additive inhibition when $\alpha > \frac{\gamma_1\gamma_2}{k_1}r$. Note that, in the latter, the inequality is structurally very different from all other stability conditions. In fact, in this case, the actuation via $\mathbf{Z_2}$ dominates $\mathbf{Z_1}$, and hence $\mathbf{Z_2}$ becomes responsible of the Integral (I) action. The detailed analysis of this network is not within the scope of this paper, and is left for future work. Finally, APIF controllers of Class 3 deteriorates the stability margin, since the right hand side of the inequalities are strictly less than one. However, this class of controllers can be useful for slow plants if the objective is to speed up the response.

3.5 Stochastic Analysis: RPA & Stationary Variance

We now investigate the effect of the APIF controllers on the stationary (steady-state) behavior of the output species $\mathbf{X_L}$ in the stochastic setting. Particularly, we examine the stationary expectation $\mathbb{E}_\pi\left[X_L\right]$ and variance $\mathrm{Var}_\pi\left[X_L\right]$. The evolution of the expectations of the various species in the closed-loop network of Figure 3 are simply given by the differential equation $\frac{d}{dt}\mathbb{E}\left[X_{cl}\right] = \mathbb{E}\left[S_{cl}\lambda_{cl}\left(X_{cl}\right)\right]$. By substituting for the closed-loop stoichiometry matrix S_{cl} and propensity function λ_{cl} given in Figure 3, we obtain the following set of differential equations that describe the evolution of the expectations for an arbitraty plant

$$\begin{cases} \dfrac{d}{dt}\mathbb{E}\left[X\right] = \mathbb{E}\left[S\lambda(X)\right] + \mathbb{E}\left[h(z_1, z_2, x_1, x_L)\right] \\ \dfrac{d}{dt}\mathbb{E}\left[Z_1\right] = \mathbb{E}\left[g(\mu, X_L)\right] - \eta\mathbb{E}\left[Z_1 Z_2\right] \\ \dfrac{d}{dt}\mathbb{E}\left[Z_2\right] = \theta\mathbb{E}\left[X_L\right] - \eta\mathbb{E}\left[Z_1 Z_2\right]. \end{cases} \tag{7}$$

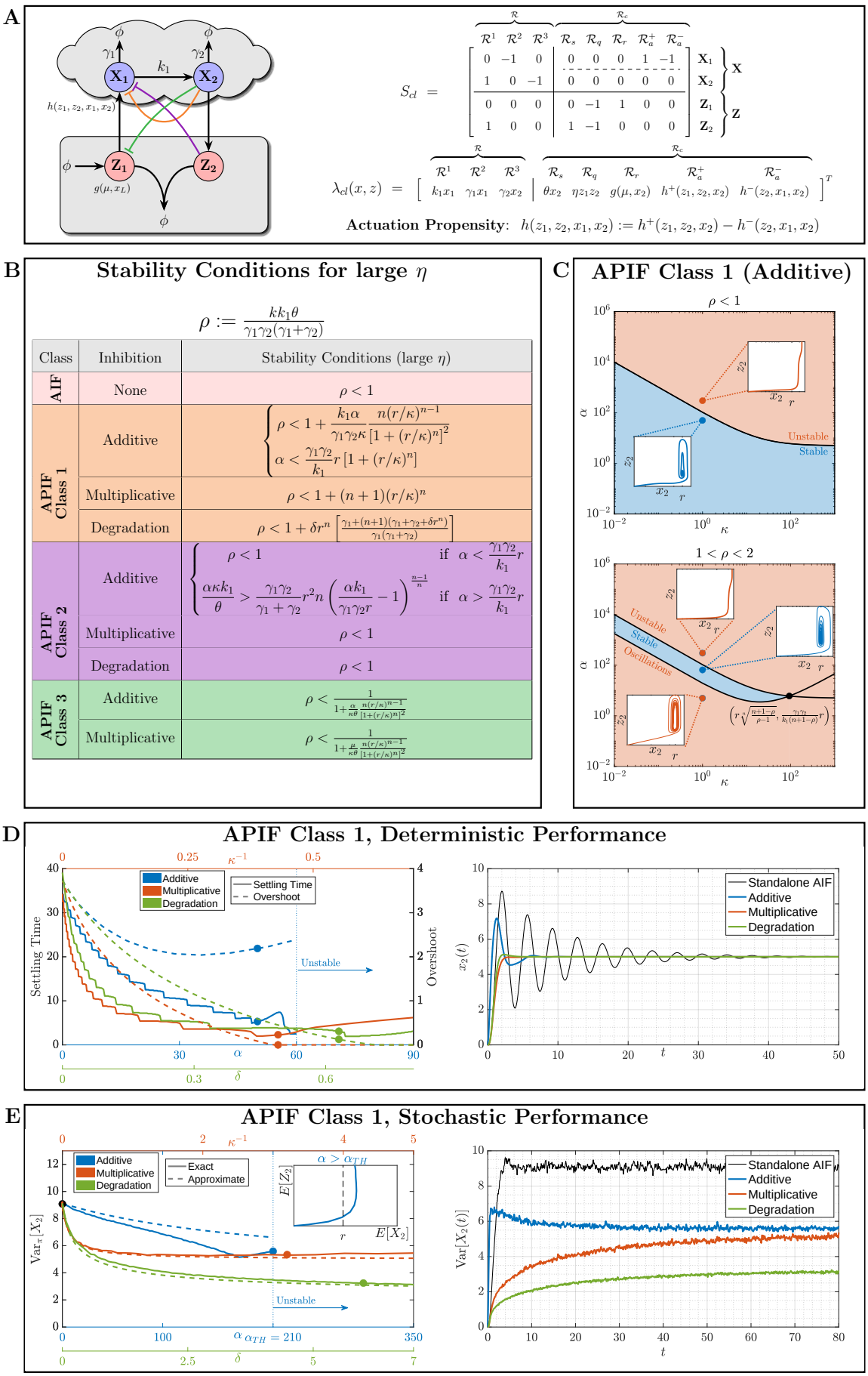

Figure 5: See caption next page.

Figure 5: **Performance of APIF Controllers.** **(A)** Gene Expression Network Controlled by APIF Controllers. **(B)** Inequalities that need to be respected by the various controllers (when η is large enough) to guarantee closed-loop stability in the deterministic setting. Multiplicative and degradation inhibition mechanisms exhibit superior stability properties. **(C)** APIF controllers of class 1 with an additive inhibition mechanism, exhibit different stability properties for different ranges of the parameter group ρ (that depends solely on the plant and the standalone AIF controller). In particular, for $\rho < 2$, proportional action can stabilize the dynamics, while for $\rho > 2$, the proportional action cannot stabilize the dynamics without re-tuning the integral action. **(D)** Settling time and overshoot for the output (X_2) response as a function of controller parameters that are relevant to the appended proportional components. Multiplicative and degradation inhibition mechanisms are capable of ameliorating the performance without risking instability as opposed to the additive inhibition mechanism. **(E)** The degradation mechanism exhibits superior stationary variance reduction. This is illustrated theoretically (see Table 1) and via simulations.

At stationarity, assuming that the closed-loop network is ergodic, the time derivatives are set to zero. Particularly, we have

$$\frac{d}{dt}\left(\mathbb{E}_\pi\left[Z_1\right]-\mathbb{E}_\pi\left[Z_2\right]\right)=0 \qquad \Longrightarrow \qquad \mathbb{E}_\pi\left[g(\mu,X_L)\right]=\theta\mathbb{E}_\pi\left[X_L\right].$$

To achieve RPA at the population level (i.e. expectations), the stationary expectation $\mathbb{E}_\pi\left[X_L\right]$ of the output species should not depend on the plant parameters. Clearly, this depends on the function g. In fact, if g is nonlinear in X_L, then there is no guarantee that RPA is achieved because the nonlinearity couples higher order moments (that may depend on the plant parameters) with $\mathbb{E}_\pi\left[X_L\right]$. As a result, RPA is not guaranteed for the APIF controllers of Class 3 in the stochastic setting, although it is guaranteed in the deterministic setting. Nonetheless if g is affine in X_L, then RPA is guaranteed (once again, assuming ergodicity). In particular, for the APIF controllers of Class 1 and 2, we have $g(\mu,X_L)=\mu$ and as a result $\mathbb{E}_\pi\left[X_L\right]=\mu/\theta$. Clearly, for these class of controllers, $\mathbb{E}_\pi\left[X_L\right]$ depends only on the control parameters μ and θ (like the deterministic setting), and thus RPA is ensured as long as the closed-loop network is ergodic.

Next, we examine the variance of the output species $\mathbf{X_L}$. Unfortunately, a general analysis for an arbitrary plant cannot be done. As a case study, we consider again the particular plant given in Panel A of Figure 5 in feedback with the APIF controller of Class 1. Even for this particular plant, one cannot derive an exact expression for $\mathrm{Var}_\pi\left[X_2\right]$. This is a consequence of the moment closure problem that stems from the inherent nonlinear nature of the antithetic motif (quadratic propensity: $\eta z_1 z_2$), and the proportional actuation (fractional propensity: $h(z_1,z_2,x_1,x_2)$). However, a tailored moment closure technique was proposed in [33] to give an approximate expression for $\mathrm{Var}_\pi\left[X_2\right]$ in the case of the APIF controller of Class 1 with additive inhibition and $n=\kappa=1$. This approximate technique exploits the fact that $\mathbb{E}_\pi\left[Z_1Z_2\right]=\mu/\eta\approx 0$ for large η; and as a result assumes that Z_2 remains close to zero. Furthermore, a linearized approximation of the function h is also exploited to circumvent the moment closure problem (see Appendix C for more details). Applying this approximate technique to our more general controllers allows us to give a general (approximate) expression for $\mathrm{Var}_\pi\left[X_2\right]$ that encompasses all three types of inhibitions with an arbitrary hill coefficient $n\geq 1$. The results are summarized in Table 1, where a general formula is given for any choice of h. Recall that

$$h(z_1,x_1,x_2):=h^+(z_1,x_2)-h^-(z_1,x_1,x_2), \qquad \partial h(z_1,x_1,x_2)=:\begin{bmatrix}\sigma_1 & -\sigma_3 & -\sigma_4\end{bmatrix}, \qquad \sigma_1>0,\quad \sigma_3,\sigma_4\geq 0.$$

Furthermore, recall from (6) that $K_{P_1}=\sigma_4$ and $K_I=\sigma_5\frac{\sigma_1\bar{z}_1+\sigma_2\bar{z}_2}{\bar{z}_1+\bar{z}_2}$. Since in the limit of large η, $\bar{z}_2\approx 0$ (refer to Appendix C), and for Class 1 APIF controllers we have that $\sigma_5=1$, then $K_I\approx\sigma_1$ (for large η).

Stationary Variance $\mathrm{Var}_\pi\left[X_2\right]\approx r\left[\frac{(\gamma_1+\gamma_2+\sigma_3)(\gamma_1\gamma_2+\gamma_2\sigma_3+\sigma_1k_1)+k_1\gamma_2(\gamma_1+\sigma_4)}{(\gamma_1+\gamma_2+\sigma_3)(\gamma_1\gamma_2+\gamma_2\sigma_3+k_1\sigma_4)-\sigma_1k_1\theta}\right]$					
Controller	$h^+(z_1,x_2)$	$h^-(x_1,x_2)$	$\sigma_1=K_I$	σ_3	$\sigma_4=K_{P_1}$
AIF	kz_1	0	k	0	0
APIF Class 1 (Additive Inhibition)	$kz_1+\frac{\alpha}{1+(x_2/\kappa)^n}$	0	k	0	$\frac{\alpha}{r}\frac{n(r/\kappa)^n}{[1+(r/\kappa)^n]^2}$
APIF Class 1 (Multiplicative Inhibition)	$\frac{kz_1}{1+(x_2/\kappa)^n}$	0	$\frac{k}{1+(r/\kappa)^n}$	0	$\frac{\gamma_1\gamma_2}{k_1}\frac{n(r/\kappa)^n}{1+(r/\kappa^n)}$
APIF Class 1 (Degradation Inhibition)	kz_1	$\delta x_1x_2^n$	k	δr^n	$n\frac{\delta\gamma_2}{k_1}r^n$

Table 1: Output Variance for the gene expression network regulated by the APIF controllers of Class 1.

Observe that the denominator of the variance expression is positive when the deterministic setting is stable (see (14)). Hence this expression is only valid when the deterministic setting is stable; otherwise, this approximation is meaningless. One can easily see from the general expression in Table 1 that $\mathrm{Var}_\pi\left[X_2\right]$ is monotonically increasing in $\sigma_1\approx K_I$ and monotonically decreasing in $\sigma_4=K_{P_1}$. Therefore, this approximate formula for the variance suggests that increasing the integral gain K_I (resp. proportional gain K_P) increases (resp. decreases) the stationary variance of the output species $\mathbf{X_2}$. This conclusion extends the results in [33] to more general proportional actuations involving different mechanisms of inhibitions with cooperativity ($n\geq 1$).

Particularly, for the case of additive inhibition (which is similar to the previous works in [33] and [35] with $\kappa = n = 1$), α tunes the proportional gain only. In fact increasing α increases $\sigma_4 = K_{P_1}$ and thus decreases the stationary variance as illustrated in Panel E of Figure 5 through both stochastic simulations and the approximate formula. However, this inhibition mechanism has the disadvantage that α, similar to the deterministic setting, cannot exceed a threshold where ergodicity is lost. Additionally, the accuracy of the approximate formula deteriorates, as illustrated in Panel E, when α gets closer to the verge of losing stability. As a result, α has to be tuned carefully. In contrast, for the case of multiplicative inhibition, tuning κ automatically tunes both the proportional and integral gain in a beneficial manner. More precisely, decreasing κ enough ($\kappa < r$), increases the proportional gain $K_{P_1} = \sigma_4$ and decreases the integral gain $K_I \approx \sigma_1$, simultaneously. This has the effect of decreasing the variance without risking loss of stability as illustrated in Panel E. Similarly, for the case of degradation inhibition, increasing δ automatically increases the proportional gain and the degradation rate of the input species $\mathbf{X_1}$ (through σ_3). This also has the effect of decreasing the variance without risking loss of stability as illustrated in Panel E. In fact, multiplicative and degradation inhibitions provide a structural property of decreasing the stationary variance of the output species $\mathbf{X_2}$. That is, the relevant controller parameters (κ and δ) doesn't have to be fine tuned to decrease the variance and not risk loss of stability. Furthermore, it is clear from Table 1 that increasing the hill coefficient n will boost the proportional gains $\sigma_4 = K_P$ and thus ameliorate the effectiveness of proportional component in decreasing the stationary variance.

4 Antithetic Proportional-Integral-Derivative Feedback Controllers

In this section, we append a Derivative (D) control action to the APIF (Class 1) controller of Figure 3. The proposed motif, depicted in Panel A of Figure 6, yields a PID architecture whose P, I and D components are inseparable as described in Panel E of Figure 1. The main advantage of the proposed APIDF controller is its simplicity. Observe that, compared to the APIF (Class 1), no additional controller species are added, and only one additional reaction is required to produce $\mathbf{Z_1}$ catalytically from $\mathbf{X_L}$ at a rate $\beta < \theta$. Intuitively, the proposed motif involves an antithetic integral action cascaded with an incoherent feedforward loop. More precisely, the output species $\mathbf{X_L}$ directly inhibits $\mathbf{X_1}$ and simultaneously produces it via the intermediate species $\mathbf{Z_1}$. This incoherent feedforward loop gives rise to a Proportional (P) and Derivative (D) action simultaneously in an inseparable fashion as will be shown next. The closed loop network with the stoichiometry matrix and propensity function are all shown in Figure 6.

The deterministic dynamics of the closed loop system are given by

$$\begin{cases} \dot{x} = f(x) + h(z_1, x_1, x_L)e_1 \\ \dot{z}_1 = \mu + \beta x_L - \eta z_1 z_2 \\ \dot{z}_2 = \theta x_L - \eta z_1 z_2, \end{cases} \tag{8}$$

where $f(x) = S\lambda(x)$. Similar to the APIF controllers, the actuation propensity h can take different forms as illustrated in the table of Figure 6, Panel A. The output component of the fixed point can be easily calculated to be

$$\bar{x}_L = \frac{\mu}{\theta - \beta}. \tag{9}$$

Note that $\bar{x}_L$ is positive and well defined under the imposed condition $\beta < \theta$. This means that RPA is achieved, and the parameters μ, θ and β serve as knobs for tuning the set point.

To analytically verify that the proposed architecture indeed involves a PID control action, we carry out a linear perturbation analysis similar to that carried out for the APIF controllers. Once again, let $\begin{bmatrix}\tilde{x}^T & \tilde{z}_1 & \tilde{z}_2\end{bmatrix}^T$ denote the perturbation from the fixed point $\begin{bmatrix}\bar{x}^T & \bar{z}_1 & \bar{z}_2\end{bmatrix}^T$ of (8). We also assume that the reference signal μ is allowed to slightly vary in time around a nominal reference $\bar{\mu}$. That is, we have

$$\tilde{x}(t) = x(t) - \bar{x}; \qquad \tilde{z}_1(t) = z_1(t) - \bar{z}_1; \qquad \tilde{z}_2(t) = z_2(t) - \bar{z}_2; \qquad \tilde{\mu}(t) = \mu(t) - \bar{\mu}.$$

The linearized dynamics can thus be written as

$$\begin{aligned} \dot{\tilde{x}} &= A\tilde{x} + (\sigma_1 \tilde{z}_1 - \sigma_3 \tilde{x}_1 - \sigma_4 \tilde{x}_L)\, e_1 \\ \dot{\tilde{z}}_1 &= \tilde{\mu} + \beta \tilde{x}_L - \eta \bar{z}_2 \tilde{z}_1 - \eta \bar{z}_1 \tilde{z}_2 \\ \dot{\tilde{z}}_2 &= \theta \tilde{x}_L - \eta \bar{z}_2 \tilde{z}_1 - \eta \bar{z}_1 \tilde{z}_2, \end{aligned}$$

where $A := \partial f(\bar{x})$, $\partial h(\bar{z}_1, \bar{x}_1, \bar{x}_L) =: \begin{bmatrix}\sigma_1 & -\sigma_3 & -\sigma_4\end{bmatrix}$ such that $\sigma_1 > 0$ and $\sigma_3, \sigma_4 \geq 0$.

A

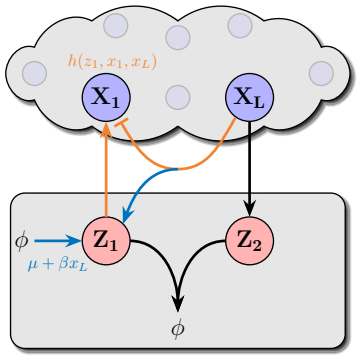

$$S_{cl} = \begin{array}{c} \begin{array}{cccccccc} \overbrace{\mathcal{R}^1 \;\; \mathcal{R}^2 \;\; \cdots \;\; \mathcal{R}^K}^{\mathcal{R}} & \overbrace{\mathcal{R}_s \;\; \mathcal{R}_q \;\; \mathcal{R}_r \;\; \mathcal{R}_a^+ \;\; \mathcal{R}_a^-}^{\mathcal{R}_c} & & \end{array} \\ \left[\begin{array}{c|ccccc} S & 0 & 0 & 0 & 1 & -1 \\ \hline & & & 0 & & \\ \hline & 0 & 0 & 0 & 0 & 0 \\ \hline 0 & 0 & -1 & 1 & 0 & 0 \\ & 1 & -1 & 0 & 0 & 0 \end{array}\right] \end{array} \begin{array}{c} \mathbf{X}_1 \\ \mathbf{X}_2 \\ \vdots \\ \mathbf{X}_{L-1} \\ \mathbf{X}_L \\ \mathbf{Z}_1 \\ \mathbf{Z}_2 \end{array}$$

$$\lambda_{cl}(x,z) = \left[\begin{array}{c|ccccc} \overbrace{\mathcal{R}^1 \;\; \mathcal{R}^2 \;\; \cdots \;\; \mathcal{R}^K}^{\mathcal{R}} & \overbrace{\mathcal{R}_s \;\; \mathcal{R}_q \;\; \mathcal{R}_r \;\; \mathcal{R}_a^+ \;\; \mathcal{R}_a^-}^{\mathcal{R}_c} \\ \lambda(x) & \theta x_L \;\; \eta z_1 z_2 \;\; \mu + \beta x_L \;\; h^+(z_1, x_L) \;\; h^-(x_1, x_L) \end{array}\right]^T$$

Actuation Propensity: $h(z_1, x_1, x_L) := h^+(z_1, x_L) - h^-(x_1, x_L)$

Reference Rxn: $\mathcal{R}_r$	Sensing Rxn: $\mathcal{R}_s$	Sequestration Rxn: $\mathcal{R}_q$
$\phi \xrightarrow{\mu + \beta x_L} \mathbf{Z_1}$	$\mathbf{X_L} \xrightarrow{\theta} \mathbf{X_L} + \mathbf{Z_2}$	$\mathbf{Z_1} + \mathbf{Z_2} \xrightarrow{\eta} \phi$

Inhibition Type	Actuation Rxns	Actuation Propensity h
Additive	$\mathcal{R}_a^+ : \;\; \phi \longrightarrow \mathbf{X_1}$	$kz_1 + \frac{\alpha}{1+(x_L/\kappa)^n}$
Multiplicative	$\mathcal{R}_a^+ : \;\; \phi \longrightarrow \mathbf{X_1}$	$\frac{kz_1}{1+(x_L/\kappa)^n}$
Degradation	$\mathcal{R}_a^+ : \;\; \mathbf{Z_1} \longrightarrow \mathbf{Z_1} + \mathbf{X_1}$ $\mathcal{R}_a^- : \;\; \mathbf{X_1} + \mathbf{X_L} \longrightarrow \mathbf{X_L}$	$kz_1 - \delta x_1 x_L^n$

B

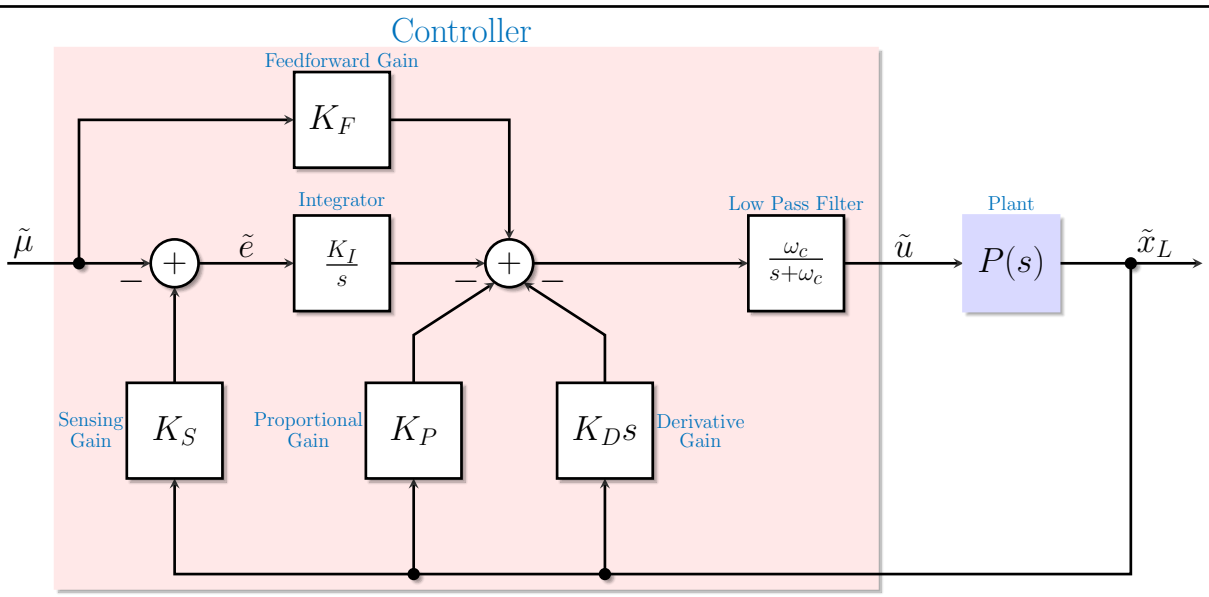

Inhibition	K_I	K_P	K_D	K_F
Additive	$k\frac{\bar{z}_1}{\bar{z}_1+\bar{z}_2}$	$\frac{\alpha}{\kappa}\frac{n(\bar{x}_L/\kappa)^{n-1}}{[1+(\bar{x}_L/\kappa)^n]^2} - \beta\frac{k}{\eta(\bar{z}_1+\bar{z}_2)}$	$\frac{\alpha/\kappa}{\eta(\bar{z}_1+\bar{z}_2)}\frac{n(\bar{x}_L/\kappa)^{n-1}}{[1+(\bar{x}_L/\kappa)^n]^2}$	$\frac{k}{\eta(\bar{z}_1+\bar{z}_2)}$
Multiplicative	$\frac{k}{1+(\bar{x}_L/\kappa)^n}\frac{\bar{z}_1}{\bar{z}_1+\bar{z}_2}$	$\frac{k}{1+(\bar{x}_L/\kappa)^n}\left[\frac{\bar{z}_1}{\kappa}\frac{n(\bar{x}_L/\kappa)^{n-1}}{1+(\bar{x}_L/\kappa)^n} - \frac{\beta}{\eta(\bar{z}_1+\bar{z}_2)}\right]$	$\frac{k\bar{z}_1/\kappa}{\eta(\bar{z}_1+\bar{z}_2)}\frac{n(\bar{x}_L/\kappa)^{n-1}}{[1+(\bar{x}_L/\kappa)^n]^2}$	$\frac{1}{1+(\bar{x}_L/\kappa)^n}\frac{k}{\eta(\bar{z}_1+\bar{z}_2)}$
Degradation	$k\frac{\bar{z}_1}{\bar{z}_1+\bar{z}_2}$	$n\delta\bar{x}_1\bar{x}_L^{n-1} - \frac{\beta k}{\eta(\bar{z}_1+\bar{z}_2)}$	$\frac{n\delta\bar{x}_1\bar{x}_L^{n-1}}{\eta(\bar{z}_1+\bar{z}_2)}$	$\frac{k}{\eta(\bar{z}_1+\bar{z}_2)}$

Figure 6: **Antithetic Proportional-Integral-Derivative Feedback (APIDF) Controllers. (A) APIDF Control Network.** An additional production reaction (marked in blue) is appended to the APIF controller of class 1 (see Figure 3) to obtain an additional derivative action. Intuitively, this additional reaction introduces an incoherent feedforward pathway from $\mathbf{X_L}$ to $\mathbf{X_1}$ that is cascaded with the standalone AIF controller. Similar to the previously introduced APIF controllers, three different biologically-relevant inhibition mechanisms are considered. **(B) APIDF Controller Block Diagram.** Similar to the block diagram of the APIF controllers depicted in Figure 4, this block diagram represents the dynamics of the linearized closed-loop system obtained by the proposed APIDF controller with all three inhibition mechanisms. The table shows the PID gains as a function of the various biological parameters.

Taking the Laplace transforms yields

$$\begin{aligned}
\tilde{x}_L(s) &= e_L^T \left(sI - \bar{A}\right)^{-1} e_1 \tilde{u}(s); \qquad \text{where} \quad \bar{A} := A - \sigma_3 e_1 e_1^T \\
\tilde{u}(s) &= \sigma_1 \tilde{z}_1(s) - \sigma_4 \tilde{x}_L(s) \\
\tilde{z}_1(s) &= \frac{\tilde{\mu}(s) + \beta \tilde{x}_L(s) - \eta \bar{z}_1 \tilde{z}_2(s)}{s + \eta \bar{z}_2} \\
\tilde{z}_2(s) &= \frac{\theta \tilde{x}_L(s) - \eta \bar{z}_2 \tilde{z}_1(s)}{s + \eta \bar{z}_1}.
\end{aligned}$$

Next, we express $\tilde{z}_1(s)$ and $\tilde{z}_2(s)$ in terms of $\tilde{\mu}(s), \tilde{x}_L(s)$ and the error $\tilde{e}(s) := \tilde{\mu}(s) - (\theta - \beta)\, \tilde{x}_L(s)$ as

$$\begin{aligned}
\tilde{z}_1(s) &= \left[\tilde{\mu}(s) + \beta \tilde{x}_L(s) + \frac{\eta \bar{z}_1}{s} \tilde{e}(s)\right] \frac{1}{s + \eta\left(\bar{z}_1 + \bar{z}_2\right)} \\
\tilde{z}_2(s) &= \left[\theta \tilde{x}_L(s) - \frac{\eta \bar{z}_2}{s} \tilde{e}(s)\right] \frac{1}{s + \eta\left(\bar{z}_1 + \bar{z}_2\right)}.
\end{aligned}$$

The feedback control action $\tilde{u}(s)$ can thus be written as

$$\begin{aligned}
\tilde{u}(s) &= \left[\sigma_1 \tilde{\mu}(s) + \frac{\eta \sigma_1 \bar{z}_1}{s} \tilde{e}(s) + \sigma_1 \beta \tilde{x}_L(s)\right] \frac{1}{s + \eta\left(\bar{z}_1 + \bar{z}_2\right)} - \sigma_4 \tilde{x}_L(s) \\
&= \left[\sigma_1 \tilde{\mu}(s) + \frac{\eta \sigma_1 \bar{z}_1}{s} \tilde{e}(s) - \sigma_4 s \tilde{x}_L(s) - \left(\sigma_4 \eta (\bar{z}_1 + \bar{z}_2) - \sigma_1 \beta\right) \tilde{x}_L(s)\right] \frac{1}{s + \eta\left(\bar{z}_1 + \bar{z}_2\right)}.
\end{aligned}$$

This is the controller transfer function that relates the control action $\tilde{u}$ to the reference signal $\tilde{\mu}$, the error signal $\tilde{e}$ and the plant output $\tilde{x}_L$ in the Laplace domain. Therefore, equipped with the controller and plant transfer functions given by

$$\begin{aligned}
&\textbf{Controller:} \quad \tilde{u}(s) = \left[K_F \tilde{\mu}(s) + \frac{K_I}{s} \tilde{e}(s) - \Big(K_P + K_D s\Big) \tilde{x}_L(s)\right] \frac{\omega_c}{s + \omega_c} \\
&\textbf{Plant:} \quad \tilde{x}_L(s) = P(s) \tilde{u}(s); \\
&\text{where:} \quad \begin{cases} K_F = \dfrac{\sigma_1}{\eta(\bar{z}_1 + \bar{z}_2)}, \quad K_I = \sigma_1 \dfrac{\bar{z}_1}{\bar{z}_1 + \bar{z}_2}, \quad K_S = \theta - \beta, \qquad K_P = \sigma_4 - \dfrac{\sigma_1 \beta}{\eta(\bar{z}_1 + \bar{z}_2)}, \\ K_D = \dfrac{\sigma_4}{\eta(\bar{z}_1 + \bar{z}_2)} \quad \omega_c = \eta(\bar{z}_1 + \bar{z}_2), \quad P(s) = e_L^T \left(sI - \bar{A}\right)^{-1} e_1, \end{cases}
\end{aligned} \tag{10}$$

we can now draw the block diagram shown in Panel B of Figure 6 which compactly encompasses the proposed APIDF architectures with three different inhibition mechanisms. Note that for the proposed controller architecture to properly function as a PID controller, β has to be strictly positive. If $\beta = 0$, it can be shown that the low pass filter annihilates the effect of the derivative component. Observe that the various controller parameters $(\eta, \theta, \beta, ...)$ appear mutually in the various PID gains and cutoff frequency. This is the consequence of having an inseparable PID controller. Recall that for the previously proposed APIF controllers, the sequestration reaction is assumed to strong (η is large). In contrast, for the proposed two-species APIDF, η cannot be large because the derivative gain $K_D := \frac{\sigma_4}{\eta(\bar{z}_1 + \bar{z}_2)}$ becomes negligible. As a result, to obtain a complete PID architecture, η should play the role of a tuning parameter that is small enough to control the derivative gain K_D.

Next, we investigate the generality of the proposed PID controllers. That is, we aim at answering the following question: Are there enough degrees of freedom in the controller to freely tune the PID gains (K_P, K_I, K_D) and cutoff frequency ω_c? To answer this question, we consider a particular plant in feedback with the proposed APIDF controller depicted in Figure 7. It is proved in Appendix B that the achievable PID gains and cutoff frequency are restricted to the following sets

$$\begin{aligned}
&\textbf{Additive Inhibition:} \qquad \mathcal{S}_A = \left\{(K_P, K_I, K_D, \omega_c) : K_P < K_D \omega_c < \frac{n}{n+1}(K_P + \tau)\right\} \\
&\textbf{Multiplicative Inhibition:} \quad \mathcal{S}_M = \left\{(K_P, K_I, K_D, \omega_c) : K_P < K_D \omega_c < \min\{n\tau, K_P + \tau\}\right\} \\
&\textbf{Degradation Inhibition:} \qquad \mathcal{S}_D = \left\{(K_P, K_I, K_D, \omega_c) : K_P < K_D \omega_c < \frac{n}{n-1}(K_P + \tau)\right\},
\end{aligned} \tag{11}$$

where $\tau := \frac{\gamma_1 \gamma_2}{k_1}$ is a rate constant that depends solely on the plant. Appendix B also provides exact formulas that show how to tune the controller parameters $\mu, \theta, \eta, \kappa, \alpha, \beta, \delta, ...$ to achieve a given set of PID gains (K_P, K_I, K_D) and cutoff frequency ω_c. Several remarks are worth noting here. Firstly, observe that $\mathcal{S}_A \subset \mathcal{S}_M \subset S_D$. This

means that more possible values of the PID gains and the cutoff frequency are achievable with degradation than with multiplicative and additive inhibitions. In fact, for $n = 1$, $\mathcal{S}_D$ becomes independent of the plant and $K_D\omega_c$ has to respect a lower bound only. This is as opposed to $\mathcal{S}_M$ and $\mathcal{S}_A$ where the plant rate constant τ imposes an upper bound on $K_D\omega_c$. Secondly, it is clear that not all PID gains and cutoff frequencies are achievable. This is the price that we pay to keep the PID controller simple, that is, involve only two species $\mathbf{Z_1}$ and $\mathbf{Z_2}$. However, although these sets limit the achievable gains and cutoff frequency, there is still enough room that allows us to leverage the benefits of the proposed PID controller and achieve various performance objectives as will be demonstrated in the subsequent sections.

4.1 Derivative Control Action Stabilizes the Dynamics but Boosts the Variance

To study the effects of the (inseparable) Derivative control action with different inhibition mechanisms, we consider the closed loop network of Figure 7 Panel A. The plant is the same as the one in Figure 5, however the controller is different. The Proportional and Integral gains are fixed to be $K_P = 0.25$ and $K_I = 1.2$. The cutoff frequency is also fixed to be $\omega_c = 10$. We only vary the Derivative gain K_D to asses its influence on the transient response and the stationary variance. The plant parameters are set to $k_1 = \gamma_1 = 2, \gamma_2 = 1$ except for the case of additive inhibition where $\gamma_2 = 2$ to make the dynamics more stable and circumvent the possible instabilities that might emerge as shown previously in Figure 5, Panel C. The values of the various controller network parameters can be calculated from the gains and cutoff frequency using the formulas in Appendix B, where $\theta = 2$, $n = 1$ and $\kappa = 1$ (for the additive inhibition) are fixed. The deterministic simulation results, depicted in Panel B of Figure 7, clearly shows that the Derivative gain K_D has a stabilizing effect and is capable of suppressing oscillations. Interestingly, compared to the APIF controller in Panel D of Figure 5, the derivative component adds an additional knob to improve the transient response. Particularly, recall that with additive inhibition, the APIF controller was capable to suppress the oscillations but could not get rid of the overshoot. The APIDF controller, however, is capable of removing the overshoot. Furthermore, with multiplicative and degradation inhibition, the APIF controller suppresses the oscillations at a price of slowing down the transient response. The APIDF controller, however, can do the opposite. That is, it suppresses the oscillations while keeping the initial transient response fast. Therefore, with this additional (Derivative) knob, one has an extra degree of freedom to optimize the transient response.

In the stochastic setting, the derivative component boosts the variance of the output species $\mathrm{Var}\,[X_2]$ when the inhibition mechanism is additive or multiplicative as depicted in Panel C of Figure 7. Intuitively, this is a consequence of the fact that the derivative operation is vulnerable to noise. In fact, it is well known in control theory that the D component hinders the PID controller's resilience to noise [16, 10.5], and, consequently, it is either set to zero or low-pass filtered in many industrial applications. This seems to also apply to BCRNs as well. Nonetheless, with degradation inhibition, increasing K_D reduces the stationary variance. At first, this might seem to contradict our previous observation. However, we will show next that with degradation inhibition, there is a "hidden" proportional component inside the plant of Figure 6 Panel B. This hidden proportional component has a gain K'_P that is proportional to the derivative gain K_D as depicted in Panel D of Figure 7. As a result, if K_D is increased, K'_P is also increased and thus it counteracts the variance-boosting effect of the derivative component while maintaining its benefits on the transient response.

To show this hidden proportional control action, recall that the transfer function of the plant is given by

$$\tilde{x}_L(s) = P(s)\tilde{u}(s), \qquad \text{with} \qquad P(s) = e_L^T(sI - \bar{A})^{-1}e_1, \quad \bar{A} = A - \sigma_3 e_1 e_1^T.$$

This input-output relationship of the plant can be equivalently rewritten in the time domain as

$$\dot{\tilde{x}} = A\tilde{x} + (\tilde{u} - \sigma_3\tilde{x}_1)e_1, \qquad \tilde{x}_L = e_L^T\tilde{x},$$

where $\tilde{u} := \sigma_1\tilde{z}_1 - \sigma_4\tilde{x}_L$ and $\tilde{x}_1 = e_1^T\tilde{x}$. By keeping the term $\sigma_3\tilde{x}_1$ separated, one can write the input-state relationship as $\tilde{x}(s) = (sI - A)^{-1}e_1(\tilde{u} - \sigma_3\tilde{x}_1)$. Therefore we have that

$$\begin{bmatrix}\tilde{x}_L(s)\\ \tilde{x}_1(s)\end{bmatrix} = \begin{bmatrix}e_L^T\\ e_1^T\end{bmatrix}(sI - A)^{-1}e_1\Big(\tilde{u}(s) - K'_P\tilde{x}_1(s)\Big), \qquad \text{with} \qquad K'_P := \sigma_3.$$

This equation is exactly equivalent to the block diagram in Panel D of Figure 7. Finally to show that K'_P is proportional to K_D, recall that $\sigma_3 := -\partial_{x_1}h(\bar{z}_1, \bar{x}_1, \bar{x}_L) = \delta r^n$ and $K_D = \frac{n\delta\bar{x}_1 r^{n-1}}{\eta(\bar{z}_1+\bar{z}_2)}$ from the table of Figure 6 Panel B. Hence, since $\omega_c := \eta(\bar{z}_1 + \bar{z}_2)$, we have that $K'_P = \frac{r\omega_c}{n\bar{x}_1}K_D$.

Next, we present a theoretical analysis that supports the variance-boosting effect of the derivative component. Recall that the approximate formulas derived for the stationary variance $\mathrm{Var}_\pi\,[X_2]$ in the case of the APIF controllers are valid when η is large. This requirement is essential to apply the approximate moment closure technique in Appendix C. However, for the proposed APIDF controllers, η is required to be small; otherwise, $K_D \approx 0$ and the controller operates effectively as a PI controller only. Consequently, it is difficult to derive an

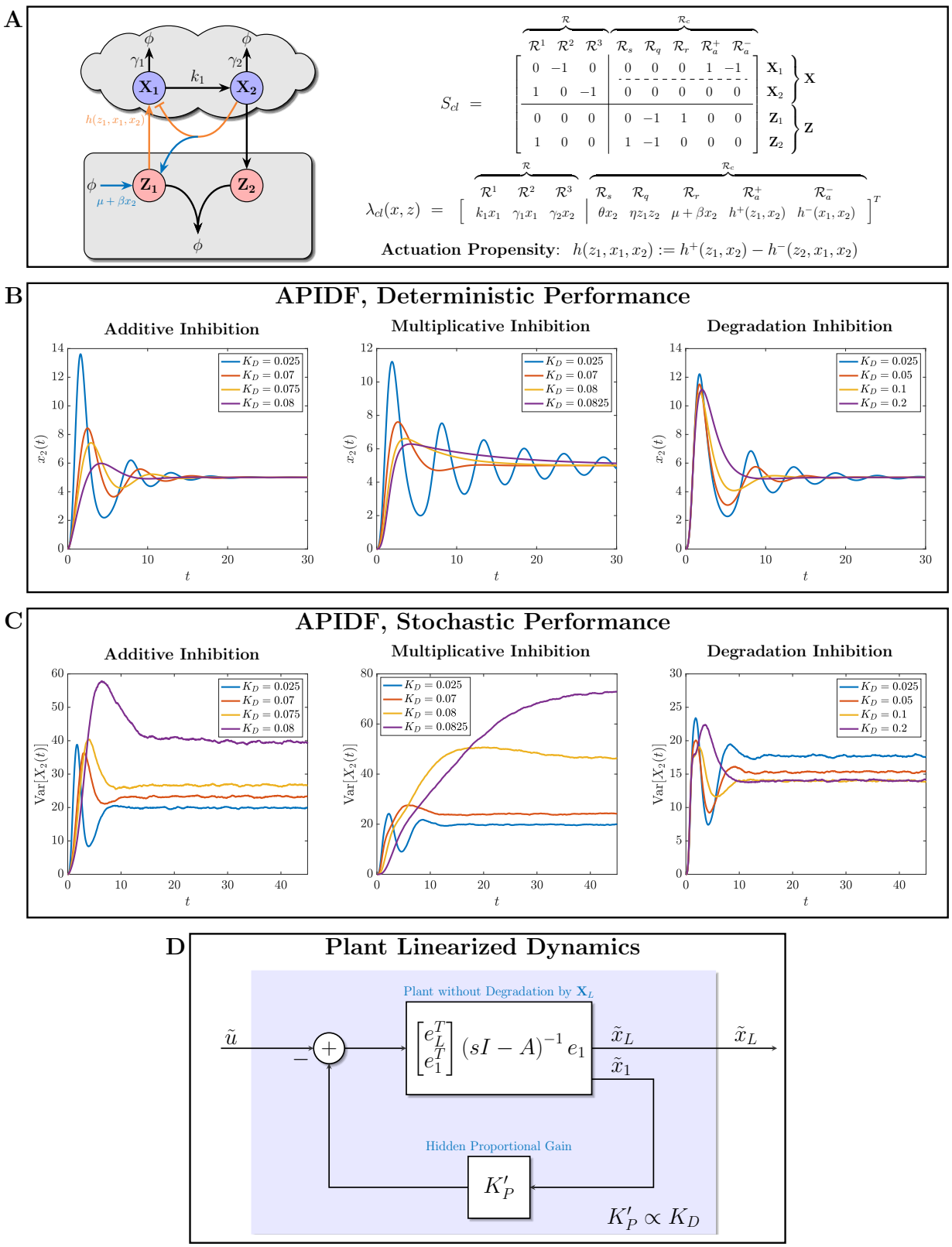

Figure 7: **Performance of APIDF Controllers. (A)** Gene Expression Network Controlled by APIDF Controllers. **(B) and (C)** The PI gains and cutoff frequency K_P, K_I and ω_c, respectively, are fixed while the derivative gain K_D is increased to asses the effect of the derivative control action on the deterministic and stochastic performances. The derivative control action appears to have a stabilizing effect on the (deterministic) transient dynamics by suppressing oscillations. For the stochastic dynamics, increasing the derivative gain seems to boost the stationary variance of the output species in the cases of additive and multiplicative inhibitions. However, with degradation inhibition, increasing the derivative gain has an opposite effect on the variance. The reason is explained in Panel **(E)** which demonstrates that the degradation inhibition gives rise to an additional (hidden) proportional control action with gain K'_P that is proportional to the derivative gain K_D. This additional (hidden) proportional component is capable of counteracting the variance-boosting effect of the derivative component while simultaneously exploiting its stabilization benefits.

approximate formula for the stationary variance $\mathrm{Var}_\pi[X_2]$ in the case of the proposed APIDF controllers (with η small).

To this end, we construct, instead, a linear "fictitious" reaction network that has a linear PID control structure (similar to Figure 1, Panel C) and analyze it. The linearity of the fictitious network is essential to circumvent the moment closure problem and, thus, obtain an exact formula for the variance. We call it a fictitious reaction network because the state variables and propensities are theoretically allowed to go negative. However, this fictitious network can be thought of as zeroth order kinetics, or a linearization of a real nonlinear reaction network whose state variables and propensities are always non-negative.

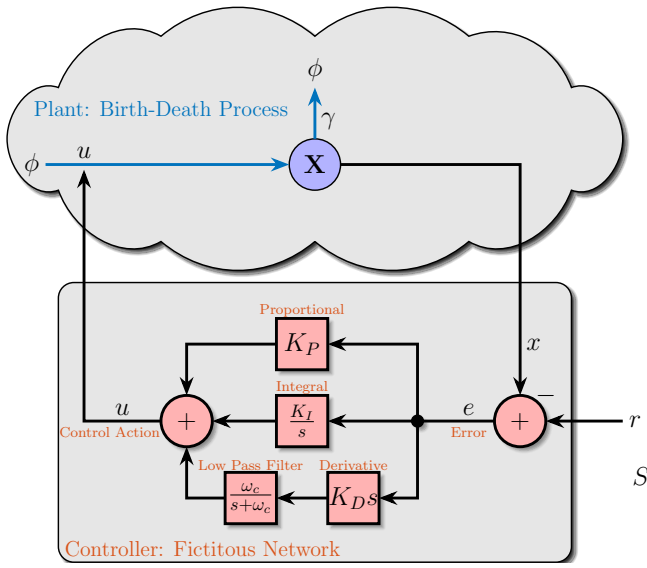

	Reaction	Fictitious Propensity
$\mathcal{R}$	$\mathbf{X} \longrightarrow \phi$	γx
$\mathcal{R}_c^1$	$\phi \longrightarrow \mathbf{Z_1}$	r
$\mathcal{R}_c^2$	$\mathbf{Z_1} \longrightarrow \phi$	x
$\mathcal{R}_c^3$	$\phi \longrightarrow \mathbf{Z_2}$	$\omega_c r$
$\mathcal{R}_c^4$	$\mathbf{Z_2} \longrightarrow \phi$	$\omega_c(z_2 + x)$
$\mathcal{R}_c^5$	$\phi \longrightarrow \mathbf{X}$	$(K_P + K_D\omega_c)r + K_I z_1$
$\mathcal{R}_c^6$	$\mathbf{X} \longrightarrow \phi$	$(K_P + K_D\omega_c)x + K_D\omega_c z_2$

$$S_{cl} = \begin{array}{c} \\ \\ \\ \end{array}\begin{array}{c|cccccc} \mathcal{R} & \overbrace{\mathcal{R}_c^1 \;\; \mathcal{R}_c^2 \;\; \mathcal{R}_c^3 \;\; \mathcal{R}_c^4 \;\; \mathcal{R}_c^5 \;\; \mathcal{R}_c^6}^{\mathcal{R}_c} & & \\ \hline -1 & 0 \;\; 0 \;\; 0 \;\; 0 \;\; 1 \;\; -1 & \mathbf{X} & \\ 0 & 1 \;\; -1 \;\; 0 \;\; 0 \;\; 0 \;\; 0 & \mathbf{Z}_1 & \mathbf{Z} \\ 0 & 0 \;\; 0 \;\; 1 \;\; -1 \;\; 0 \;\; 0 & \mathbf{Z}_2 & \end{array}$$

$$\lambda_{cl}(x,z) = \left[\begin{array}{c|cccccc} \mathcal{R} & \overbrace{\mathcal{R}_c^1 \;\; \mathcal{R}_c^2 \;\; \mathcal{R}_c^3 \;\; \mathcal{R}_c^4 \;\; \mathcal{R}_c^5 \;\; \mathcal{R}_c^6}^{\mathcal{R}_c} \\ \gamma x & r \;\; x \;\; \omega_c r \;\; \omega_c(z_2+x) \;\; (K_P+K_D\omega_c)r + K_I z_1 \;\; (K_P+K_D\omega_c)x + K_D\omega_c z_2 \end{array}\right]^T$$

Controller	**Stationary Variance** $\mathrm{Var}_\pi[X]$	**Monotonicity of** $\mathrm{Var}_\pi[X]$
I	$r\left[1 + \frac{K_I}{\gamma}\right]$	$\uparrow$ in K_I
PI	$r\left[1 + \frac{K_I}{K_P+\gamma}\right]$	$\downarrow$ in K_P
PID	$r\left[1 + \frac{\omega_c K_I(K_P+K_D\omega_c+\gamma)+\omega_c^2(K_I+K_D\omega_c)+K_D^2\omega_c^3+K_I^2}{(K_P+K_D\omega_c+\gamma)(K_I+\omega_c(K_P+\gamma))+\omega_c^2(K_P+\gamma)}\right]$	if $\omega_c > \frac{K_I}{\sqrt{K_P+\gamma}}$: $\uparrow$ in K_D if $\omega_c < \frac{K_I}{\sqrt{K_P+\gamma}}$: $\begin{cases}\uparrow \text{ in } K_D > K_D^{\mathrm{Th}} \\ \downarrow \text{ in } K_D < K_D^{\mathrm{Th}}\end{cases}$

Figure 8: **A Fictitious (non-biochemical) linear PID controller.** A fictitious reaction network is designed (upper table) that realizes the linear dynamics of the standard PID controller with filtered derivative control. This fictitious reaction network can be though of as a linearization of a realistic (nonlinear) reaction network, or a network with zeroth-order kinetics. In fact, any nonlinear PID controller will have a linearization possessing a similar architecture. Since the dynamics are linear, a formula for the stationary variance is derived and depicted in the lower table. The integral (resp. proportional) control induces an increase (resp. decrease) in the stationary variance. Furthermore, the derivative control induces a boost in the stationary variance if the cutoff frequency ω_c is large enough (mimicking a pure unfiltered derivative controller). These theoretical conclusions are consistent with the proposed nonlinear APIDF controllers.

The fictitious network is depicted in Figure 8, where we consider a plant describing a birth-death process for simplicity. More general unimolecular (linear) plants can also be considered (refer to Appendix D). Observe that the controller has the basic PID structure where the species $\mathbf{X}$ is measured, and compared to the reference r by computing the error $e := r - x$. Then the Proportional, Integral, and Derivative terms of the error are computed and summed up to obtain the control action u that is fed back to the plant as the production rate of the species $\mathbf{X}$. Note that the derivative term is passed through a low pass filter with a cutoff frequency ω_c, and thus the PID has a filtered derivative component which becomes a pure derivative in the limit as $\omega_c \to \infty$. The goal is to realize the closed-loop system as a fictitious reaction network and derive an exact formula for the stationary variance $\mathrm{Var}_\pi[X]$.

From the block diagram in Figure 8, one can immediately write down the transfer function of the controller (in the Laplace domain) as

$$u(s) = \left(\frac{K_I}{s} + K_P + K_D s \frac{\omega_c}{s + \omega_c} \right) e(s),$$

To rewrite this controller relationship in the time domain, we introduce two state variables z_1 and z_2 defined as

$$z_1(s) := \frac{e(s)}{s} \qquad \text{and} \qquad \frac{se(s)}{s + \omega_c} = \left(1 - \frac{\omega_c}{s + \omega_c} \right) e(s) =: e(s) - z_2(s).$$

The first differential equation in z_1 can be easily written as $\dot{z}_1 = r - x$. The second differential equation in z_2 can be written as $\dot{z}_2 = -\omega_c z_2 + \omega_c r - \omega_c x$. Therefore, the control action u in the time domain can be written in terms of z_1 and z_2 as

$$\begin{cases} u = (K_P + K_D\omega_c)r - (K_P + K_D\omega_c)x + K_I z_1 - K_D\omega_c z_2 \\ \dot{z}_1 = r - x \\ \dot{z}_2 = -\omega_c z_2 + \omega_c r - \omega_c x. \end{cases}$$

These *linear* equations can be realized as a set of fictitious reactions listed in the Table of Figure 8. With the list of reactions at hand, one can construct the stoichiometry matrix and propensity function that are also depicted in Figure 8. Observe that the propensity function is affine in the state variables, and as a result there is no moment closure problem, and one can derive exact expressions for the stationary expectations and variances. In fact, it is shown in Appendix D that, assuming ergodicity of the closed loop system, the stationary expectation is $\mathbb{E}_\pi[X] = r$, regardless of what the plant is. This is a consequence of the integral control action that ensures RPA. Furthermore, an exact formula for the stationary variance $\mathrm{Var}_\pi[X_2]$ is derived and shown in the lower table of Figure 8. By setting either $(K_P, K_D) = 0$ or $K_P = 0$, we obtain the stationary variance for the Integral (I) and Proportional-Integral (PI) controllers, respectively. Clearly, the integral gain K_I increases the stationary variance; whereas, the proportional gain K_P decreases it. This agrees with the simulations and theoretical analysis of our proposed APIF controllers and the previous work in [33].

The expression for the stationary variance in the case of full PID control is slightly more complicated, but two conclusions can be drawn from it. Firstly, recall that to obtain a pure (non-filtered) Derivative control, we increase the cutoff frequency ω_c to infinity. Observe that for large ω_c, the stationary variance behaves like

$$\mathrm{Var}_\pi[X] \approx r \frac{K_D\omega_c}{K_P + \gamma} \qquad (\text{for large } \omega_c),$$

which is monotonically increasing in K_D. This means that for a pure derivative control action (asymptotic limit as $\omega_c \to \infty$), the stationary variance blows up to infinity. Even for a finite cutoff frequency ω_c, it is shown in Appendix D that for $\omega_c > \frac{K_I}{\sqrt{K_P+\gamma}}$, the stationary variance is a monotonically increasing function of K_D. Otherwise, for $\omega_c < \frac{K_I}{\sqrt{K_P+\gamma}}$, the stationary variance decreases in K_D as long as K_D is less than a threshold K_D^{Th} that is calculated in Appendix D. However, above this threshold, the stationary variance increases in K_D again. This analysis implies that the derivative control action, if not low-pass filtered intensively (low cutoff frequency), boosts the stationary variance. Indeed for a pure derivative the variance blows up to infinity. This conclusion is in agreement with the simulation results of the APIDF controller in Figure 7. Secondly, observe that the stationary variance can not be less than the set point r no matter what the PID gains are. We conjecture that this is a consequence of the linearity for this PID controller. Interestingly, the proposed nonlinear APIF controllers are capable of reducing the stationary variance to values lower than the set point as illustrated in both the appoximate analytical formulas given in Table 1 and the simulations results of Figure 5. It seems that the nonlinearity of the APIF controllers is beneficial in reducing the variance to small values.

We close this section with a final remark. Although this controller describes a fictitious network, one can still use it *in silico* by artificially forcing all fictitious propensities to remain non-negative. For example, one can replace the fictitious propensity of reaction $\mathcal{R}^6$ by $\max\{(K_P + K_D\omega_c)x + K_D\omega_c z_2, 0\}$.

5 Conclusion

This paper proposes a set of (nonlinear) PID controllers that can be realized by biochemical reaction networks. The main goal of this paper is to keep the PID designs as simple as possible in order to make them amenable for biological implementations. A general framework for biomolecular feedback controllers is introduced that can be used to pave the way for other possible controllers in the future. The various PID designs are verified and assessed using theoretical tools and (deterministic and stochastic) simulations. It is shown that the details of the PID realizations (particularly, the inhibition mechanisms) have a critical effect on the targeted performance objectives such as stability, transient dynamics, and variance. We believe that research along this direction helps building high performance controllers that are capable of reliably manipulating genetic circuits for various applications.

Acknowledgments

This project has received funding from the European Research Council (ERC) under the European Union's Horizon 2020 research and innovation programme (CyberGenetics; grant agreement 743269), and from the European Union's Horizon 2020 research and innovation programme (COSY-BIO; grant agreement 766840).

Competing Interests

ETH Zürich has filed a patent application on behalf of the inventors T.F., C.H.C., M.F. and M.K. that includes the designs described (application no. EP20206417.6).

References

[1] T.-M. Yi, Y. Huang, M. I. Simon, and J. Doyle, "Robust perfect adaptation in bacterial chemotaxis through integral feedback control," *Proceedings of the National Academy of Sciences*, vol. 97, no. 9, pp. 4649–4653, 2000.

[2] D. Muzzey, C. A. Gómez-Uribe, J. T. Mettetal, and A. van Oudenaarden, "A systems-level analysis of perfect adaptation in yeast osmoregulation," *Cell*, vol. 138, no. 1, pp. 160–171, 2009.

[3] H. El-Samad, J. Goff, and M. Khammash, "Calcium homeostasis and parturient hypocalcemia: an integral feedback perspective," *Journal of theoretical biology*, vol. 214, no. 1, pp. 17–29, 2002.

[4] M. J. Dunlop, J. D. Keasling, and A. Mukhopadhyay, "A model for improving microbial biofuel production using a synthetic feedback loop," *Systems and synthetic biology*, vol. 4, no. 2, pp. 95–104, 2010.

[5] J. A. Stapleton, K. Endo, Y. Fujita, K. Hayashi, M. Takinoue, H. Saito, and T. Inoue, "Feedback control of protein expression in mammalian cells by tunable synthetic translational inhibition," *ACS synthetic biology*, vol. 1, no. 3, pp. 83–88, 2012.

[6] G. Lillacci, S. Aoki, D. Schweingruber, and M. Khammash, "A synthetic integral feedback controller for robust tunable regulation in bacteria," *BioRxiv*, p. 170951, 2017.

[7] A. H. Ng, T. H. Nguyen, M. Gomez-Schiavon, G. Dods, R. A. Langan, S. E. Boyken, J. A. Samson, L. M. Waldburger, J. E. Dueber, D. Baker, *et al.*, "Modular and tunable biological feedback control using a de novo protein switch," *Nature*, vol. 572, no. 7768, pp. 265–269, 2019.

[8] H.-H. Huang, Y. Qian, and D. Del Vecchio, "A quasi-integral controller for adaptation of genetic modules to variable ribosome demand," *Nature communications*, vol. 9, no. 1, pp. 1–12, 2018.

[9] S. K. Aoki, G. Lillacci, A. Gupta, A. Baumschlager, D. Schweingruber, and M. Khammash, "A universal biomolecular integral feedback controller for robust perfect adaptation," *Nature*, p. 1, 2019.

[10] G. Lillacci, Y. Benenson, and M. Khammash, "Synthetic control systems for high performance gene expression in mammalian cells," *Nucleic acids research*, vol. 46, no. 18, pp. 9855–9863, 2018.

[11] V. Hsiao, E. L. De Los Santos, W. R. Whitaker, J. E. Dueber, and R. M. Murray, "Design and implementation of a biomolecular concentration tracker," *ACS synthetic biology*, vol. 4, no. 2, pp. 150–161, 2015.

[12] C. L. Kelly, A. W. K. Harris, H. Steel, E. J. Hancock, J. T. Heap, and A. Papachristodoulou, "Synthetic negative feedback circuits using engineered small rnas," *Nucleic acids research*, vol. 46, no. 18, pp. 9875–9889, 2018.

[13] D. K. Agrawal, R. Marshall, V. Noireaux, and E. D. Sontag, "In vitro implementation of robust gene regulation in a synthetic biomolecular integral controller," *Nature communications*, vol. 10, no. 1, pp. 1–12, 2019.

[14] T. Frei, C.-H. Chang, M. Filo, and M. Khammash, "Genetically engineered integral feedback controllers for robust perfect adaptation in mammalian cells," *bioRxiv*, 2020.

[15] M. H. Khammash, "Robust steady-state tracking," *IEEE transactions on automatic control*, vol. 40, no. 11, pp. 1872–1880, 1995.

[16] K. J. Åström and R. M. Murray, *Feedback systems: an introduction for scientists and engineers*. Princeton university press, 2010.

[17] B. A. Francis and W. M. Wonham, "The internal model principle of control theory," *Automatica*, vol. 12, no. 5, pp. 457–465, 1976.

[18] N. Minorsky, "Directional stability of automatically steered bodies," *Journal of the American Society for Naval Engineers*, vol. 34, no. 2, pp. 280–309, 1922.

[19] R. Vilanova and A. Visioli, *PID control in the third millennium*. Springer, 2012.

[20] T. L. Blevins, "Pid advances in industrial control," *IFAC Proceedings Volumes*, vol. 45, no. 3, pp. 23–28, 2012.

[21] J. Li and Y. Li, "Dynamic analysis and pid control for a quadrotor," in *2011 IEEE International Conference on Mechatronics and Automation*, pp. 573–578, IEEE, 2011.

[22] S. Bennett, "A brief history of automatic control," *IEEE Control Systems Magazine*, vol. 16, no. 3, pp. 17–25, 1996.

[23] C. Briat, "A biology-inspired approach to the positive integral control of positive systems: The antithetic, exponential, and logistic integral controllers," *SIAM Journal on Applied Dynamical Systems*, vol. 19, no. 1, pp. 619–664, 2020.

[24] K. Oishi and E. Klavins, "Biomolecular implementation of linear i/o systems," *IET systems biology*, vol. 5, no. 4, pp. 252–260, 2011.

[25] C. Briat, C. Zechner, and M. Khammash, "Design of a synthetic integral feedback circuit: dynamic analysis and dna implementation," *ACS Synthetic Biology*, vol. 5, no. 10, pp. 1108–1116, 2016.

[26] C. Briat, A. Gupta, and M. Khammash, "Antithetic integral feedback ensures robust perfect adaptation in noisy biomolecular networks," *Cell systems*, vol. 2, no. 1, pp. 15–26, 2016.

[27] F. Xiao and J. C. Doyle, "Robust perfect adaptation in biomolecular reaction networks," in *2018 IEEE Conference on Decision and Control (CDC)*, pp. 4345–4352, IEEE, 2018.

[28] Y. Qian and D. Del Vecchio, "Realizing 'integral control'in living cells: how to overcome leaky integration due to dilution?," *Journal of The Royal Society Interface*, vol. 15, no. 139, p. 20170902, 2018.

[29] C. C. Samaniego and E. Franco, "Ultrasensitive molecular controllers for quasi-integral feedback," *Cell Systems*, 2021.

[30] N. Olsman, F. Xiao, and J. C. Doyle, "Architectural principles for characterizing the performance of antithetic integral feedback networks," *Iscience*, vol. 14, pp. 277–291, 2019.

[31] N. Olsman, A.-A. Baetica, F. Xiao, Y. P. Leong, R. M. Murray, and J. C. Doyle, "Hard limits and performance tradeoffs in a class of antithetic integral feedback networks," *Cell systems*, vol. 9, no. 1, pp. 49–63, 2019.

[32] M. Filo and M. Khammash, "Optimal parameter tuning of feedback controllers with application to biomolecular antithetic integral control," in *2019 IEEE 58th Conference on Decision and Control (CDC)*, pp. 951–957, IEEE, 2019.

[33] C. Briat, A. Gupta, and M. Khammash, "Antithetic proportional-integral feedback for reduced variance and improved control performance of stochastic reaction networks," *Journal of The Royal Society Interface*, vol. 15, no. 143, p. 20180079, 2018.

[34] A. Gupta and M. Khammash, "An antithetic integral rein controller for bio-molecular networks," in *2019 IEEE 58th Conference on Decision and Control (CDC)*, pp. 2808–2813, IEEE, 2019.

[35] M. Chevalier, M. Gómez-Schiavon, A. H. Ng, and H. El-Samad, "Design and analysis of a proportional-integral-derivative controller with biological molecules," *Cell Systems*, vol. 9, no. 4, pp. 338–353, 2019.

[36] S. Modi, S. Dey, and A. Singh, "Proportional and derivative controllers for buffering noisy gene expression," in *2019 IEEE 58th Conference on Decision and Control (CDC)*, pp. 2832–2837, IEEE, 2019.

[37] N. M. Paulino, M. Foo, J. Kim, and D. G. Bates, "Pid and state feedback controllers using dna strand displacement reactions," *IEEE Control Systems Letters*, vol. 3, no. 4, pp. 805–810, 2019.

[38] M. Whitby, L. Cardelli, M. Kwiatkowska, L. Laurenti, M. Tribastone, and M. Tschaikowski, "Pid control of biochemical reaction networks," *IEEE Transactions on Automatic Control*, 2021.

[39] W. Halter, Z. A. Tuza, and F. Allgöwer, "Signal differentiation with genetic networks," *IFAC-PapersOnLine*, vol. 50, no. 1, pp. 10938–10943, 2017.

[40] W. Halter, R. M. Murray, and F. Allgöwer, "Analysis of primitive genetic interactions for the design of a genetic signal differentiator," *Synthetic Biology*, vol. 4, no. 1, p. ysz015, 2019.

[41] C. C. Samaniego, G. Giordano, and E. Franco, "Practical differentiation using ultrasensitive molecular circuits," in *2019 18th European Control Conference (ECC)*, pp. 692–697, IEEE, 2019.

[42] C. C. Samaniego, J. Kim, and E. Franco, "Sequestration and delays enable the synthesis of a molecular derivative operator," in *2020 59th IEEE Conference on Decision and Control (CDC)*, pp. 5106–5112, IEEE, 2020.

[43] C. Guiver, H. Logemann, R. Rebarber, A. Bill, B. Tenhumberg, D. Hodgson, and S. Townley, "Integral control for population management," *Journal of Mathematical Biology*, vol. 70, no. 5, pp. 1015–1063, 2015.

[44] C. Briat and M. Khammash, "Computer control of gene expression: Robust setpoint tracking of protein mean and variance using integral feedback," in *2012 IEEE 51st IEEE Conference on Decision and Control (CDC)*, pp. 3582–3588, IEEE, 2012.

[45] C. Briat and M. Khammash, "Integral population control of a quadratic dimerization process," in *52nd IEEE Conference on Decision and Control*, pp. 3367–3372, IEEE, 2013.

[46] A. Milias-Argeitis, M. Rullan, S. K. Aoki, P. Buchmann, and M. Khammash, "Automated optogenetic feedback control for precise and robust regulation of gene expression and cell growth," *Nature communications*, vol. 7, no. 1, pp. 1–11, 2016.

APPENDIX

A Derivation of the Stability Conditions of the APIF Controllers

Consider the closed-loop network in Figure 5 Panel A where the APIF controller is in feedback with a particular plant comprised of two species $\mathbf{X_1}$ and $\mathbf{X_2}$. We now exploit the Routh-Hurwitz Criterion to derive a necessary and sufficient condition of stability for all of the proposed APIF controllers. Using the closed loop stoichiometry matrix and propensity function, shown in Figure 5, one can write the deterministic closed-loop dynamics as

$$\begin{aligned}\dot{x}_1 &= h(z_1, z_2, x_1, x_2) - \gamma_1 x_1\\ \dot{x}_2 &= k_1 x_1 - \gamma_2 x_2\\ \dot{z}_1 &= g(\mu, x_2) - \eta z_1 z_2\\ \dot{z}_2 &= \theta x_2 - \eta z_1 z_2.\end{aligned} \tag{12}$$

Hence, the Jacobian J, evaluated at the fixed point $\begin{bmatrix}\bar{x}_1 & \bar{x}_2 & \bar{z}_1 & \bar{z}_2\end{bmatrix}^T$, of the right hand side is calculated to be

$$J = \begin{bmatrix} -(\gamma_1+\sigma_3) & -\sigma_4 & \sigma_1 & -\sigma_2\\ k_1 & -\gamma_2 & 0 & 0\\ 0 & -\sigma_6 & -\eta\bar{z}_2 & -\eta\bar{z}_1\\ 0 & \theta & -\eta\bar{z}_2 & -\eta\bar{z}_1\end{bmatrix},$$

where $\partial h(\bar{z}_1, \bar{z}_2, \bar{x}_1, \bar{x}_2) =: \begin{bmatrix}\sigma_1 & -\sigma_2 & -\sigma_3 & -\sigma_4\end{bmatrix}$, and $\partial g(\mu, \bar{x}_2) =: \begin{bmatrix}\sigma_5 & -\sigma_6\end{bmatrix}$. Note that $\sigma_i \geq 0$. The characteristic polynomial $p(s) := \det(sI - J)$ is thus calculated to be

$$p(s) = s^4 + (\eta\bar{z} + \bar{\gamma}_1)\, s^3 + (\eta\bar{z}\bar{\gamma}_1 + \bar{\gamma}_2)\, s^2 + [\eta\bar{z}\bar{\gamma}_2 + k_1(\theta\sigma_2 + \sigma_1\sigma_6)]\, s + \eta k_1(\theta+\sigma_6)(\sigma_1\bar{z}_1 + \sigma_2\bar{z}_2)$$
$$\text{where} \quad \bar{z} := \bar{z}_1 + \bar{z}_2, \quad \bar{\gamma}_1 := \gamma_1 + \gamma_2 + \sigma_3, \quad \text{and} \quad \bar{\gamma}_2 := (\gamma_1+\sigma_3)\gamma_2 + k_1\sigma_4.$$

Using the characteristic polynomial we construct the Routh-Hurwitz table:

s^4	1	$\eta\bar{z}\bar{\gamma}_1 + \bar{\gamma}_2$	$\eta k_1(\theta+\sigma_6)(\sigma_1\bar{z}_1 + \sigma_2\bar{z}_2)$
s^3	$\eta\bar{z} + \bar{\gamma}_1$	$\eta\bar{z}\bar{\gamma}_2 + k_1(\theta\sigma_2 + \sigma_1\sigma_6)$	0
s^2	$\frac{\eta\bar{z}\bar{\gamma}_1(\eta\bar{z}+\bar{\gamma}_1)+\bar{\gamma}_1\bar{\gamma}_2-k_1(\theta\sigma_2+\sigma_1\sigma_6)}{\eta\bar{z}+\bar{\gamma}_1}$	$\eta k_1(\theta+\sigma_6)(\sigma_1\bar{z}_1 + \sigma_2\bar{z}_2)$	0
s^1	$\eta\bar{z}\bar{\gamma}_2 + k_1(\theta\sigma_2 + \sigma_1\sigma_6) - \frac{\eta k_1(\theta+\sigma_6)(\sigma_1\bar{z}_1+\sigma_2\bar{z}_2)(\eta\bar{z}+\bar{\gamma}_1)^2}{\eta\bar{\gamma}_1\bar{z}(\eta\bar{z}+\bar{\gamma}_1)+\bar{\gamma}_1\bar{\gamma}_2-k_1(\theta\sigma_2+\sigma_1\sigma_6)}$	0	0
s^0	$\eta k_1(\theta+\sigma_6)(\sigma_1\bar{z}_1 + \sigma_2\bar{z}_2)$	0	0

The Routh-Hurwitz criterion states that the necessary and sufficient condition of local stability of the fixed point is obtained by forcing all the entries of the first column to be positive. Therefore the exact necessary and sufficient conditions of stability of the fixed point are

$$\eta\bar{z}\bar{\gamma}_1(\eta\bar{z}+\bar{\gamma}_1) + \bar{\gamma}_1\bar{\gamma}_2 > k_1(\theta\sigma_2+\sigma_1\sigma_6) \quad \text{and} \quad \eta\bar{z}\bar{\gamma}_2 + k_1(\theta\sigma_2+\sigma_1\sigma_6) > \frac{\eta k_1(\theta+\sigma_6)(\sigma_1\bar{z}_1+\sigma_2\bar{z}_2)(\eta\bar{z}+\bar{\gamma}_1)^2}{\eta\bar{\gamma}_1\bar{z}(\eta\bar{z}+\bar{\gamma}_1)+\bar{\gamma}_1\bar{\gamma}_2-k_1(\theta\sigma_2+\sigma_1\sigma_6)}. \tag{13}$$

This condition of stability is cumbersome and not easy to compare for different APIF controllers (that is, different σ_i's and $\bar{z}$). However, one can obtain a simpler but approximate condition of stability for the case of strong sequestration (asymptotic limit as $\eta \to \infty$). In fact, the first condition in (13) is always satisfied when $\eta \to \infty$ assuming that σ_1, σ_2 and σ_6 are finite (which can be easily checked to be a valid assumption for the proposed APIF controllers). To simplify the second condition in (13), we first examine the asymptotic behavior of $\bar{z}_1$ and $\bar{z}_2$ as $\eta \to \infty$. For any $\eta > 0$, we have that $\bar{z}_1\bar{z}_2 = \theta\bar{x}_2/\eta$. Thus, as long as $\bar{x}_2$ is finite, we have that $\bar{z}_1\bar{z}_2 = 0$ in the limit as $\eta \to \infty$. This means that we have two possibilities in the asymptotic limit as $\eta \to \infty$: if $\bar{z}_1 > 0$ then $\bar{z}_2 = 0$, and if $\bar{z}_2 > 0$ then $\bar{z}_1 = 0$. As a result, as $\eta \to \infty$, the first condition of stability is always satisfied. The second condition of stability in the limit as $\eta \to \infty$ takes one of the two forms

$$\begin{cases}\sigma_1 k_1(\theta+\sigma_6) < \bar{\gamma}_1\bar{\gamma}_2 & \text{and} \quad (\bar{z}_1 > 0, \bar{z}_2 = 0)\\ \sigma_2 k_1(\theta+\sigma_6) < \bar{\gamma}_1\bar{\gamma}_2 & \text{and} \quad (\bar{z}_1 = 0, \bar{z}_2 > 0).\end{cases}$$

This can be rewritten as

$$\begin{cases}\sigma_1 k_1(\theta+\sigma_6) < (\gamma_1+\gamma_2+\sigma_3)(\gamma_1\gamma_2+\sigma_3\gamma_2+k_1\sigma_4) & \text{and} \quad (\bar{z}_1 > 0, \bar{z}_2 = 0)\\ \sigma_2 k_1(\theta+\sigma_6) < (\gamma_1+\gamma_2+\sigma_3)(\gamma_1\gamma_2+\sigma_3\gamma_2+k_1\sigma_4) & \text{and} \quad (\bar{z}_1 = 0, \bar{z}_2 > 0).\end{cases} \tag{14}$$

Equations (14) provide the approximate stability conditions compactly for all the proposed APIF controllers. To this end, the stability conditions for each APIF controller are obtained by simply computing σ_i's, $\bar{z}_1$, and $\bar{z}_2$ for each particular controller architecture, and then take the limit as $\eta \to \infty$. The calculation results are tabulated below, where r is the desired set point and is equal to μ/θ for APIF controllers of Class 1 and 2, but is given by (4) and (5) for the APIF controller of Class 3.

Class	Inhibition	σ_i's	$\bar{z}_1(\eta \to \infty)$	$\bar{z}_2(\eta \to \infty)$
AIF	None	$\sigma_1 = k, \quad \sigma_5 = 1$ $\sigma_2 = \sigma_3 = \sigma_4 = \sigma_6 = 0$	$\frac{\gamma_1\gamma_2 r}{kk_1}$	0
APIF Class 1	Additive	$\sigma_1 = k, \quad \sigma_5 = 1$ $\sigma_4 = \frac{\alpha}{\kappa}\frac{n(r/\kappa)^{n-1}}{[1+(r/\kappa)^n]^2}$ $\sigma_2 = \sigma_3 = \sigma_6 = 0$	$\frac{1}{k}\left[\frac{\gamma_1\gamma_2 r}{k_1} - \frac{\alpha}{1+(r/\kappa)^n}\right]$	0
	Multiplicative	$\sigma_1 = \frac{k}{1+(r/\kappa)^n}, \quad \sigma_5 = 1$ $\sigma_4 = \frac{\gamma_1\gamma_2}{k_1}\frac{n(r/\kappa)^n}{1+(r/\kappa)^n}$ $\sigma_2 = \sigma_3 = \sigma_6 = 0$	$\frac{\gamma_1\gamma_2 r}{kk_1}[1+(r/\kappa)^n]$	0
	Degradation	$\sigma_1 = k, \quad \sigma_5 = 1, \quad \sigma_3 = \delta r^n$ $\sigma_4 = nr^n\frac{\delta\gamma_2}{k_1}$ $\sigma_2 = \sigma_6 = 0$	$\frac{\gamma_2 r}{kk_1}(\gamma_1 + \delta r^n)$	0
APIF Class 2	Additive	$\sigma_1 = k, \quad \sigma_5 = 1$ $\sigma_2 = \frac{\alpha}{\kappa}\frac{n(\bar{z}_2/\kappa)^n}{1+(\bar{z}_2/\kappa)^n}$ $\sigma_3 = \sigma_4 = \sigma_6 = 0$	$\begin{cases} \frac{1}{k}\left(\frac{\gamma_1\gamma_2 r}{k_1} - \alpha\right) & \text{if } \alpha < \frac{\gamma_1\gamma_2 r}{k_1} \\ 0 & \text{if } \alpha > \frac{\gamma_1\gamma_2 r}{k_1} \end{cases}$	$\begin{cases} 0 & \text{if } \alpha < \frac{\gamma_1\gamma_2 r}{k_1} \\ \kappa\sqrt[n]{\frac{\alpha k_1}{\gamma_1\gamma_2 r} - 1} & \text{if } \alpha > \frac{\gamma_1\gamma_2 r}{k_1} \end{cases}$
	Multiplicative	$\sigma_1 = k, \quad \sigma_5 = 1$ $\sigma_2 = \frac{k\bar{z}_1}{\kappa}\frac{n(\bar{z}_2/\kappa)^{n-1}}{[1+(\bar{z}_2/\kappa)^n]^2}$ $\sigma_3 = \sigma_4 = \sigma_6 = 0$	$\frac{\gamma_1\gamma_2 r}{kk_1}$	0
	Degradation	$\sigma_1 = k, \quad \sigma_5 = 1$ $\sigma_2 = n\frac{\delta\gamma_2 r}{k_1}\bar{z}_2^{n-1}, \quad \sigma_3 = \delta\bar{z}_2^n$ $\sigma_4 = \sigma_6 = 0$	$\frac{\gamma_1\gamma_2 r}{kk_1}$	0
APIF Class 3	Additive	$\sigma_1 = k, \quad \sigma_5 = 1$ $\sigma_6 = \frac{\alpha}{\kappa}\frac{n(r/\kappa)^{n-1}}{[1+(r/\kappa)^n]^2}$ $\sigma_2 = \sigma_3 = \sigma_4 = 0$	$\frac{\gamma_1\gamma_2 r}{kk_1}$	0
	Multiplicative	$\sigma_1 = k, \quad \sigma_5 = \frac{1}{1+(r/\kappa)^n}$ $\sigma_6 = \frac{\mu}{\kappa}\frac{n(r/\kappa)^{n-1}}{[1+(r/\kappa)^n]^2}$ $\sigma_2 = \sigma_3 = \sigma_4 = 0$	$\frac{\gamma_1\gamma_2 r}{kk_1}$	0

Based on the table and (14), one can write the stability conditions for each APIF controller. The various stability conditions are tabulated in Figure 5 Panel B.

B Span of the APIDF controller in the PID parameter space

Lemma 1. *Consider the closed loop network given in Figure 7 Panel A whose plant is comprised of two species and is in feedback with the proposed APIDF controller with additive inhibition and hill coefficient n. Let $\tau := \frac{\gamma_1\gamma_2}{k_1}$ be a rate constant that depends solely on the plant. Then any given set of PID gains (K_P, K_I, K_D) and cutoff frequency ω_c satisfying the following constraint*

$$K_P < K_D\omega_c < \frac{n}{n+1}(K_P + \tau), \tag{15}$$

can be obtained by setting the controller parameters as

$$\begin{aligned}
\alpha &= K_D\omega_c \frac{(\kappa^n + r^n)^2}{nr^{n-1}\kappa^n} \\
\eta &= \frac{K_I\omega_c/r}{\tau - \frac{\kappa^n+r^n}{nr^n}K_D\omega_c} \\
k^{\pm} &= \frac{\omega_c\left(\tau - \frac{\kappa^n+r^n}{nr^n}K_D\omega_c\right)}{2\theta}\left[1 \pm \sqrt{1 - \frac{4K_I\theta^{\pm}}{\omega_c\left(\tau - \frac{\kappa^n+r^n}{nr^n}K_D\omega_c\right)}}\right] \\
\beta^{\pm} &= \frac{2\theta(K_D\omega_c - K_P)}{\left(\tau - \frac{\kappa^n+r^n}{nr^n}K_D\omega_c\right)\left[1 \pm \sqrt{1 - \frac{4K_I\theta^{\pm}}{\omega_c\left(\tau - \frac{\kappa^n+r^n}{nr^n}K_D\omega_c\right)}}\right]},
\end{aligned} \tag{16}$$

where r is the desired set point, and κ and $\theta^{\pm}$ are free parameters that respect the following conditions

$$\begin{cases}
\kappa & < \; r\sqrt[n]{\frac{n}{K_D\omega_c}\left[\tau - (K_D\omega_c - K_P)\right] - 1} \\
\theta^{+} & < \; \left[1 - \frac{K_D\omega_c - K_P}{\tau - \frac{\kappa^n+r^n}{nr^n}K_D\omega_c}\right]\frac{\omega_c}{K_I}\left(K_D\omega_c - K_P\right), \quad \textit{if} \quad 1 < \frac{2(K_D\omega_c - K_P)}{\tau - \frac{\kappa^n+r^n}{nr^n}K_D\omega_c} < 2 \\
\theta^{\pm} & < \; \frac{\omega_c}{4K_I}\left(\tau - \frac{\kappa^n + r^n}{nr^n}K_D\omega_c\right), \quad \textit{if} \quad 1 > \frac{2(K_D\omega_c - K_P)}{\tau - \frac{\kappa^n+r^n}{nr^n}K_D\omega_c} \\
\theta^{-} & > \; \left[1 - \frac{K_D\omega_c - K_P}{\tau - \frac{\kappa^n+r^n}{nr^n}K_D\omega_c}\right]\frac{\omega_c}{K_I}\left(K_D\omega_c - K_P\right), \quad \textit{if} \quad 1 > \frac{2(K_D\omega_c - K_P)}{\tau - \frac{\kappa^n+r^n}{nr^n}K_D\omega_c}.
\end{cases}$$

Proof. For the closed loop system under consideration, the actuation propensity is given by $h(z_1, x_2) = kz_1 + \frac{\alpha}{1+(x_2/\kappa)^n}$, and the closed loop dynamics are given by

$$\begin{aligned}
\dot{x}_1 &= kz_1 + \frac{\alpha}{1 + (x_2/\kappa)^n} - \gamma_1 x_1 \\
\dot{x}_2 &= k_1 x_1 - \gamma_2 x_2 \\
\dot{z}_1 &= \mu + \beta x_2 - \eta z_1 z_2 \\
\dot{z}_2 &= \theta x_2 - \eta z_1 z_2.
\end{aligned}$$

The fixed point is thus given by

$$\begin{bmatrix}\bar{x}_1 & \bar{x}_2 & \bar{z}_1 & \bar{z}_2\end{bmatrix} = \begin{bmatrix}\frac{\gamma_2 r}{k_1} & r & \frac{1}{k}\left(\tau r - \frac{\alpha}{1+(r/\kappa)^n}\right) & \frac{k\theta r}{\eta}\frac{1}{\tau r - \frac{\alpha}{1+(r/\kappa)^n}}\end{bmatrix},$$

where $r := \frac{\mu}{\theta - \beta}$ and $\tau := \frac{\gamma_1\gamma_2}{k_1}$. Furthermore, the partial derivatives of h are given by

$$\sigma_1 := \partial_{z_1} h(\bar{z}_1, \bar{x}_2) = k; \qquad \sigma_4 := -\partial_{x_2} h(\bar{z}_1, \bar{x}_2) = \frac{\alpha}{r}\frac{n(r/\kappa)^n}{\left[1 + (r/\kappa)^n\right]^2}.$$

By substituting the expressions of $\bar{x}_2, \bar{z}_1, \bar{z}_2, \sigma_1$ and σ_4 in (10), we obtain the following set of nonlinear algebraic equations

$$\begin{aligned}
\sigma_4 = K_D\omega_c \quad &\Longrightarrow \quad \frac{\alpha}{r}\frac{n(r/\kappa)^n}{\left[1 + (r/\kappa)^n\right]^2} = K_D\omega_c \\
\sigma_1\eta\bar{z}_1 = K_I\omega_c \quad &\Longrightarrow \quad \eta\left(\tau r - \frac{\alpha}{1 + (r/\kappa)^n}\right) = K_I\omega_c \\
\eta(\bar{z}_1 + \bar{z}_2) = \omega_c \quad &\Longrightarrow \quad \frac{\eta}{k}\left(\tau r - \frac{\alpha}{1 + (r/\kappa)^n}\right) + \frac{k\theta r}{\tau r - \frac{\alpha}{1+(r/\kappa)^n}} = \omega_c \\
\sigma_1\beta = (K_D\omega_c - K_P)\omega_c \quad &\Longrightarrow \quad k\beta = (K_D\omega_c - K_P)\omega_c.
\end{aligned} \tag{17}$$

The goal is to solve for the controller parameters $\alpha, \beta, \eta, \theta, \mu, \kappa, k$, and n given the PID gains (K_P, K_I, K_D), the cutoff frequency ω_c, the set point r, and plant time constant τ. The equations in (17) can be solved to obtain

$$\begin{aligned}
\alpha &= K_D\omega_c \frac{(\kappa^n + r^n)^2}{nr^{n-1}\kappa^n} \\
\eta &= \frac{K_I\omega_c/r}{\tau - \frac{\kappa^n+r^n}{nr^n}K_D\omega_c} \\
k^{\pm} &= \frac{\omega_c\left(\tau - \frac{\kappa^n+r^n}{nr^n}K_D\omega_c\right)}{2\theta}\left[1 \pm \sqrt{1 - \frac{4K_I\theta}{\omega_c\left(\tau - \frac{\kappa^n+r^n}{nr^n}K_D\omega_c\right)}}\right] \\
\beta^{\pm} &= \frac{2\theta(K_D\omega_c - K_P)}{\left(\tau - \frac{\kappa^n+r^n}{nr^n}K_D\omega_c\right)\left[1 \pm \sqrt{1 - \frac{4K_I\theta}{\omega_c\left(\tau - \frac{\kappa^n+r^n}{nr^n}K_D\omega_c\right)}}\right]},
\end{aligned}$$

where θ, κ, and n are free parameters that should satisfy certain conditions to ensure that the controller parameters are positive real numbers. First, we require that $\eta > 0$. This imposes a condition on the free parameter κ and restricts the allowed values of K_D and ω_c as follows.

$$\tau - \frac{\kappa^n + r^n}{nr^n}K_D\omega_c > 0 \qquad \Longrightarrow \qquad \kappa < r\sqrt[n]{\frac{n\tau}{K_D\omega_c} - 1} \quad \text{with} \quad K_D\omega_c < n\tau. \tag{18}$$

Next, we require that $k^{\pm}$ to be a real number. This imposes a condition on the free parameter θ.

$$\frac{4K_I\theta}{\omega_c\left(\tau - \frac{\kappa^n+r^n}{nr^n}K_D\omega_c\right)} < 1 \qquad \Longrightarrow \qquad \theta < \frac{\omega_c}{4K_I}\left(\tau - \frac{\kappa^n + r^n}{nr^n}K_D\omega_c\right). \tag{19}$$

Furthermore, we require that $\beta^{\pm} > 0$. This restricts the allowed values of K_D, K_P and ω_c as follows.

$$K_D\omega_c - K_P > 0 \qquad \Longrightarrow \qquad K_D\omega_c > K_P. \tag{20}$$

Finally, we require that the output $\bar{x}_2 = \frac{\mu}{\theta - \beta^{\pm}} > 0$, or equivalently $\beta^{\pm} < \theta$. We have

$$\begin{aligned}
&\frac{2\theta(K_D\omega_c - K_P)}{\left(\tau - \frac{\kappa^n+r^n}{nr^n}K_D\omega_c\right)\left[1 \pm \sqrt{1 - \frac{4K_I\theta}{\omega_c\left(\tau - \frac{\kappa^n+r^n}{nr^n}K_D\omega_c\right)}}\right]} < \theta \\
&\Longrightarrow \qquad \frac{2(K_D\omega_c - K_P)}{\tau - \frac{\kappa^n+r^n}{nr^n}K_D\omega_c} < 1 \pm \sqrt{1 - \frac{4K_I\theta}{\omega_c\left(\tau - \frac{\kappa^n+r^n}{nr^n}K_D\omega_c\right)}}.
\end{aligned} \tag{21}$$

Observe that if $\frac{2(K_D\omega_c - K_P)}{\tau - \frac{\kappa^n+r^n}{nr^n}K_D\omega_c} > 2$, then there is no $\theta > 0$ that satisfies the condition above (for both $\beta^{\pm}$). This imposes an additional condition on the free parameter κ and restricts the allowed values of K_D, ω_c and K_P as follows.

$$\frac{2(K_D\omega_c - K_P)}{\tau - \frac{\kappa^n+r^n}{nr^n}K_D\omega_c} < 2 \qquad \Longrightarrow \qquad \kappa < r\sqrt[n]{\frac{n}{K_D\omega_c}\left[\tau - (K_D\omega_c - K_P)\right] - 1} \quad \text{with} \quad K_D\omega_c < \frac{n}{n+1}(\tau + K_P). \tag{22}$$

It is easy to see that the upper bounds on κ and $K_D\omega_c$ given in (22) dominate the previously obtained upper bounds in (18) since $K_P < K_D\omega_c < n\tau$. Under conditions (22), we seek for $\theta > 0$ that satisfies (21). Two cases arise here.

First, if $1 < \frac{2(K_D\omega_c - K_P)}{\tau - \frac{\kappa^n+r^n}{nr^n}K_D\omega_c} < 2$, then β^- is rejected, and the condition becomes

$$\begin{aligned}
&\frac{2(K_D\omega_c - K_P)}{\tau - \frac{\kappa^n+r^n}{nr^n}K_D\omega_c} < 1 + \sqrt{1 - \frac{4K_I\theta^+}{\omega_c\left(\tau - \frac{\kappa^n+r^n}{nr^n}K_D\omega_c\right)}} \\
&\Longrightarrow \qquad \theta^+ < \left[1 - \frac{K_D\omega_c - K_P}{\tau - \frac{\kappa^n+r^n}{nr^n}K_D\omega_c}\right]\frac{\omega_c}{K_I}\left(K_D\omega_c - K_P\right).
\end{aligned} \tag{23}$$

It is also easy to see that condition (23) dominates condition (19) when $1 < \frac{2(K_D\omega_c - K_P)}{\tau - \frac{\kappa^n+r^n}{nr^n}K_D\omega_c} < 2$.

Second, if $\frac{2(K_D\omega_c - K_P)}{\tau - \frac{\kappa^n+r^n}{nr^n}K_D\omega_c} < 1$, then both $\beta^{\pm} > 0$ are possible. In fact, under this condition, only (19) is enough to satisfy $\beta^+ < \theta$. However, for β^-, we have

$$\begin{aligned}
&\frac{2(K_D\omega_c - K_P)}{\tau - \frac{\kappa^n+r^n}{nr^n}K_D\omega_c} < 1 - \sqrt{1 - \frac{4K_I\theta^-}{\omega_c\left(\tau - \frac{\kappa^n+r^n}{nr^n}K_D\omega_c\right)}} \\
&\Longrightarrow \qquad \theta^- > \left[1 - \frac{K_D\omega_c - K_P}{\tau - \frac{\kappa^n+r^n}{nr^n}K_D\omega_c}\right]\frac{\omega_c}{K_I}\left(K_D\omega_c - K_P\right).
\end{aligned} \tag{24}$$

Note that (19) and (24) provide an upper and lower bounds for θ when $\frac{2(K_D\omega_c - K_P)}{\tau - \frac{\kappa^n + r^n}{nr^n} K_D\omega_c} < 1$. □

Lemma 2. *Consider the closed loop network given in Figure 7 Panel A whose plant is comprised of two species and is in feedback with the proposed APIDF controller with multiplicative inhibition and hill coefficient n. Let $\tau := \frac{\gamma_1\gamma_2}{k_1}$ be a plant rate constant. Then any given set of PID gains (K_P, K_I, K_D) and cutoff frequency ω_c satisfying the following constraint*

$$K_P < K_D\omega_c < \min\{n\tau, K_P + \tau\} \tag{25}$$

can be obtained by setting the controller parameters as

$$\begin{aligned}
\kappa &= r\sqrt[n]{\frac{n\tau}{K_D\omega_c} - 1} \\
\eta &= \frac{K_I\omega_c}{\tau r} \\
k^{\pm} &= \frac{\tau\omega_c}{2\theta\left(1 - \frac{K_D\omega_c}{n\tau}\right)}\left[1 \pm \sqrt{1 - \frac{4K_I\theta}{\tau\omega_c}}\right] \\
\beta^{\pm} &= \frac{2\theta(K_D\omega_c - K_P)}{\tau\left[1 \pm \sqrt{1 - \frac{4K_I\theta}{\tau\omega_c}}\right]},
\end{aligned} \tag{26}$$

where r is the desired set point, and θ is a free parameter that respects the following condition

$$\begin{cases}
\theta^+ & < \dfrac{\omega_c}{K_I\tau}(K_D\omega_c - K_P)(\tau + K_P - K_D\omega_c) & \text{if } K_D\omega_c > \dfrac{\tau}{2} + K_P \\
\theta^{\pm} & < \dfrac{\tau\omega_c}{4K_I} & \text{if } K_D\omega_c < \dfrac{\tau}{2} + K_P \\
\theta^- & > \dfrac{\omega_c}{K_I\tau}(K_D\omega_c - K_P)(\tau + K_P - K_D\omega_c) & \text{if } K_D\omega_c < \dfrac{\tau}{2} + K_P.
\end{cases}$$

Proof. For the closed loop system under consideration, the actuation propensity is given by $h(z_1, x_2) = \frac{kz_1}{1+(x_2/\kappa)^n}$, and the closed loop dynamics are given by

$$\begin{aligned}
\dot{x}_1 &= \frac{kz_1}{1 + (x_2/\kappa)^n} - \gamma_1 x_1 \\
\dot{x}_2 &= k_1 x_1 - \gamma_2 x_2 \\
\dot{z}_1 &= \mu + \beta x_2 - \eta z_1 z_2 \\
\dot{z}_2 &= \theta x_2 - \eta z_1 z_2.
\end{aligned}$$

The fixed point is thus given by

$$\begin{bmatrix}\bar{x}_1 & \bar{x}_2 & \bar{z}_1 & \bar{z}_2\end{bmatrix} = \begin{bmatrix}\frac{\gamma_2 r}{k_1} & r & \frac{\tau r}{k}\left[1 + (r/\kappa)^n\right] & \frac{k\theta}{\eta\tau[1+(r/\kappa)^n]}\end{bmatrix},$$

where $r := \frac{\mu}{\theta - \beta}$ and $\tau := \frac{\gamma_1\gamma_2}{k_1}$. Furthermore, the partial derivatives of h are given by

$$\sigma_1 := \partial_{z_1} h(\bar{z}_1, \bar{x}_2) = \frac{k}{1 + (r/\kappa)^n}; \qquad \sigma_4 := -\partial_{x_2} h(\bar{z}_1, \bar{x}_2) = \tau\frac{n(r/\kappa)^n}{1 + (r/\kappa)^n}.$$

By substituting the expressions of $\bar{x}_2, \bar{z}_1, \bar{z}_2, \sigma_1$ and σ_4 in (10), we obtain

$$\begin{aligned}
\sigma_4 = K_D\omega_c \quad &\Longrightarrow \quad \kappa = r\sqrt[n]{\frac{n\tau}{K_D\omega_c} - 1} \quad \text{with} \quad K_D\omega_c < n\tau \\
\sigma_1\eta\bar{z}_1 = K_I\omega_c \quad &\Longrightarrow \quad \eta = \frac{K_I\omega_c}{\tau r} \\
\eta(\bar{z}_1 + \bar{z}_2) = \omega_c \quad &\Longrightarrow \quad k^{\pm} = \frac{\tau\omega_c}{2\theta\left(1 - \frac{K_D\omega_c}{n\tau}\right)}\left[1 \pm \sqrt{1 - \frac{4K_I\theta}{\tau\omega_c}}\right] \quad \text{with} \quad \theta < \frac{\tau\omega_c}{4K_I} \\
\sigma_1\beta = (K_D\omega_c - K_P)\omega_c \quad &\Longrightarrow \quad \beta^{\pm} = \frac{2\theta(K_D\omega_c - K_P)}{\tau\left[1 \pm \sqrt{1 - \frac{4K_I\theta}{\tau\omega_c}}\right]} \quad \text{with} \quad K_D\omega_c > K_P.
\end{aligned} \tag{27}$$

Finally, we require that the output $\bar{x}_2 = \frac{\mu}{\theta - \beta^{\pm}} > 0$, or equivalently $\beta^{\pm} < \theta$. We have

$$\frac{2\theta(K_D\omega_c - K_P)}{\tau\left[1 \pm \sqrt{1 - \frac{4K_I\theta}{\tau\omega_c}}\right]} < \theta \qquad \Longrightarrow \qquad \frac{K_D\omega_c - K_P}{\tau} < \frac{1}{2}\left[1 \pm \sqrt{1 - \frac{4K_I\theta}{\tau\omega_c}}\right]. \tag{28}$$

Observe that if $K_D\omega_c - K_P > \tau$, then there is no $\theta > 0$ that can satisfy (28). This imposes the condition that needs to be satisfied: $K_D\omega_c < K_P + \tau$. Under the latter condition we seek for $\theta > 0$ that satisfies (28). Two cases arise here.

First, if $\frac{1}{2} < \frac{K_D\omega_c - K_P}{\tau} < 1$, then β^- is rejected and condition (28) becomes

$$\frac{K_D\omega_c - K_P}{\tau} < \frac{1}{2}\left[1 + \sqrt{1 - \frac{4K_I\theta^+}{\tau\omega_c}}\right] \qquad \Longrightarrow \qquad \theta^+ < \frac{\omega_c}{K_I\tau}(K_D\omega_c - K_P)(\tau + K_P - K_D\omega_c),$$

which dominates the condition $\theta^+ < \frac{\tau\omega_c}{4K_I}$ when $\frac{1}{2} < \frac{K_D\omega_c - K_P}{\tau} < 1$.

Second, if $\frac{K_D\omega_c - K_P}{\tau} < \frac{1}{2}$, then both $\beta^\pm > 0$ are possible. In fact, under this condition, only $\theta^+ < \frac{\tau\omega_c}{4K_I}$ is enough to satisfy $\beta^+ < \theta^+$. However, for β^-, we have

$$\frac{K_D\omega_c - K_P}{\tau} < \frac{1}{2}\left[1 \pm \sqrt{1 - \frac{4K_I\theta}{\tau\omega_c}}\right] \qquad \Longrightarrow \qquad \theta^- > \frac{\omega_c}{K_I\tau}\left(K_D\omega_c - K_P\right)\left(\tau + K_P - K_D\omega_c\right).$$

Therefore, under the condition $\frac{K_D\omega_c - K_P}{\tau} < \frac{1}{2}$, there is a lower and upper bounds on θ^-. □

Lemma 3. *Consider the closed loop network given in Figure 7 Panel A whose plant is comprised of two species and is in feedback with the proposed APIDF controller with degradation inhibition. Let $\tau := \frac{\gamma_1\gamma_2}{k_1}$ be a plant rate constant. Then any given set of PID gains (K_P, K_I, K_D) and cutoff frequency ω_c satisfying the following constraint*

$$K_P < K_D\omega_c < \frac{n}{n-1}(K_P + \tau) \tag{29}$$

can be obtained by setting the controller parameters as

$$\begin{aligned}
\delta &= \frac{K_D\omega_c}{n\tau r^n}\gamma_1 \\
\eta &= \frac{K_I\omega_c}{\tau r\left[1 + (\delta/\gamma_1)r^n\right]} \\
k^\pm &= \frac{\omega_c\left(\tau + \frac{K_D\omega_c}{n}\right)}{2\theta}\left[1 \pm \sqrt{1 - \frac{4K_I\theta}{\tau\omega_c\left[1 + (\delta/\gamma_1)r^n\right]}}\right] \\
\beta^\pm &= \frac{2\theta(K_D\omega_c - K_P)}{\left(\tau + \frac{K_D\omega_c}{n}\right)\left[1 \pm \sqrt{1 - \frac{4K_I\theta}{\tau\omega_c[1+(\delta/\gamma_1)r^n]}}\right]},
\end{aligned} \tag{30}$$

where r is the desired set point, and θ is a free parameter that respects the following condition

$$\begin{cases}
\theta^+ < \dfrac{\tau\omega_c\left[1 + (\delta/\gamma_1)r^n\right]}{K_I\left(\tau + \frac{K_D\omega_c}{n}\right)}\left(1 - \dfrac{K_D\omega_c - K_P}{\tau + \frac{K_D\omega_c}{n}}\right)(K_D\omega_c - K_P) & \text{if } K_D\omega_c > \dfrac{n}{2n-1}(\tau + 2K_P) \\
\theta^\pm < \dfrac{\tau\omega_c}{4K_I}\left[1 + (\delta/\gamma_1)r^n\right] & \text{if } K_D\omega_c < \dfrac{n}{2n-1}(\tau + 2K_P) \\
\theta^- > \dfrac{\tau\omega_c\left[1 + (\delta/\gamma_1)r^n\right]}{K_I\left(\tau + \frac{K_D\omega_c}{n}\right)}\left(1 - \dfrac{K_D\omega_c - K_P}{\tau + \frac{K_D\omega_c}{n}}\right)(K_D\omega_c - K_P) & \text{if } K_D\omega_c < \dfrac{n}{2n-1}(\tau + 2K_P).
\end{cases}$$

Proof. For the closed loop system under consideration, the actuation propensity is given by $h(z_1, x_2) = kz_1 - \delta x_1 x_2^n$, and the closed loop dynamics are given by

$$\begin{aligned}
\dot{x}_1 &= kz_1 - \delta x_1 x_2^n - \gamma_1 x_1 \\
\dot{x}_2 &= k_1 x_1 - \gamma_2 x_2 \\
\dot{z}_1 &= \mu + \beta x_2 - \eta z_1 z_2 \\
\dot{z}_2 &= \theta x_2 - \eta z_1 z_2.
\end{aligned}$$

The fixed point is thus given by

$$\begin{bmatrix}\bar{x}_1 & \bar{x}_2 & \bar{z}_1 & \bar{z}_2\end{bmatrix} = \begin{bmatrix}\frac{\gamma_2 r}{k_1} & r & \frac{\tau r}{k}\left[1 + (\delta/\gamma_1)r^n\right] & \frac{k\theta}{\eta\tau[1+(\delta/\gamma_1)r^n]}\end{bmatrix},$$

where $r := \frac{\mu}{\theta - \beta}$ and $\tau := \frac{\gamma_1\gamma_2}{k_1}$. Furthermore, the partial derivatives of h are given by

$$\sigma_1 := \partial_{z_1} h(\bar{z}_1, \bar{x}_2) = k; \qquad \sigma_4 := -\partial_{x_2} h(\bar{z}_1, \bar{x}_2) = n\tau(\delta/\gamma_1)r^n.$$

By substituting the expressions of $\bar{x}_2, \bar{z}_1, \bar{z}_2, \sigma_1$ and σ_4 in (10), we obtain the following set of nonlinear algebraic equations

$$\begin{aligned}
\sigma_4 = K_D\omega_c \quad &\Longrightarrow \quad \delta = \frac{K_D\omega_c}{n\tau r^n}\gamma_1 \\
\sigma_1\eta\bar{z}_1 = K_I\omega_c \quad &\Longrightarrow \quad \eta = \frac{K_I\omega_c}{\tau r\left[1+(\delta/\gamma_1)r^n\right]} \\
\eta(\bar{z}_1+\bar{z}_2) = \omega_c \quad &\Longrightarrow \quad k^{\pm} = \frac{\omega_c\left(\tau+\frac{K_D\omega_c}{n}\right)}{2\theta}\left[1\pm\sqrt{1-\frac{4K_I\theta}{\tau\omega_c\left[1+(\delta/\gamma_1)r^n\right]}}\right] \\
\sigma_1\beta = (K_D\omega_c - K_P)\omega_c \quad &\Longrightarrow \quad \beta^{\pm} = \frac{2\theta(K_D\omega_c-K_P)}{\left(\tau+\frac{K_D\omega_c}{n}\right)\left[1\pm\sqrt{1-\frac{4K_I\theta}{\tau\omega_c[1+(\delta/\gamma_1)r^n]}}\right]} \quad \text{with} \quad K_D\omega_c > K_P,
\end{aligned} \tag{31}$$

where $\theta < \frac{\tau\omega_c}{4K_I}\left[1+(\delta/\gamma_1)r^n\right]$ has to be satisfied to guarantee that $k^{\pm}$ is a real number.

Finally, we require that the output $\bar{x}_2 = \frac{\mu}{\theta-\beta^{\pm}} > 0$, or equivalently $\beta^{\pm} < \theta$. We have

$$\frac{2\theta(K_D\omega_c-K_P)}{\left(\tau+\frac{K_D\omega_c}{n}\right)\left[1\pm\sqrt{1-\frac{4K_I\theta}{\tau\omega_c[1+(\delta/\gamma_1)r^n]}}\right]} < \theta \qquad \Longrightarrow \qquad \frac{K_D\omega_c-K_P}{\tau+\frac{K_D\omega_c}{n}} < \frac{1}{2}\left[1\pm\sqrt{1-\frac{4K_I\theta}{\tau\omega_c\left[1+(\delta/\gamma_1)r^n\right]}}\right]. \tag{32}$$

Observe that if $K_D\omega_c - K_P > \tau + \frac{K_D\omega_c}{n}$, then there is no $\theta > 0$ that can satisfy (32). This imposes the condition that needs to be satisfied: $K_D\omega_c < \frac{n}{n-1}(K_P+\tau)$. Under the latter condition we seek for $\theta > 0$ that satisfies (32). Two cases arise here.

First, if $\frac{1}{2} < \frac{K_D\omega_c-K_P}{\tau+\frac{K_D\omega_c}{n}} < 1$, then β^- is rejected and condition (32) becomes

$$\begin{aligned}
&\frac{K_D\omega_c-K_P}{\tau+\frac{K_D\omega_c}{n}} < \frac{1}{2}\left[1+\sqrt{1-\frac{4K_I\theta^+}{\tau\omega_c\left[1+(\delta/\gamma_1)r^n\right]}}\right] \\
\Longrightarrow \qquad &\theta^+ < \frac{\tau\omega_c\left[1+(\delta/\gamma_1)r^n\right]}{K_I\left(\tau+\frac{K_D\omega_c}{n}\right)}\left(1-\frac{K_D\omega_c-K_P}{\tau+\frac{K_D\omega_c}{n}}\right)(K_D\omega_c-K_P),
\end{aligned}$$

which dominates the previous condition $\theta < \frac{\tau\omega_c}{4K_I}\left[1+(\delta/\gamma_1)r^n\right]$ when $\frac{1}{2} < \frac{K_D\omega_c-K_P}{\tau+\frac{K_D\omega_c}{n}} < 1$.

Second, if $\frac{K_D\omega_c-K_P}{\tau+\frac{K_D\omega_c}{n}} < \frac{1}{2}$, then both $\beta^{\pm} > 0$ are possible. In fact, under this condition, only $\theta^+ < \frac{\tau\omega_c}{4K_I}\left[1+(\delta/\gamma_1)r^n\right]$ is enough to satisfy $\beta^+ < \theta^+$. However, for β^-, we have

$$\begin{aligned}
\frac{K_D\omega_c-K_P}{\tau} < \frac{1}{2}\left[1\pm\sqrt{1-\frac{4K_I\theta}{\tau\omega_c}}\right] \qquad &\Longrightarrow \qquad \theta^- > \frac{\omega_c}{K_I\tau}(K_D\omega_c-\tau)(\tau+K_P-K_D\omega_c) \\
&\Longrightarrow \qquad \theta^- > \frac{\tau\omega_c\left[1+(\delta/\gamma_1)r^n\right]}{K_I\left(\tau+\frac{K_D\omega_c}{n}\right)}\left(1-\frac{K_D\omega_c-K_P}{\tau+\frac{K_D\omega_c}{n}}\right)(K_D\omega_c-K_P).
\end{aligned}$$

Therefore, under the condition $\frac{K_D\omega_c-K_P}{\tau+\frac{K_D\omega_c}{n}} < \frac{1}{2}$, there is a lower and upper bounds on θ^-. □

C Stationary Variance Approximation for the APIF Controllers

Consider the closed loop network depicted in Panel A of Figure 5 where a gene expression plant is connected in feedback with a class of APIF controllers. The goal of this section is to derive an approximate formula for the stationary variance of the output species $\mathbf{X_2}$. We only consider APIF controllers of Class 1. First, we consider a general plant to write down the evolution equations of the variance. Then, we derive a closed formula for the output stationary variance in the case of the particular gene expression plant given in Panel A of Figure 5.

C.1 Evolution of the Covariances for a General Plant

Let $X_{cl} := \begin{bmatrix} X \\ Z \end{bmatrix}$ denote the closed loop state variable encrypting the copy numbers of the plant and controller species $\mathbf{X}$ and $\mathbf{Z}$, respectively. Define the instantaneous covariance of the closed loop state variable as

$$\mathrm{Cov}\left[X_{cl}(t)\right] := \mathbb{E}\left[\Big(X_{cl}(t)-\mathbb{E}\left[X_{cl}(t)\right]\Big)\Big(X_{cl}(t)-\mathbb{E}\left[X_{cl}(t)\right]\Big)^T\right],$$

whose evolution is described by the following differential equation (we drop the time variable for notational convenience)

$$\frac{d}{dt}\mathrm{Cov}\left[X_{cl}\right] = S_{cl}\mathcal{D}\big(\mathbb{E}\left[\lambda_{cl}(X_{cl})\right]\big)S_{cl}^T + S_{cl}\mathrm{Cov}\left[\lambda_{cl}(X_{cl}), X_{cl}\right] + \mathrm{Cov}\left[X_{cl}, \lambda_{cl}(X_{cl})\right]S_{cl}^T, \tag{33}$$

where S_{cl} and λ_{cl}, depicted in Figure 3, denote the closed loop stoichiometry matrix and propensity function, respectively. Note that $\mathcal{D}$ is the diagonal operator such that for any vector x, $\mathcal{D}(x)$ is a diagonal matrix whose diagonal entries are x. Define the matrices and vector

$$S_m := \begin{bmatrix} 0 & 0 & 0 & 1 & -1 \\ \vdots & \vdots & \vdots & 0 & 0 \\ \vdots & \vdots & \vdots & \vdots & \vdots \\ 0 & 0 & 0 & 0 & 0 \end{bmatrix}_{L\times 5}, \quad S_c := \begin{bmatrix} 0 & -1 & 1 & 0 & 0 \\ 1 & -1 & 0 & 0 & 0 \end{bmatrix}, \quad \lambda_c(x,z) := \begin{bmatrix} \theta x_L \\ \eta z_1 z_2 \\ \mu \\ h^+(z_1, x_L) \\ h^-(x_1, x_L) \end{bmatrix},$$

so that the closed loop stoichiometry matrix and propensity function can be written as $S_{cl} = \begin{bmatrix} S & S_m \\ 0 & S_c \end{bmatrix}$ and $\lambda_{cl}(x,z) = \begin{bmatrix} \lambda(x) \\ \lambda_c(x,z) \end{bmatrix}$, respectively. Note that h^+ and h^- are functions that can take the forms given in Figure 3. By substituting the plant and controller components of X_{cl}, S_{cl}, and λ_{cl} in (33), we proceed as follows

$$\begin{aligned}\frac{d}{dt}\begin{bmatrix} \mathrm{Cov}\left[X\right] & \mathrm{Cov}\left[X,Z\right] \\ \mathrm{Cov}\left[Z,X\right] & \mathrm{Cov}\left[Z\right] \end{bmatrix} &= \begin{bmatrix} S & S_m \\ 0 & S_c \end{bmatrix}\begin{bmatrix} \mathcal{D}\big(\mathbb{E}\left[\lambda(X)\right]\big) & 0 \\ 0 & \mathcal{D}\big(\mathbb{E}\left[\lambda_c(X,Z)\right]\big) \end{bmatrix}\begin{bmatrix} S^T & 0 \\ S_m^T & S_c^T \end{bmatrix} \\ &+ \begin{bmatrix} S & S_m \\ 0 & S_c \end{bmatrix}\begin{bmatrix} \mathrm{Cov}\left[\lambda(X), X\right] & \mathrm{Cov}\left[\lambda(X), Z\right] \\ \mathrm{Cov}\left[\lambda_c(X,Z), X\right] & \mathrm{Cov}\left[\lambda_c(X,Z), Z\right] \end{bmatrix} \\ &+ \begin{bmatrix} \mathrm{Cov}\left[X, \lambda(X)\right] & \mathrm{Cov}\left[X, \lambda_c(X,Z)\right] \\ \mathrm{Cov}\left[Z, \lambda(X)\right] & \mathrm{Cov}\left[Z, \lambda_c(X,Z)\right] \end{bmatrix}\begin{bmatrix} S^T & 0 \\ S_m^T & S_c^T \end{bmatrix}\end{aligned}$$

Thus we have

$$\begin{aligned}\frac{d}{dt}\mathrm{Cov}\left[X\right] &= S\mathcal{D}\big(\mathbb{E}\left[\lambda(X)\right]\big)S^T + S_m\mathcal{D}\big(\mathbb{E}\left[\lambda_c(X,Z)\right]\big)S_m^T + S\mathrm{Cov}\left[\lambda(X), X\right] + S_m\mathrm{Cov}\left[\lambda_c(X,Z), X\right] \\ &\quad + \mathrm{Cov}\left[X, \lambda(X)\right]S^T + \mathrm{Cov}\left[X, \lambda_c(X,Z)\right]S_m^T \\ \frac{d}{dt}\mathrm{Cov}\left[X,Z\right] &= S_m\mathcal{D}\big(\mathbb{E}\left[\lambda_c(X,Z)\right]\big)S_c^T + S\mathrm{Cov}\left[\lambda(X), Z\right] + S_m\mathrm{Cov}\left[\lambda_c(X,Z), Z\right] + \mathrm{Cov}\left[X, \lambda_c(X,Z)\right]S_c^T \\ \frac{d}{dt}\mathrm{Cov}\left[Z\right] &= S_c\mathcal{D}\big(\mathbb{E}\left[\lambda_c(X,Z)\right]\big)S_c^T + S_c\mathrm{Cov}\left[\lambda_c(X,Z), Z\right] + \mathrm{Cov}\left[Z, \lambda_c(X,Z)\right]S_c^T.\end{aligned}$$

Next, by substituting for S_m, S_c and $\lambda_c(X,Z)$ and doing some algebraic calculations, we obtain

$$\begin{cases} \frac{d}{dt}\mathrm{Cov}\left[X\right] = S\mathcal{D}\big(\mathbb{E}\left[\lambda(X)\right]\big)S^T + \mathbb{E}\left[h\left(Z_1, X_1, X_l\right)\right]e_1e_1^T + S\mathrm{Cov}\left[\lambda(X), X\right] + e_1\mathrm{Cov}\left[h\left(Z_1, X_1, X_L\right), X\right] \\ \qquad\qquad + \mathrm{Cov}\left[X, \lambda(X)\right]S^T + \mathrm{Cov}\left[X, h\left(Z_1, X_1, X_L\right)\right]e_1^T \\ \frac{d}{dt}\mathrm{Cov}\left[X, Z_1\right] = S\mathrm{Cov}\left[\lambda(X), Z_1\right] + \mathrm{Cov}\left[h(Z_1, X_1, X_L), Z_1\right]e_1 - \eta\mathrm{Cov}\left[X, Z_1Z_2\right] \\ \frac{d}{dt}\mathrm{Cov}\left[X, Z_2\right] = S\mathrm{Cov}\left[\lambda(X), Z_2\right] + \mathrm{Cov}\left[h(Z_1, X_1, X_L), Z_2\right]e_1 - \eta\mathrm{Cov}\left[X, Z_1Z_2\right] + \theta\mathrm{Cov}\left[X, X_L\right] \\ \frac{d}{dt}\mathrm{Var}\left[Z_1\right] = \mu + \eta\mathbb{E}\left[Z_1Z_2\right] - 2\eta\mathrm{Cov}\left[Z_1, Z_1Z_2\right] \\ \frac{d}{dt}\mathrm{Var}\left[Z_2\right] = \theta\mathbb{E}\left[X_L\right] + \eta\mathbb{E}\left[Z_1Z_2\right] - 2\eta\mathrm{Cov}\left[Z_2, Z_1Z_2\right] + 2\theta\mathrm{Cov}\left[X_L, Z_2\right] \\ \frac{d}{dt}\mathrm{Cov}\left[Z_1, Z_2\right] = \eta\mathbb{E}\left[Z_1Z_2\right] - \eta\mathrm{Cov}\left[Z_1 + Z_2, Z_1Z_2\right] + \theta\mathrm{Cov}\left[X_L, Z_1\right], \end{cases} \tag{34}$$

where, as in Figure 3, the actuation propensity function is defined as $h(z_1, x_1, x_L) := h^+(z_1, x_L) - h^-(x_1, x_L)$, and e_i is a vector whose entries are all zeros except the ith entry is one. Note that h does not depend on z_2 in this section because only APIF controllers of Class 1 are considered. The set of differential equations in (34) describe the evolution of the various covariances in the closed loop network. Observe that it does not involve first and second order moments only (expectations and covariances), but also third order moments like $\mathrm{Cov}\left[X, Z_1Z_2\right]$ and $\mathrm{Cov}\left[Z_1 + Z_2, Z_1Z_2\right]$ that have there own differential equations. This, in addition to the nonlinearity of λ and h (in general), give rise to the moment closure problem.

C.2 Steady-State (Stationary) Analysis

Let $\mathbb{E}_\pi[\cdot], \mathrm{Var}_\pi[\cdot]$, and $\mathrm{Cov}_\pi[\cdot,\cdot]$ denote the the stationary expectation, variance and covariance, respectively. Assuming that the closed loop system is ergodic, the various time derivatives in (7) and (34) are set to zero at stationarity. Particularly, we have the following relationships that hold regardless of what the plant is

$$\begin{aligned}
\frac{d}{dt}\left(\mathbb{E}_\pi[Z_1]-\mathbb{E}_\pi[Z_2]\right)=0 \quad &\Longrightarrow \quad \mathbb{E}_\pi[X_L]=\frac{\mu}{\theta}\\
\frac{d}{dt}\mathbb{E}_\pi[Z_1]=0 \quad &\Longrightarrow \quad \mathbb{E}_\pi[Z_1Z_2]=\frac{\mu}{\eta}\\
\frac{d}{dt}\mathrm{Var}_\pi[Z_1]=0 \quad &\Longrightarrow \quad \mathrm{Cov}_\pi[Z_1,Z_1Z_2]=\frac{\mu}{\eta}\\
\frac{d}{dt}\left(\mathrm{Var}_\pi[Z_1]+\mathrm{Var}_\pi[Z_2]-2\mathrm{Cov}_\pi[Z_1,Z_2]\right)=0 \quad &\Longrightarrow \quad \mathrm{Cov}_\pi[X_L,Z_1-Z_2]=\frac{\mu}{\theta}\\
\frac{d}{dt}\mathrm{Var}_\pi[Z_2]=0 \quad &\Longrightarrow \quad \mathrm{Cov}_\pi[Z_2,Z_1Z_2]=\frac{\mu+\theta\mathrm{Cov}_\pi[X_L,Z_2]}{\eta}.
\end{aligned} \tag{35}$$

These relationships will be useful in what follows, particularly in the asymptotic limit as $\eta\to\infty$.

C.3 Application to Gene Expression

Consider the case where the plant is simple gene expression described in Panel A of Figure 5. The plant stoichiometry matrix and propensity vector are given by

$$S=\begin{bmatrix}0 & -1 & 0\\ 1 & 0 & -1\end{bmatrix} \qquad \text{and} \qquad \lambda(x)=\begin{bmatrix}k_1x_1\\ \gamma_1x_1\\ \gamma_2x_2\end{bmatrix}.$$

Then, by substituting S and λ in (7) and (34), we obtain the the following set of differential equations for the expectations and covariances

$$\begin{cases}
\frac{d}{dt}\mathbb{E}[X_1]=\mathbb{E}[h(Z_1,X_1,X_2)]-\gamma_1\mathbb{E}[X_1]\\
\frac{d}{dt}\mathbb{E}[X_2]=k_1\mathbb{E}[X_1]-\gamma_2\mathbb{E}[X_2]\\
\frac{d}{dt}\mathbb{E}[Z_1]=\mu-\eta\mathbb{E}[Z_1Z_2]\\
\frac{d}{dt}\mathbb{E}[Z_2]=\theta\mathbb{E}[X_2]-\eta\mathbb{E}[Z_1Z_2],
\end{cases}$$

$$\begin{cases}
\frac{d}{dt}\mathrm{Var}[X_1]=\gamma_1\mathbb{E}[X_1]+\mathbb{E}[h(Z_1,X_1,X_2)]-2\gamma_1\mathrm{Var}[X_1]+2\mathrm{Cov}[X_1,h(Z_1,X_1,X_2)]\\
\frac{d}{dt}\mathrm{Var}[X_2]=\gamma_2\mathbb{E}[X_2]+k_1\mathbb{E}[X_1]-2\gamma_2\mathrm{Var}[X_2]+2k_1\mathrm{Cov}[X_1,X_2]\\
\frac{d}{dt}\mathrm{Cov}[X_1,X_2]=k_1\mathrm{Var}[X_1]-(\gamma_1+\gamma_2)\mathrm{Cov}[X_1,X_2]+\mathrm{Cov}[X_2,h(Z_1,X_1,X_2)]\\
\frac{d}{dt}\mathrm{Cov}[X_1,Z_1]=-\gamma_1\mathrm{Cov}[X_1,Z_1]+\mathrm{Cov}[h(Z_1,X_1,X_2),Z_1]-\eta\mathrm{Cov}[X_1,Z_1Z_2]\\
\frac{d}{dt}\mathrm{Cov}[X_1,Z_2]=-\gamma_1\mathrm{Cov}[X_1,Z_2]+\mathrm{Cov}[h(Z_1,X_1,X_2),Z_2]-\eta\mathrm{Cov}[X_1,Z_1Z_2]+\theta\mathrm{Cov}[X_1,X_2]\\
\frac{d}{dt}\mathrm{Cov}[X_2,Z_1]=-\gamma_2\mathrm{Cov}[X_2,Z_1]+k_1\mathrm{Cov}[X_1,Z_1]-\eta\mathrm{Cov}[X_2,Z_1Z_2]\\
\frac{d}{dt}\mathrm{Cov}[X_2,Z_2]=-\gamma_2\mathrm{Cov}[X_2,Z_2]+k_1\mathrm{Cov}[X_1,Z_2]-\eta\mathrm{Cov}[X_2,Z_1Z_2]+\theta\mathrm{Var}[X_2]\\
\frac{d}{dt}\mathrm{Var}[Z_1]=\mu+\eta\mathbb{E}[Z_1Z_2]-2\eta\mathrm{Cov}[Z_1Z_2,Z_1]\\
\frac{d}{dt}\mathrm{Var}[Z_2]=\theta\mathbb{E}[X_2]+\eta\mathbb{E}[Z_1Z_2]-2\eta\mathrm{Cov}[Z_1Z_2,Z_2]+2\theta\mathrm{Cov}[X_2,Z_2]\\
\frac{d}{dt}\mathrm{Cov}[Z_1,Z_2]=\eta\mathbb{E}[Z_1Z_2]-\eta\mathrm{Cov}[Z_1Z_2,Z_1+Z_2]+\theta\mathrm{Cov}[X_2,Z_1]
\end{cases}$$

Steady-State (Stationary) Analysis: Assuming that the closed loop system is ergodic, the time derivatives at stationarity are set to zero. We have

$$\mathbb{E}_\pi[X_2]=\frac{\mu}{\theta}; \qquad \mathbb{E}_\pi[X_1]=\frac{\gamma_2}{k_1}\frac{\mu}{\theta}; \qquad \mathbb{E}_\pi[h(Z_1,X_1,X_2)]=\frac{\gamma_1\gamma_2}{k_1}\frac{\mu}{\theta}; \qquad \mathbb{E}_\pi[Z_1Z_2]=\frac{\mu}{\eta};$$

To compute the steady-state variance $\mathrm{Var}_\pi[X_2]$, we use the following set of algebraic equations

$$\begin{aligned}
\frac{d}{dt}\mathrm{Var}_\pi[X_2] = 0 \quad &\Longrightarrow \quad \mathrm{Var}_\pi[X_2] = \frac{\mu}{\theta} + \frac{k_1}{\gamma_2}\mathrm{Cov}_\pi[X_1, X_2] \\
\frac{d}{dt}\mathrm{Cov}_\pi[X_1, X_2] = 0 \quad &\Longrightarrow \quad \mathrm{Cov}_\pi[X_1, X_2] = \frac{k_1}{\gamma_1+\gamma_2}\mathrm{Var}_\pi[X_1] + \frac{1}{\gamma_1+\gamma_2}\mathrm{Cov}_\pi[X_2, h(Z_1, X_1, X_2)] \\
\frac{d}{dt}\mathrm{Var}_\pi[X_1] = 0 \quad &\Longrightarrow \quad \mathrm{Var}_\pi[X_1] = \frac{\gamma_2}{k_1}\frac{\mu}{\theta} + \frac{1}{\gamma_1}\mathrm{Cov}_\pi[X_1, h(Z_1, X_1, X_2)] \\
\frac{d}{dt}\mathrm{Cov}_\pi[X_2, Z_1 - Z_2] = 0 \quad &\Longrightarrow \quad \mathrm{Cov}_\pi[X_1, Z_1 - Z_2] = \frac{\gamma_2}{k_1}\frac{\mu}{\theta} + \frac{\theta}{k_1}\mathrm{Var}_\pi[X_2],
\end{aligned} \tag{36}$$

where the last equality follows by exploiting the fact that $\mathrm{Cov}_\pi[X_2, Z_1 - Z_2] = \mu/\theta$ from (35). Observe that these algebraic equations cannot be solved exactly for $\mathrm{Var}_\pi[X_2]$ because of the moment closure problem. However, to proceed, we give an approximation for the covariance terms $\mathrm{Cov}_\pi[X_i, h(Z_1, X_1, X_2)]$ for $i = 1, 2$. The approximation essentially (1) exploits a second order Taylor expansion of the function h around the stationary expected values , and (2) exploits the fact that for large η, $\mathbb{E}_\pi[Z_1 Z_2] = \frac{\mu}{\eta} \approx 0$ and Z_2 is assumed to be close to zero unlike Z_1 which takes positive values actuating the plant. In fact, these approximations are summarized below.

$$\begin{aligned}
&\mathbb{E}_\pi[Z_1 Z_2] \approx 0, \qquad \mathrm{Cov}_\pi[X_1, Z_2] \approx 0, \qquad \mathrm{Cov}_\pi[X_2, Z_2] \approx 0 \\
&h(Z_1, X_1, X_2) \approx \bar{h} + \begin{bmatrix}\partial_{z_1}\bar{h} & \partial_{x_1}\bar{h} & \partial_{x_2}\bar{h}\end{bmatrix}\begin{bmatrix} Z_1 - \mathbb{E}_\pi[Z_1] \\ X_1 - \mathbb{E}_\pi[X_1] \\ X_2 - \mathbb{E}_\pi[X_2]\end{bmatrix} \\
&\qquad + \frac{1}{2}\begin{bmatrix} Z_1 - \mathbb{E}_\pi[Z_1] \\ X_1 - \mathbb{E}_\pi[X_1] \\ X_2 - \mathbb{E}_\pi[X_2]\end{bmatrix}^T \begin{bmatrix} \partial^2_{z_1}\bar{h} & \partial_{z_1}\partial_{x_1}\bar{h} & \partial_{z_1}\partial_{x_2}\bar{h} \\ \partial_{x_1}\partial_{z_1}\bar{h} & \partial^2_{x_1}\bar{h} & \partial_{x_1}\partial_{x_2}\bar{h} \\ \partial_{x_2}\partial_{z_1}\bar{h} & \partial_{x_2}\partial_{x_1}\bar{h} & \partial^2_{x_2}\bar{h}\end{bmatrix}\begin{bmatrix} Z_1 - \mathbb{E}_\pi[Z_1] \\ X_1 - \mathbb{E}_\pi[X_1] \\ X_2 - \mathbb{E}_\pi[X_2]\end{bmatrix},
\end{aligned}$$

where $\bar{h} := h\Big(\mathbb{E}_\pi[Z_1], \mathbb{E}_\pi[X_1], \mathbb{E}_\pi[X_2]\Big)$. Using Appendix F (with $X := \begin{bmatrix} Z_1 & X_1 & X_2\end{bmatrix}^T$, $F(X) = X_1$, and $G(X) = h(Z_1, X_1, X_2)$), we can approximate $\mathrm{Cov}_\pi[X_1, h(Z_1, X_1, X_2)]$ up to first order (or second order if the stationary distribution is close to a normal distribution) as

$$\begin{aligned}
\mathrm{Cov}_\pi[X_1, h(Z_1, X_1, X_2)] &\approx \begin{bmatrix}0 & 1 & 0\end{bmatrix}\begin{bmatrix} \mathrm{Var}_\pi[Z_1] & \mathrm{Cov}_\pi[Z_1, X_1] & \mathrm{Cov}_\pi[Z_1, X_2] \\ \mathrm{Cov}_\pi[X_1, Z_1] & \mathrm{Var}_\pi[X_1] & \mathrm{Cov}_\pi[X_1, X_2] \\ \mathrm{Cov}_\pi[X_2, Z_1] & \mathrm{Cov}_\pi[X_2, X_1] & \mathrm{Var}_\pi[X_2]\end{bmatrix}\begin{bmatrix}\partial_{z_1}\bar{h} \\ \partial_{x_1}\bar{h} \\ \partial_{x_2}\bar{h}\end{bmatrix} \\
&\approx \sigma_1 \mathrm{Cov}_\pi[X_1, Z_1] - \sigma_3 \mathrm{Var}_\pi[X_1] - \sigma_4 \mathrm{Cov}_\pi[X_1, X_2],
\end{aligned}$$

where

$$\begin{aligned}
\sigma_1 &:= \partial_{z_1} h(\mathbb{E}_\pi[Z_1], \mathbb{E}_\pi[X_1], \mathbb{E}_\pi[X_2]) > 0 \\
\sigma_3 &:= -\partial_{x_1} h(\mathbb{E}_\pi[Z_1], \mathbb{E}_\pi[X_1], \mathbb{E}_\pi[X_2]) \geq 0 \\
\sigma_4 &:= -\partial_{x_2} h(\mathbb{E}_\pi[Z_1], \mathbb{E}_\pi[X_1], \mathbb{E}_\pi[X_2]) \geq 0.
\end{aligned}$$

Similarly, we can approximate $\mathrm{Cov}_\pi[X_2, h(Z_1, X_1, X_2)]$ as

$$\begin{aligned}
\mathrm{Cov}_\pi[X_2, h(Z_1, X_1, X_2)] &\approx \begin{bmatrix}0 & 0 & 1\end{bmatrix}\begin{bmatrix} \mathrm{Var}_\pi[Z_1] & \mathrm{Cov}_\pi[Z_1, X_1] & \mathrm{Cov}_\pi[Z_1, X_2] \\ \mathrm{Cov}_\pi[X_1, Z_1] & \mathrm{Var}_\pi[X_1] & \mathrm{Cov}_\pi[X_1, X_2] \\ \mathrm{Cov}_\pi[X_2, Z_1] & \mathrm{Cov}_\pi[X_2, X_1] & \mathrm{Var}_\pi[X_2]\end{bmatrix}\begin{bmatrix}\partial_{z_1}\bar{h} \\ \partial_{x_1}\bar{h} \\ \partial_{x_2}\bar{h}\end{bmatrix} \\
&\approx \sigma_1 \mathrm{Cov}_\pi[X_2, Z_1] - \sigma_3 \mathrm{Cov}_\pi[X_2, X_1] - \sigma_4 \mathrm{Var}_\pi[X_2].
\end{aligned}$$

Invoking the approximations $\mathrm{Cov}_\pi[X_1, Z_2] \approx \mathrm{Cov}_\pi[X_2, Z_2] \approx 0$ and the last equation in (36), we obtain

$$\begin{aligned}
\mathrm{Cov}_\pi[X_1, Z_1] &\approx \mathrm{Cov}_\pi[X_1, Z_1 - Z_2] = \frac{\gamma_2}{k_1}\frac{\mu}{\theta} + \frac{\theta}{k_1}\mathrm{Var}_\pi[X_2] \\
\mathrm{Cov}_\pi[X_2, Z_1] &\approx \mathrm{Cov}_\pi[X_2, Z_1 - Z_2] = \frac{\mu}{\theta}.
\end{aligned}$$

Then we have

$$\begin{aligned}
\mathrm{Cov}_\pi[X_1, h(Z_1, X_1, X_2)] &\approx \sigma_1\frac{\gamma_2}{k_1}\frac{\mu}{\theta} + \sigma_1\frac{\theta}{k_1}\mathrm{Var}_\pi[X_2] - \sigma_3 \mathrm{Var}_\pi[X_1] - \sigma_4 \mathrm{Cov}_\pi[X_1, X_2] \\
\mathrm{Cov}_\pi[X_2, h(Z_1, X_1, X_2)] &\approx \sigma_1\frac{\mu}{\theta} - \sigma_3 \mathrm{Cov}_\pi[X_1, X_2] - \sigma_4 \mathrm{Var}_\pi[X_2].
\end{aligned}$$

Finally, by substituting for $\mathrm{Cov}_\pi\left[X_1, h(Z_1, X_1, X_2)\right]$ and $\mathrm{Cov}_\pi\left[X_2, h(Z_1, X_1, X_2)\right]$ in (36), we obtain the following set of algebraic (approximate) equations

$$\begin{aligned}
\mathrm{Var}_\pi\left[X_2\right] &\approx \frac{\mu}{\theta} + \frac{k_1}{\gamma_2}\mathrm{Cov}_\pi\left[X_1, X_2\right] \\
\mathrm{Cov}_\pi\left[X_1, X_2\right] &\approx \frac{k_1}{\gamma_1+\gamma_2}\mathrm{Var}_\pi\left[X_1\right] + \frac{1}{\gamma_1+\gamma_2}\left(\sigma_1\frac{\mu}{\theta} - \sigma_4\mathrm{Var}_\pi\left[X_2\right] - \sigma_3\mathrm{Cov}\left[X_1, X_2\right]\right) \\
\mathrm{Var}_\pi\left[X_1\right] &\approx \frac{\gamma_2}{k_1}\frac{\mu}{\theta} + \frac{1}{\gamma_1}\left(\sigma_1\frac{\gamma_2}{k_1}\frac{\mu}{\theta} + \sigma_1\frac{\theta}{k_1}\mathrm{Var}_\pi\left[X_2\right] - \sigma_3\mathrm{Var}_\pi\left[X_1\right] - \sigma_4\mathrm{Cov}_\pi\left[X_1, X_2\right]\right).
\end{aligned}$$

This can be written in matrix form as

$$\begin{bmatrix} 1+\frac{\sigma_3}{\gamma_1} & -\frac{\sigma_1}{\gamma_1}\frac{\theta}{k_1} & \frac{\sigma_4}{\gamma_1} \\ 0 & 1 & -\frac{k_1}{\gamma_2} \\ -k_1 & \sigma_4 & \gamma_1+\gamma_2+\sigma_3 \end{bmatrix} \begin{bmatrix} \mathrm{Var}_\pi\left[X_1\right] \\ \mathrm{Var}_\pi\left[X_2\right] \\ \mathrm{Cov}_\pi\left[X_1, X_2\right] \end{bmatrix} = \begin{bmatrix} \left(1+\frac{\sigma_1}{\gamma_1}\right)\frac{\gamma_2}{k_1}\frac{\mu}{\theta} \\ \frac{\mu}{\theta} \\ \sigma_1\frac{\mu}{\theta} \end{bmatrix}.$$

Finally, solving for $\mathrm{Var}_\pi\left[X_2\right]$, we arrive at

$$\mathrm{Var}_\pi\left[X_2\right] \approx \frac{\mu}{\theta}\left[\frac{\left(\gamma_1+\gamma_2+\sigma_3\right)\left(\gamma_1\gamma_2+\gamma_2\sigma_3+\sigma_1 k_1\right) + k_1\gamma_2(\gamma_1+\sigma_4)}{\left(\gamma_1+\gamma_2+\sigma_3\right)\left(\gamma_1\gamma_2+\gamma_2\sigma_3+k_1\sigma_4\right) - \sigma_1 k_1\theta}\right].$$

This is a general formula that encompasses the standalone AIF controller and the three APIF controllers of Class 1, that are addressed as a special case next.

AIF: For this controller, the propensities of the actuation reactions are given by

$$h^+(z_1, x_2) = kz_1 \qquad \text{and} \qquad h^-(x_1, x_2) = 0,$$

which implies that $h(z_1, x_1, x_2) = kz_1$. Then $\sigma_1 = k$ and $\sigma_3 = \sigma_4 = 0$.

APIF of Class 1 with Additive Inhibition: The propensities of the actuation reactions are given by

$$h^+(z_1, x_2) = kz_1 + \frac{\alpha}{1+(x_2/\kappa)^n} \qquad \text{and} \qquad h^-(x_1, x_2) = 0,$$

which implies that $h(z_1, x_1, x_2) = kz_1 + \frac{\alpha}{1+(x_2/\kappa)^n}$. Then we have

$$\sigma_1 = k, \qquad \sigma_3 = 0, \qquad \text{and} \quad \sigma_4 = \frac{\alpha}{r}\frac{n(r/\kappa)^n}{\left[1+(r/\kappa)^n\right]^2}.$$

APIF of Class 1 with Multiplicative Inhibition: The propensities of the actuation reactions are given by

$$h^+(z_1, x_2) = \frac{kz_1}{1+(x_2/\kappa)^n} \qquad \text{and} \qquad h^-(x_1, x_2) = 0,$$

which implies that $h(z_1, x_1, x_2) = \frac{kz_1}{1+(x_2/\kappa)^n}$. Then we have

$$\sigma_1 = \frac{k}{1+(r/\kappa)^n}, \qquad \sigma_3 = 0, \qquad \text{and} \qquad \sigma_4 = \frac{k\mathbb{E}_\pi\left[Z_1\right]}{r}\frac{n(r/\kappa)^n}{\left[1+(r/\kappa)^n)\right]^2}.$$

We are left with approximating $\mathbb{E}_\pi\left[Z_1\right]$. This can be done by recalling that $\mathbb{E}_\pi\left[h(Z_1, X_1, X_2)\right] = \frac{\gamma_1\gamma_2}{k_1}\frac{\mu}{\theta}$ and using a first order Taylor series expansion of h around stationarity. That is

$$\begin{aligned}
\mathbb{E}_\pi\left[h\Big(\mathbb{E}_\pi\left[Z_1\right], \mathbb{E}_\pi\left[X_1\right], \mathbb{E}_\pi\left[X_2\right]\Big)\right] &\approx \frac{\gamma_1\gamma_2}{k_1}r \\
\frac{k\mathbb{E}_\pi\left[Z_1\right]}{1+(r/\kappa)^n} &\approx \frac{\gamma_1\gamma_2}{k_1}r \\
\mathbb{E}_\pi\left[Z_1\right] &\approx \frac{\gamma_1\gamma_2}{kk_1}r\left[1+(r/\kappa)^n\right].
\end{aligned}$$

Finally, substituting for $\mathbb{E}_\pi\left[Z_1\right]$ in σ_4 yields

$$\sigma_4 = \frac{\gamma_1\gamma_2}{k_1}\frac{n(r/\kappa)^n}{1+(r/\kappa^n)}.$$

APIF of Class 1 with Degradation Inhibition: The propensities of the actuation reactions are given by

$$h^+(z_1, x_2) = kz_1 \qquad \text{and} \qquad h^-(x_1, x_2) = \delta x_1 x_2^n,$$

which implies that $h(z_1, x_1, x_2) = kz_1 - \delta x_1 x_2^n$. Then we have

$$\sigma_1 = k, \qquad \sigma_3 = \delta r^n, \qquad \text{and} \quad \sigma_4 = n\frac{\delta\gamma_2}{k_1} r^n.$$

The results are summarized in Table 1.

D Stochastic Analysis of the Fictitious PID Controller

Consider the closed loop network depicted in Figure 8 but with a general (linear) unimolecular plant that constitutes L species denote by $\mathbf{X} := \{\mathbf{X_1}, \mathbf{X_2}, \mathbf{X_L}\}$. First we write down the evolution equations of the covaraince for the general linear plant. Then we derive a closed formula for the stationary variance of the output species $\mathbf{X_L}$ when $L = 1$.

D.1 Evolution of the Expectations and Covariances for a General Unimolecular Plant

Let $X_{cl} := \begin{bmatrix} X \\ Z \end{bmatrix}$ denote the closed loop state variable encrypting the copy numbers of the plant and controller species $\mathbf{X}$ and $\mathbf{Z}$, respectively. Let S_{cl} and λ_{cl} denote the closed loop stoichiometry matrix and propensity function, respectively. By exploiting the structure of the controller in Figure 8, we can write the closed loop stoichiometry matrix and propensity function as

$$S_{cl} = \begin{bmatrix} S & S_m \\ 0 & S_c \end{bmatrix} \quad \text{with} \quad S_m := \begin{bmatrix} 0 & 0 & 0 & 0 & 1 & -1 \\ \vdots & \vdots & \vdots & \vdots & 0 & 0 \\ \vdots & \vdots & \vdots & \vdots & \vdots & \vdots \\ 0 & 0 & 0 & 0 & 0 & 0 \end{bmatrix}_{L\times 6} \quad \text{and} \quad S_c := \begin{bmatrix} 1 & -1 & 0 & 0 & 0 & 0 \\ 0 & 0 & 1 & -1 & 0 & 0 \end{bmatrix}$$

$$\lambda_{cl}(x_{cl}) = W_{cl} x_{cl} + w_{cl}; \quad W_{cl} := \begin{bmatrix} W & 0 \\ W_{c_1} & W_{c_2} \end{bmatrix}; \quad w_{cl} := \begin{bmatrix} w \\ w_c \end{bmatrix};$$

$$W_{c_1} := \begin{bmatrix} 0 \\ e_L^T \\ 0 \\ \omega_c e_L^T \\ 0 \\ (K_P + K_D\omega_c) e_L^T \end{bmatrix}_{6\times L}; \quad W_{c_2} := \begin{bmatrix} 0 & 0 \\ 0 & 0 \\ 0 & 0 \\ 0 & \omega_c \\ K_I & 0 \\ 0 & K_D\omega_c \end{bmatrix}; \quad w_c := \begin{bmatrix} r \\ 0 \\ \omega_c r \\ 0 \\ (K_P + K_D\omega_c) r \\ 0 \end{bmatrix},$$

where $\lambda(x) = Wx + w$ is the affine propensity function the general unimolecular plant.

D.1.1 Evolution of Expectations

The evolution of the first moment is described by the following differential equation

$$\frac{d}{dt}\mathbb{E}\left[X_{cl}(t)\right] = S_{cl}\mathbb{E}\left[\lambda_{cl}\Big(X(t), Z(t)\Big)\right] = S_{cl}\left(W_{cl}\mathbb{E}\left[X_{cl}\right] + w_{cl}\right) =: A\mathbb{E}\left[X_{cl}\right] + b,$$

where

$$A = \begin{bmatrix} S & S_m \\ 0 & S_c \end{bmatrix} \begin{bmatrix} W & 0 \\ W_{c_1} & W_{c_2} \end{bmatrix} = \begin{bmatrix} SW + S_m W_{c_1} & S_m W_{c_2} \\ S_c W_{c_1} & S_c W_{c_2} \end{bmatrix} = \begin{bmatrix} SW - (K_P + K_D\omega_c) e_1 e_L^T & K_I e_1 & -K_D\omega_c e_1 \\ -e_L^T & 0 & 0 \\ -\omega_c e_L^T & 0 & -\omega_c \end{bmatrix}$$

$$b = \begin{bmatrix} S & S_m \\ 0 & S_c \end{bmatrix} \begin{bmatrix} w \\ w_c \end{bmatrix} = \begin{bmatrix} Sw + S_m w_c \\ S_c w_c \end{bmatrix} = \begin{bmatrix} Sw + (K_P + K_D\omega_c) r e_1 \\ r \\ \omega_c r \end{bmatrix}.$$

Therefore, the evolution of the expectations is governed by the following set of differential equations

$$\begin{cases} \dfrac{d}{dt}\mathbb{E}\left[X\right] = SW\mathbb{E}\left[X\right] + Sw + \mathbb{E}\left[U\right] e_1; \qquad U := -(K_P + K_D\omega_c) X_L + K_I Z_1 - K_D\omega_c Z_2 + (K_P + K_D\omega_c) r \\ \dfrac{d}{dt}\mathbb{E}\left[Z_1\right] = r - \mathbb{E}\left[X_L\right] \\ \dfrac{d}{dt}\mathbb{E}\left[Z_2\right] = -\omega_c\mathbb{E}\left[Z_2\right] + \omega_c\left(r - \mathbb{E}\left[X_L\right]\right). \end{cases}$$

D.1.2 Evolution of the Covariances

Define the covariance of the closed loop state variable as

$$\mathrm{Cov}\left[X_{cl}(t)\right] := \mathbb{E}\left[\Big(X_{cl}(t) - \mathbb{E}\left[X_{cl}(t)\right]\Big)\Big(X_{cl}(t) - \mathbb{E}\left[X_{cl}(t)\right]\Big)^T\right].$$

The evolution of the covariances is described by the following differential equation (we drop the time variable for notational convenience)

$$\begin{aligned}\frac{d}{dt}\mathrm{Cov}\left[X_{cl}\right] &= S_{cl}\mathcal{D}\big(\mathbb{E}\left[\lambda_{cl}(X_{cl})\right]\big)S_{cl}^T + S_{cl}\mathrm{Cov}\left[\lambda_{cl}(X_{cl}), X_{cl}\right] + \mathrm{Cov}\left[X_{cl}, \lambda_{cl}(X_{cl})\right]S_{cl}^T \\ &= S_{cl}\mathcal{D}\big(W_{cl}\mathbb{E}\left[X_{cl}\right] + w_{cl}\big)S_{cl}^T + S_{cl}W_{cl}\mathrm{Cov}\left[X_{cl}\right] + \mathrm{Cov}\left[X_{cl}\right]W_{cl}^T S_{cl}^T.\end{aligned}$$

Note that $\mathcal{D}$ is the diagonal operator such that for any vector x, $\mathcal{D}(x)$ is a diagonal matrix whose diagonal entries are x. Therefore, the dynamics of the covariance can be rewritten, in matrix form, as a differential Lyapunov equation

$$\begin{aligned}&\frac{d}{dt}\mathrm{Cov}\left[X_{cl}\right] = A\mathrm{Cov}\left[X_{cl}\right] + \mathrm{Cov}\left[X_{cl}\right]A^T + Q, \\ &\text{where} \qquad A := \begin{bmatrix} SW - (K_P + K_D\omega_c)e_1e_L^T & K_Ie_1 & -K_D\omega_ce_1 \\ -e_L^T & 0 & 0 \\ -\omega_ce_L^T & 0 & -\omega_c \end{bmatrix} \\ &\qquad Q(t) := \left[\begin{array}{c|cc} S\mathcal{D}\left(W\mathbb{E}\left[X(t)\right] + w\right)S^T + \mathbb{E}\left[V(t)\right]e_1e_1^T & \multicolumn{2}{c}{0} \\ \hline 0 & \mathbb{E}\left[X_L(t)\right] + r & 0 \\ & 0 & \omega_c(\mathbb{E}\left[X_L(t)\right] + \mathbb{E}\left[Z_2(t)\right] + r) \end{array}\right] \\ &\qquad V(t) := (K_P + K_D\omega_c)(X_L(t) + r) + K_IZ_1(t) + K_D\omega_cZ_2(t).\end{aligned}$$

Particularly, we the following differential equations for $\mathrm{Var}\left[Z_1\right], \mathrm{Var}\left[Z_2\right]$ and $\mathrm{Cov}\left[Z_1, Z_2\right]$, regardless of what the plant is:

$$\begin{cases} \frac{d}{dt}\mathrm{Var}\left[Z_1\right] = \mathbb{E}\left[X_L\right] + r - 2\mathrm{Cov}\left[X_L, Z_1\right] \\ \frac{d}{dt}\mathrm{Var}\left[Z_2\right] = \omega_c\left(r + \mathbb{E}\left[X_L\right] + \mathbb{E}\left[Z_2\right] - 2\mathrm{Cov}\left[X_L, Z_2\right] - 2\mathrm{Var}\left[Z_2\right]\right) \\ \frac{d}{dt}\mathrm{Cov}\left[Z_1, Z_2\right] = -\mathrm{Cov}\left[X_L, Z_2\right] - \omega_c\mathrm{Cov}\left[Z_1, X_L\right] - \omega_c\mathrm{Cov}\left[Z_1, Z_2\right]. \end{cases}$$

D.2 Stationary Analysis for a General Unimolecular Plant

Let $\mathbb{E}_\pi\left[\cdot\right], \mathrm{Var}_\pi\left[\cdot\right]$, and $\mathrm{Cov}_\pi\left[\cdot,\cdot\right]$ denote the the stationary expectation, variance and covariance. Assuming ergodicity of the closed loop system, the various time derivatives are set to zero at stationarity. We have the following relationships, regardless of what the plant is

$$\begin{aligned} \frac{d}{dt}\mathbb{E}_\pi\left[Z_1\right] = 0 \quad &\Longrightarrow \quad \mathbb{E}_\pi\left[X_L\right] = r \\ \frac{d}{dt}\mathbb{E}_\pi\left[Z_2\right] = 0 \quad &\Longrightarrow \quad \mathbb{E}_\pi\left[Z_2\right] = 0 \\ \frac{d}{dt}\mathrm{Var}_\pi\left[Z_1\right] = 0 \quad &\Longrightarrow \quad \mathrm{Cov}_\pi\left[X_L, Z_1\right] = r \\ \frac{d}{dt}\mathrm{Var}_\pi\left[Z_2\right] = 0 \quad &\Longrightarrow \quad \mathrm{Cov}_\pi\left[Z_2, X_l + Z_2\right] = r \\ \frac{d}{dt}\mathrm{Cov}_\pi\left[Z_1, Z_2\right] = 0 \quad &\Longrightarrow \quad \mathrm{Cov}_\pi\left[Z_2, X_L + \omega_cZ_1\right] = -\omega_cr. \end{aligned}$$

Stationary Expectations: Define $\hat{X} := \begin{bmatrix} X_1 & \cdots & X_{L-1} \end{bmatrix}^T$ so that $X = \begin{bmatrix} \hat{X}^T & X_L \end{bmatrix}^T$. Furthermore, partition the matrix $W := \begin{bmatrix} W_1 & W_L \end{bmatrix}$ where W_L is a column vector. At stationary, we have $\mathbb{E}_\pi\left[X_L\right] = r$ and

$\mathbb{E}_\pi[Z_2] = 0$ and thus

$$\begin{aligned}
& S\left(W\mathbb{E}_\pi[X] + w\right) + K_I\mathbb{E}_\pi[Z_1]\, e_1 = 0 \\
\implies \quad & S\left(\begin{bmatrix} W_1 & W_L \end{bmatrix}\begin{bmatrix} \mathbb{E}_\pi\left[\hat{X}\right] \\ r \end{bmatrix} + w\right) + K_I\mathbb{E}_\pi[Z_1]\, e_1 = 0 \\
\implies \quad & S\left(W_1\mathbb{E}_\pi\left[\hat{X}\right] + W_L r + w\right) + K_I\mathbb{E}_\pi[Z_1]\, e_1 = 0 \\
\implies \quad & SW_1\mathbb{E}_\pi\left[\hat{X}\right] + K_I\mathbb{E}_\pi[Z_1]\, e_1 = -S(W_L r + w) \\
\implies \quad & \begin{bmatrix} SW_1 & K_I e_1 \end{bmatrix}\begin{bmatrix} \mathbb{E}_\pi\left[\hat{X}\right] \\ \mathbb{E}_\pi[Z_1] \end{bmatrix} = -S(W_L r + w).
\end{aligned}$$

The last equation is a system of linear equations that can be solved for $\mathbb{E}_\pi\left[\hat{X}_1\right]$ and $\mathbb{E}_\pi[Z_1]$.

Stationary Covariances: The stationary covariance satisfies the following algebraic Lyapunov equation

$$A\mathrm{Cov}_\pi[X_{cl}] + \mathrm{Cov}_\pi[X_{cl}]\, A^T + Q_{ss} = 0,$$

where

$$Q_{ss} := \left[\begin{array}{c|cc} S\mathcal{D}\left(W\mathbb{E}_\pi[X] + w\right) S^T + \left(2r(K_P + K_D\omega_c) + K_I\mathbb{E}_\pi[Z_1]\right) e_1 e_1^T & \multicolumn{2}{c}{0} \\ \hline 0 & 2r & 0 \\ & 0 & 2\omega_c r \end{array}\right].$$

D.3 Application to a Plant with One Species

Consider the case where the plant is comprised of only one species given in Figure 8. The plant stoichiometry matrix and propensity vector are given by

$$S = -1 \qquad \text{and} \qquad \lambda(x) = \gamma x.$$

That is, $W = \gamma$ and $w = 0$ and the index $L = 1$ is suppressed. Then we have

$$\begin{aligned}
A &:= \begin{bmatrix} -(K_P + K_D\omega_c + \gamma) & K_I & -K_D\omega_c \\ -1 & 0 & 0 \\ -\omega_c & 0 & -\omega_c \end{bmatrix} \\
Q(t) &:= \begin{bmatrix} \gamma\mathbb{E}[X(t)] + \mathbb{E}[V(t)] & 0 & 0 \\ 0 & \mathbb{E}[X(t)] + r & 0 \\ 0 & 0 & \omega_c(\mathbb{E}[X] + \mathbb{E}[Z_2] + r) \end{bmatrix} \\
V(t) &:= (K_P + K_D\omega_c)(X(t) + r) + K_I Z_1(t) + K_D\omega_c Z_2(t) \\
b &:= \begin{bmatrix} (K_P + K_D\omega_c)r \\ r \\ \omega_c r \end{bmatrix}.
\end{aligned}$$

Deterministic Stability: The differential equation describing the deterministic dynamics (or equivalently the expectation dynamics) is given by

$$\dot{x}_{cl} = Ax_{cl} + b.$$

The characteristic polynomial is given by

$$p(s) := \det(sI - A) = s^3 + (K_P + K_D\omega_c + \omega_c + \gamma)\, s^2 + (K_I + \omega_c K_P + \omega_c\gamma)\, s + \omega_c K_I.$$

To determine the stability conditions, we construct the Routh table.

s^3	1	$K_I + \omega_c K_P + \omega_c\gamma$
s^2	$(K_P + K_D\omega_c + \omega_c + \gamma)$	$\omega_c K_I$
s^1	$\frac{\omega_c^2(K_P+\gamma)+(K_P+K_D\omega_c+\gamma)(K_I+\omega_c K_P+\omega_c\gamma)}{K_P+K_D\omega_c+\omega_c+\gamma}$	0
s^0	$\omega_c K_I$	0

Clearly the deterministic dynamics (and first moment dynamics) are unconditionally stable for all $\omega_c, K_I, K_P, K_D, \gamma > 0$.

Expectation and Covariance Evolution: The evolution of the expectations are governed by the following set of differential equations

$$\begin{cases} \frac{d}{dt}\mathbb{E}\left[X_1\right] = -\gamma\mathbb{E}\left[X\right] + \mathbb{E}\left[U\right]; \qquad U := (K_P + K_D\omega_c)(r - X) + K_I Z_1 - K_D\omega_c Z_2 \\ \frac{d}{dt}\mathbb{E}\left[Z_1\right] = r - \mathbb{E}\left[X\right] \\ \frac{d}{dt}\mathbb{E}\left[Z_2\right] = -\omega_c\mathbb{E}\left[Z_2\right] + \omega_c\left(r - \mathbb{E}\left[X\right]\right). \end{cases}$$

and the evolution of the covariances are governed by the following differential Lyapunov equation

$$\begin{aligned} &\frac{d}{dt}\mathrm{Cov}\left[X_{cl}\right] = A\mathrm{Cov}\left[X_{cl}\right] + \mathrm{Cov}\left[X_{cl}\right]A^T + Q, \\ \text{where} \qquad &A := \begin{bmatrix} -(K_P + K_D\omega_c + \gamma) & K_I & -K_D\omega_c \\ -1 & 0 & 0 \\ -\omega_c & 0 & -\omega_c \end{bmatrix} \\ &Q := \begin{bmatrix} \gamma\mathbb{E}\left[X\right] + \mathbb{E}\left[V\right] & 0 & 0 \\ 0 & \mathbb{E}\left[X\right] + r & 0 \\ 0 & 0 & \omega_c(\mathbb{E}\left[X\right] + \mathbb{E}\left[Z_2\right] + r) \end{bmatrix} \\ &V := (K_P + K_D\omega_c)(X_2 + r) + K_I Z_1 + K_D\omega_c Z_2. \end{aligned}$$

Steady-State (Stationary) Analysis: Assuming that the closed loop system is ergodic, the time derivatives of the stationary variances and covariances are set to zero. We have

$$\mathbb{E}_\pi\left[X\right] = r; \qquad \mathbb{E}_\pi\left[Z_2\right] = 0; \qquad \mathbb{E}_\pi\left[Z_1\right] = \frac{\gamma}{K_I}r.$$

To calculate the steady-state variance $\mathrm{Var}_\pi\left[X\right]$, we solve the algebraic Lyapunov equation

$$A\mathrm{Cov}_\pi\left[X_{cl}\right] + \mathrm{Cov}_\pi\left[X_{cl}\right]A^T + Q_{ss} = 0; \quad \text{with} \quad Q_{ss} := \begin{bmatrix} 2\left(\gamma + K_P + K_D\omega_c\right)r + & 0 & 0 \\ 0 & 2r & 0 \\ 0 & 0 & 2\omega_c r \end{bmatrix}.$$

Finally, we obtain

$$\mathrm{Var}_\pi\left[X\right] = r\left(1 + \frac{\omega_c K_I(K_P + K_D\omega_c + \gamma) + \omega_c^2(K_I + K_D\omega_c) + K_D^2\omega_c^3 + K_I^2}{(K_P + K_D\omega_c + \gamma)(K_I + \omega_c(K_P + \gamma)) + \omega_c^2(K_P + \gamma)}\right).$$

The derivative component in the controller is filtered with a cutoff frequency ω_c. The larger ω_c is, the more the filtered derivative resembles a pure derivative controller. In fact, in the asymptotic limit as $\omega_c \to \infty$, the stationary variance grows like $\frac{K_D\omega_c}{K_P+\gamma}$ to infinity. This also shows that for large ω_c, the stationary variance increases with the derivative gain.

Let us study the effect of K_D on the stationary variance for finite values of the cutoff frequency ω_c. For simplicity, let $\bar{K}_P := K_P + \gamma$. We have

$$\begin{aligned} \frac{d}{dK_D}\mathrm{Var}_\pi\left[X\right] &= r\left(\frac{c_2K_D^2 + 2c_1K_D + c_0}{T^2}\right) \\ c_2 &:= \omega_c^4\left(K_I + \omega_c\bar{K}_P\right) \\ c_1 &:= \omega_c^3\bar{K}_P\left(\omega_c^2 + \omega_c\bar{K}_P + K_I\right) \\ c_0 &:= \omega_c\left(\omega_c^2 + \omega_c\bar{K}_P + K_I\right)\left(\omega_c^2\bar{K}_P - K_I^2\right) \\ T &:= (\bar{K}_P + K_D\omega_c)(K_I + \omega_c\bar{K}_P) + \omega_c^2\bar{K}_P. \end{aligned}$$

The derivative of the stationary variance with respect to K_D can be zero for the following two values of K_D

$$K_D^\pm = \frac{-c_1 \pm \sqrt{c_1^2 - c_2c_0}}{c_2}.$$

Clearly K_D^- is either negative or imaginary. On the other hand, K_D^+ is either negative or imaginary when $c_0 > 0$. This means that for $c_0 > 0$, the derivative is positive for all $K_D \geq 0$. But when $c_0 < 0$, one can show that $K_D^+ > 0$ for all parameters ω_c, K_P, and K_D. This follows because

$$\begin{aligned} c_1^2 - c_2c_0 &= \omega_c^6\bar{K}_P^2\left[\omega_c^2 + \omega_c\bar{K}_P + K_I\right]^2 - \omega_c^5\left[K_I + \omega_c\bar{K}_P\right]\left(\omega_c^2 + \omega_c\bar{K}_P + K_I\right)\left(\omega_c^2\bar{K}_P - K_I^2\right) \\ &= \omega_c^5\left[\omega_c^2 + \omega_c\bar{K}_P + K_I\right]\left[\omega_c\bar{K}_P^2[\omega_c + \omega_c\bar{K}_P + K_I] - [K_I + \omega_c\bar{K}_P][\omega_c^2\bar{K}_P - K_I^2]\right] \\ &= \omega_c^5\left[\omega_c^2 + \omega_c\bar{K}_P + K_I\right]\left[\left(K_I^2 - \omega_c^2\bar{K}_P\right)\left(K_I + \omega_c\bar{K}_P\right) + \omega_c\bar{K}_P^2\left(K_I + \omega_c\bar{K}_P + \omega_c^2\right)\right], \end{aligned}$$

which shows that $c_1^2 - c_2 c_0 > 0$ when $K_I^2 - \omega_c^2 \bar{K}_P > 0$ (i.e. $c_0 < 0$). This calculation verifies that K_D^+ is a real number. Finally, it is straight forward to see that it is also positive when $c_0 < 0$. The conclusion that can be drawn here is that when $\omega_c > K_I/\sqrt{K_P + \gamma}$, the stationary variance $\mathrm{Var}_\pi[X]$ increases with K_D. But when $\omega_c < K_I/\sqrt{K_P + \gamma}$, the stationary variance $\mathrm{Var}_\pi[X]$ first decreases with K_D until $K_D = K_D^{\mathrm{Th}} := \frac{-c_1 + \sqrt{c_1^2 - c_2 c_0}}{c_2}$, after which the stationary variance starts to increase. The results are summarized in the table of Figure 8.

E Useful Covariance Identities

Let X, Y and Z be two vector-valued random variables of possibly different dimensions. Let $X := \begin{bmatrix} X_1 \\ X_2 \end{bmatrix}$ and $Y := \begin{bmatrix} Y_1 \\ Y_2 \end{bmatrix}$, where X_1, X_2, Y_1 and Y_2 are all vector-valued random variables. Let A and B be two deterministic matrices with suitable dimensions. Furthermore, let b be a deterministic vector. We have the following identities.

1. $\mathrm{Cov}[X, Y] := \mathbb{E}\left[\big(X - \mathbb{E}[X]\big)\big(Y - \mathbb{E}[Y]\big)^T\right] = \mathbb{E}\left[XY^T\right] - \mathbb{E}[X]\,\mathbb{E}\left[Y^T\right]$
2. $\mathrm{Cov}[X, Y] = \mathrm{Cov}[Y, X]^T$
3. $\mathrm{Cov}[b, X] = 0$
4. $\mathrm{Cov}[AX, BY] = A\mathrm{Cov}[X, Y]\,B^T$.
5. $\mathrm{Cov}[X, Y] = \begin{bmatrix}\mathrm{Cov}[X, Y_1] & \mathrm{Cov}[X, Y_2]\end{bmatrix} = \begin{bmatrix}\mathrm{Cov}[X_1, Y] \\ \mathrm{Cov}[X_2, Y]\end{bmatrix} = \begin{bmatrix}\mathrm{Cov}[X_1, Y_1] & \mathrm{Cov}[X_1, Y_2] \\ \mathrm{Cov}[X_2, Y_1] & \mathrm{Cov}[X_2, Y_2]\end{bmatrix}$
6. $\mathrm{Cov}[X_1 + X_2, Y_1 + Y_2] = \mathrm{Cov}[X_1, Y_1] + \mathrm{Cov}[X_1, Y_2] + \mathrm{Cov}[X_2, Y_1] + \mathrm{Cov}[X_2, Y_2]$
7. $\mathrm{Cov}\left[b^T X, X^T A X\right] = \sum_{i,j,k} b_k A_{ij} \mathrm{Cov}[X_k, X_i X_j]$
8. $\mathrm{Cov}\left[X^T A X, X^T B X\right] = \sum_{i,j,k,l} A_{ij} B_{k,l} \mathrm{Cov}[X_i X_j, X_k X_l]$

The proofs of 1 through 6 are straight forward. The proofs of 7 and 8 are given below.

Proof of 7.

$$\begin{aligned}
\mathrm{Cov}\left[b^T X, X^T A X\right] &= \mathbb{E}\left[b^T X X^T A X\right] - \mathbb{E}\left[b^T X\right]\mathbb{E}\left[X^T A X\right] \\
&= \mathbb{E}\left[\sum_k b_k X_k \sum_{i,j} A_{ij} X_i X_j\right] - \mathbb{E}\left[\sum_k b_k X_k\right]\mathbb{E}\left[\sum_{i,j} A_{ij} X_i X_j\right] \\
&= \sum_{i,j,k} b_k A_{ij}\Big(\mathbb{E}[X_k X_i X_j] - \mathbb{E}[X_k]\,\mathbb{E}[X_i X_j]\Big) \\
&= \sum_{i,j,k} b_k A_{ij} \mathrm{Cov}[X_k, X_i X_j]
\end{aligned}$$

□

Proof of 8.

$$\begin{aligned}
\mathrm{Cov}\left[X^T A X, X^T B X\right] &= \mathbb{E}\left[X^T A X X^T B X\right] - \mathbb{E}\left[X^T A X\right]\mathbb{E}\left[X^T B X\right] \\
&= \mathbb{E}\left[\sum_{i,j} A_{ij} X_i X_j \sum_{k,l} B_{kl} X_k X_l\right] - \mathbb{E}\left[\sum_{i,j} A_{ij} X_i X_j\right]\mathbb{E}\left[\sum_{k,l} B_{kl} X_k X_l\right] \\
&= \sum_{i,j,k,l} A_{ij} B_{kl}\Big(\mathbb{E}[X_i X_j X_k X_l] - \mathbb{E}[X_i X_j]\,\mathbb{E}[X_k X_l]\Big) \\
&= \sum_{i,j,k,l} A_{ij} B_{kl} \mathrm{Cov}[X_i X_j, X_k X_l]
\end{aligned}$$

□

F Useful Expectation and Covariance Approximations

Let $F, G : \mathbb{R}^n \to \mathbb{R}$ and $X \in \mathbb{R}^n$. We have the following approximations

1. $\mathbb{E}[F(X)] \approx F(\mathbb{E}[X]) + \frac{1}{2}\text{tr}\left\{\partial^2 F(\mathbb{E}[X])\text{Cov}[X]\right\}$
2. $\text{Cov}[F(X), G(X)] \approx \partial F(\mathbb{E}[X])\text{Cov}[X]\,\partial G(\mathbb{E}[X])^T$
3. If X follows a multivariate normal distribution, we have

$$\text{Cov}[F(X), G(X)] \approx \partial F(\mathbb{E}[X])\text{Cov}[X]\,\partial G(\mathbb{E}[X])^T + \frac{1}{2}\text{tr}\left\{\partial^2 F(\mathbb{E}[X])\text{Cov}[X]\,\partial^2 G(\mathbb{E}[X])\text{Cov}[X]\right\}.$$

Note that (1) and (3) are second order approximations while (2) is a first order approximation.

Proof of 1. A second order approximation of F around the expected value of X, denoted here as $\bar{X}$ for convenience, can be written as

$$F(X) \approx F(\bar{X}) + \partial F(\bar{X})(X - \bar{X}) + \frac{1}{2}(X - \bar{X})^T \partial^2 F(\bar{X})(X - \bar{X}),$$

where $\partial F(\bar{X})$ (resp. $\partial^2 F(\bar{X})$) is a row vector (resp. square matrix) whose dimension is n (resp. $n \times n$) that represents the directional derivative of F (respectively Hessian), evaluated at $\bar{X}$. Taking the expectation of $F(X)$ yields

$$\begin{aligned}\mathbb{E}[F(X)] &\approx F(\bar{X}) + \frac{1}{2}\mathbb{E}\left[(X - \bar{X})^T \partial^2 F(\bar{X})(X - \bar{X})\right] \\ &\approx F(\bar{X}) + \frac{1}{2}\text{tr}\left\{\partial^2 F(\bar{X})\text{Cov}[X]\right\},\end{aligned}$$

where the first approximate equality follows from the fact that $\mathbb{E}\left[X - \bar{X}\right] = 0$, and the second approximate equality follows from the circular property of the trace operator. □

Proof of 2. Using a first order Taylor expansion for F and G around the expectation of X, denoted here by $\bar{X}$ for convenience, we proceed as follows

$$\begin{aligned}\text{Cov}[F(X), G(X)] &\approx \text{Cov}\left[F(\bar{X}) + \partial F(\bar{X})(X - \bar{X}), G(\bar{X}) + \partial G(\bar{X})(X - \bar{X})\right] \\ &\approx \text{Cov}\left[\partial F(\bar{X})(X - \bar{X}), \partial G(\bar{X})(X - \bar{X})\right] \\ &\approx \partial F(\bar{X})\text{Cov}\left[X - \bar{X}\right]\partial G(\bar{X})^T,\end{aligned}$$

which follows by exploiting identity 4 in Appendix E. The proof is complete since $\text{Cov}\left[X - \bar{X}\right] = \text{Cov}[X]$. □

Proof of 3. Using a second order Taylor expansion for F and G around the expectation of X, denoted here by $\bar{X}$, we proceed as follows

$$\begin{aligned}&\text{Cov}[F(X), G(X)] \\ &\approx \text{Cov}\left[F(\bar{X}) + \partial F(\bar{X})(X - \bar{X}) + \frac{1}{2}(X - \bar{X})^T \partial^2 F(\bar{X})(X - \bar{X}), G(\bar{X}) + \partial G(\bar{X})(X - \bar{X}) + \frac{1}{2}(X - \bar{X})^T \partial^2 G(\bar{X})(X - \bar{X})\right] \\ &\approx \text{Cov}\left[\partial F(\bar{X})(X - \bar{X}) + \frac{1}{2}(X - \bar{X})^T \partial^2 F(\bar{X})(X - \bar{X}), \partial G(\bar{X})(X - \bar{X}) + \frac{1}{2}(X - \bar{X})^T \partial^2 G(\bar{X})(X - \bar{X})\right] \\ &\approx \partial F(\bar{X})\text{Cov}\left[X - \bar{X}\right]\partial G(\bar{X})^T + \frac{1}{2}\partial F(\bar{X})\text{Cov}\left[X - \bar{X}, (X - \bar{X})^T \partial^2 G(\bar{X})(X - \bar{X})\right] \\ &\qquad + \frac{1}{2}\text{Cov}\left[(X - \bar{X})^T \partial^2 F(\bar{X})(X - \bar{X}), X - \bar{X}\right]\partial G(\bar{X})^T \\ &\qquad + \frac{1}{4}\text{Cov}\left[(X - \bar{X})^T \partial^2 F(\bar{X})(X - \bar{X}), (X - \bar{X})^T \partial^2 G(\bar{X})(X - \bar{X})\right]\end{aligned}$$

Define the following deterministic vectors $a := \partial F(\bar{X})^T$ and $b := \partial G(\bar{X})^T$ and define the following symmetric matrices $A := \partial^2 F(\bar{X})$ and $B := \partial^2 G(\bar{X})$. Then we have

$$\begin{aligned}\text{Cov}[F(X), G(X)] \approx a^T\text{Cov}\left[X - \bar{X}\right]b &+ \frac{1}{2}\text{Cov}\left[a^T(X - \bar{X}), (X - \bar{X})^T B(X - \bar{X})\right] \\ &+ \frac{1}{2}\text{Cov}\left[b^T(X - \bar{X}), (X - \bar{X})^T A(X - \bar{X})\right] \\ &+ \frac{1}{4}\text{Cov}\left[(X - \bar{X})^T A(X - \bar{X}), (X - \bar{X})^T B(X - \bar{X})\right].\end{aligned}$$

Now, let's calculate each term separately. First we have that $\mathrm{Cov}\left[X-\bar{X}\right] = \mathrm{Cov}\left[X\right]$. The second term is calculated next using property 7.

$$\mathrm{Cov}\left[a^T(X-\bar{X}),(X-\bar{X})^T B(X-\bar{X})\right] = \sum_{i,j,k} a_k B_{i,j} \mathrm{Cov}\left[X_k-\bar{X}_k,(X_i-\bar{X}_i)(X_j-\bar{X}_j)\right] = 0,$$

because the odd central moments of a multivariate normal distribution are all zeros. The second term is also zero for the same reason. We are left with the last term which we calculate using property 8.

$$\begin{aligned}\mathrm{Cov}\left[(X-\bar{X})^T A(X-\bar{X}),(X-\bar{X})^T B(X-\bar{X})\right] &= \sum_{i,j,k,l} A_{ij}B_{kl}\mathbb{E}\left[(X_i-\bar{X}_i)(X_j-\bar{X}_j)(X_k-\bar{X}_k)(X_l-\bar{X}_l)\right] \\ &\quad - \sum_{i,j,k,l} A_{ij}B_{kl}\mathbb{E}\left[(X_i-\bar{X}_i)(X_j-\bar{X}_j)\right]\mathbb{E}\left[(X_k-\bar{X}_k)(X_l-\bar{X}_l)\right]\end{aligned}$$

Using the fourth and second order moments of the multivariate normal distribution, we can write the right hand side as

$$\begin{aligned}&\sum_{i,j,k,l} A_{ij}B_{kl}\Big(\mathrm{Cov}\left[X_i,X_j\right]\mathrm{Cov}\left[X_k,X_l\right] + \mathrm{Cov}\left[X_i,X_l\right]\mathrm{Cov}\left[X_j,X_k\right] + \mathrm{Cov}\left[X_i,X_k\right]\mathrm{Cov}\left[X_l,X_j\right] - \mathrm{Cov}\left[X_i,X_j\right]\mathrm{Cov}\left[X_k,X_l\right]\Big) \\ &\quad = \sum_{i,j,k,l} A_{ij}B_{kl}\Big(\mathrm{Cov}\left[X_i,X_l\right]\mathrm{Cov}\left[X_j,X_k\right] + \mathrm{Cov}\left[X_i,X_k\right]\mathrm{Cov}\left[X_l,X_j\right]\Big) \\ &\quad = 2\sum_{i,j,k,l} A_{ij}B_{kl}\mathrm{Cov}\left[X_i,X_l\right]\mathrm{Cov}\left[X_j,X_k\right],\end{aligned}$$

where the last equality follows because A is symmetric. Now let's write the sum in matrix form by exploiting the symmetry of A and B.

$$\begin{aligned}\sum_{i,j,k,l} A_{ij}B_{kl}\mathrm{Cov}\left[X_i,X_l\right]\mathrm{Cov}\left[X_j,X_k\right] &= \sum_{i,j,k,l} A_{ji}\mathrm{Cov}\left[X_i,X_l\right]B_{lk}\mathrm{Cov}\left[X_k,X_j\right] \\ &= \sum_{j,l}\left(\sum_i A_{ji}\mathrm{Cov}\left[X_i,X_l\right]\right)\left(\sum_k B_{lk}\mathrm{Cov}\left[X_k,X_j\right]\right) \\ &= \sum_{j,l} A_j\mathrm{Cov}\left[X,X_l\right]B_l\mathrm{Cov}\left[X,X_j\right] \\ &= \sum_j A_j\left(\sum_l \mathrm{Cov}\left[X,X_l\right]B_l\right)\mathrm{Cov}\left[X,X_j\right] \\ &= \sum_j A_j\mathrm{Cov}\left[X\right]B\mathrm{Cov}\left[X,X_j\right] \\ &= \sum_j e_j^T A\mathrm{Cov}\left[X\right]B\mathrm{Cov}\left[X\right]e_j = \mathrm{tr}\left\{A\mathrm{Cov}\left[X\right]B\mathrm{Cov}\left[X\right]\right\}.\end{aligned}$$

Therefore, we have

$$\mathrm{Cov}\left[F(X),G(X)\right] \approx \partial F(\bar{X})\mathrm{Cov}\left[X\right]\partial G(\bar{X})^T + \frac{1}{2}\mathrm{tr}\left\{\partial^2 F(\bar{X})\mathrm{Cov}\left[X\right]\partial^2 G(\bar{X})\mathrm{Cov}\left[X\right]\right\}.$$

□